EFFECTIVE RELAYING MECHANISMS IN FUTURE DEVICE TO DEVICE COMMUNICATION

A thesis presented in partial fulfilment of the requirements for the degree of

Doctor of Philosophy

in

School of Food and Advanced Technology

at Massey University, Palmerston North,

New Zealand.

Syeda Kanwal Zaidi

2020

Contents

Abstract **viii**

Acknowledgements **ix**

1 Introduction **1**

1.1 Rationale of the Study 3
1.2 Research Motivation 6
1.3 Research Objectives 8
1.4 Scope and Limitations 8
1.5 Research Contributions 9
1.6 Related Publications and Awards 10
1.7 Thesis Structure and Outline 12

2 Evaluating the Ergodic Rate in SWIPT-Aided Hybrid NOMA **13**

2.1 Introduction 13
2.2 Preliminaries 15
2.2.1 System Model 15
2.2.2 SWIPT based Transmission Model 15
2.3 Performance Analysis: Ergodic Rates 17
2.3.1 Downlink Ergodic Rate 17
2.3.2 Uplink Ergodic Rate 18
2.4 Observations 20
2.5 Conclusion 22

Appendices **23**

A DRC 16 Form 24

3 Two-Way SWIPT-Aided Hybrid NOMA Relaying for Out-of-Coverage Devices **25**
3.1 Introduction . . . 26
3.1.1 Related Works and Motivation . . . 26
3.1.2 Contributions . . . 28
3.1.3 Organisation and Notations . . . 28
3.2 The System Model . . . 29
3.2.1 Wireless Powered NOMA Relays (WPNR) . . . 29
3.2.2 Channel Model Description . . . 30
3.3 Operation Modes . . . 30
3.3.1 Downlink Transmission . . . 30
3.3.2 Uplink Transmission . . . 32
3.4 Performance Analysis of the system . . . 33
3.4.1 Outage Analysis . . . 33
3.4.2 System Throughput . . . 35
3.4.3 Rate Analysis . . . 36
3.5 Numerical Results and Discussion . . . 37
3.5.1 Effect of Transmit Power . . . 37
3.5.2 Effect of distance and transmission angle . . . 41
3.5.3 Uplink and Downlink Transmission . . . 43
3.6 Conclusion . . . 44

Appendices **46**
A Proof of Proposition 1 . . . 47
B Proof of Proposition 3 . . . 47
C Proof of Proposition 5 . . . 49
D Proof of Proposition 6 . . . 51
E DRC 16 Form . . . 52

4 Outage Analysis of Ground-Aerial NOMA with Distinct Instantaneous Channel Gain Ranking **54**
4.1 Introduction . . . 55
4.1.1 Contributions . . . 58
4.2 System Model and Assumptions . . . 59
4.3 Transmission Theoretic Model . . . 61
4.3.1 NOMA-based Model . . . 61
4.3.2 OMA-based Model . . . 63
4.4 Performance Analysis . . . 63
4.4.1 Downlink Transmission . . . 64

4.4.2 Uplink Transmission 66
4.5 Numerical Studies 69
4.5.1 Instantaneous Distinct Signal Power Assumption 69
4.5.2 Downlink Transmissions 72
4.5.3 Uplink Transmissions 76
4.6 Conclusion and Future Work 79

Appendices **81**
A Proof of Corollary 1 82
B Proof of Theorem 1 83
C Proof of Theorem 2 84
D Proof of Theorem 3 85
E Proof of Theorem 4 86
F DRC 16 Form 87

5 Conclusion and Future Directions **90**
5.1 Conclusion 90
5.2 Future Research Directions 92
5.2.1 Extension of WPNRs on a large scale network 92
5.2.2 Ground Aerial NOMA Aided Relays 92

Bibliography **94**

List of Tables

3.1 Communication Slots 30
3.2 Important Symbols 31
3.3 Simulation Parameters 38

4.1 Simulation Parameters 70

List of Figures

1.1 Generations of Wireless Communications [1]. 2
1.2 Key technologies. 5
1.3 An Illustration of Device to Device Relaying [2]. 6

2.1 Transmission Block Structure. 15
2.2 System Ergodic Rate vs SNR, $\beta_e = \alpha_d = 0.5$. 21
2.3 Downlink and Uplink Rate with variable β_e. 21
2.4 Uplink Rate with variable β_e and α_d, SNR= 30 dB. 22
A.1 DRC 16 -Chapter 2. 24

3.1 Proposed System Model for Hybrid NOMA with SWIPT. 29
3.2 Downlink Outage Probability 39
3.3 Uplink Outage Probability 40
3.4 System Throughput-delay-limited transmission mode. 41
3.5 Ergodic Rate- Delay-tolerant transmission mode 42
3.6 Effect of distance and transmission angle on rate 43
3.7 Ergodic Rate with varying SNR and ρ. 44
E.1 DRC 16 -Chapter 3. 53

4.1 System Model. 59
4.2 Impact of α_g on $IDSP_g$ with $m_d = 2$, $\mathcal{R}_\mathcal{D} = \mathcal{R}_\mathcal{G} = 50m, h_d = 50m$. . . . 70
4.3 Impact of $\mathcal{R}_\mathcal{G}$ on $IDSP_g$ with $m_d = 2, \mathcal{R}_\mathcal{D} = 50m, \alpha_d = 2.05, h_d = 50m$. 71
4.4 Impact of $\mathcal{R}_\mathcal{D}$ on $IDSP_d$ with $m_d = 2, \mathcal{R}_\mathcal{G} = 50m, \alpha_g = 2, h_d = 50m$. . . 71
4.5 Impact of h_d on $IDSP_g$ with $\alpha_d = 2.05, \alpha_g = 2$. 72
4.6 Outage of user d and user g in DL transmission, $\beta_{SIC} = 0.1$. 73
4.7 Outage of user d and user g in DL transmission vs. Power allocation, $\beta_{SIC} = 0.1$. 74
4.8 Comparison of Outage of user d and user g in DL transmission with baseline scheme. 74

4.9 Outage Probability of the users vs. α_g, $p_{\mathcal{S}} = 30$dB, h_d= 50m, β_{SIC}= 0.1, $\mathcal{R}_{\mathcal{T}}^{x_{dl}^d} = 0.1$ bps, and $\mathcal{R}_{\mathcal{T}}^{x_{dl}^g} = 0.5$ bps. 75
4.10 Outage Probability of user d vs. h_d, $\alpha_d = 2.05, \alpha_g = 1.992, \beta_{SIC} = 0.1$. . 75
4.11 Downlink System Throughput (NOMA vs. OMA), $h_d = 50m$, $m_d = 2$, $\beta_{SIC} = 0.1$ $\mathcal{R}_{\mathcal{T}}^{x_{dl}^d} = 0.1$ bps, and $\mathcal{R}_{\mathcal{T}}^{x_{dl}^g} = 0.5$ bps. 76
4.12 Outage of user d and user g in UL transmission, $\beta_{SIC} = 0.1$. 77
4.13 Comparison of Outage of user d and user g in UL transmission with baseline scheme. 77
4.14 Outage of user d and user g vs. α_g, $\alpha_d = 2.05$, $\beta_{SIC} = 0.1$, $m_d = 2$, $h_d = 50m$, $\mathcal{R}_{\mathcal{T}}^{x_{ul}^d} = 0.01$ bps, and $\mathcal{R}_{\mathcal{T}}^{x_{ul}^g} = 0.1$ bps. 78
4.15 Outage of user d vs. h_d, $\beta_{SIC} = 0.1$, $\alpha_d = 2$, $\alpha_d = 1.992$, $\mathcal{R}_{\mathcal{T}}^{x_{ul}^d} = 0.01$ bps, and $\mathcal{R}_{\mathcal{T}}^{x_{ul}^g} = 0.1$ bps. 78
4.16 Uplink System Throughput (NOMA vs. OMA), $\beta_{SIC} = 0.1$, $\mathcal{R}_{\mathcal{T}}^{x_{ul}^d} = 0.01$ bps, and $\mathcal{R}_{\mathcal{T}}^{x_{ul}^g} = 0.1$ bps. 79
F.1 DRC 16 -Chapter 4. 89

Abstract

Future wireless networks embrace a large number of assorted network-enabled devices such as mobile phones, sensor nodes, drones, smart gears, etc., with different applications and purpose, but they all share one common characteristic which is the dependence on strong network connectivity. Growing demand of internet-connected devices and data applications is burdensome for the currently deployed cellular wireless networks. For this reason, future networks are likely to embrace cutting-edge technological advancements in network infrastructure such as, small cells, device-to-device communication, non-orthogonal multiple access scheme (NOMA), multiple-input-multiple out, etc., to increase spectral efficiency, improve network coverage, and reduce network latency. Individual devices acquire network connectivity by accessing radio resources in orthogonal manner which limits spectrum utilisation resulting in data congestion and latency in dense cellular networks. NOMA is a prominent scheme in which multiple users are paired together and access radio resources by slicing the power domain. While several research works study power control mechanisms by base station to communicate with NOMA users, it is equally important to maintain distinction between the users in uplink communication. Furthermore, these users in a NOMA pair are able to perform cooperative relaying where one device assists another device in a NOMA pair to increase signal diversity. However, the benefits of using a NOMA pair in improving network coverage is still overlooked. With a varierty of cellular connected devices, use of NOMA is studied on devices with similar channel characteristics and the need of adopting NOMA for aerial devices has not been investigated. Therefore, this research establishes a novel mechanism to offer distinction in uplink communication for NOMA pair, a relaying scheme to extend the coverage of a base station by utilising NOMA pair and a ranking scheme for ground and aerial devices to access radio resources by NOMA.

Acknowledgements

Praises and thanks to Almighty Allah for blessing me with the strength to complete this dissertation. I would like to thank my supervisor Syed Faraz Hasan for his continuous guidance, kind support and remarkable leadership. His motivation, dedication and attention to my work have pushed out the best from me. I am equally thankful to my co-supervisor Xiang Gui for being an excellent mentor, without his constant support the research would not have been completed. I honestly feel that I have the best duo of supervisors for my PhD research.

Many thanks to Telecommunication and Network Engineering (TNE) Group for their input to my research. I am very grateful to Donald Bailey and Murray Milner for their counselling and support through the platform of IEEE NZ Central Section. Thank you Massey University for MU doctoral scholarship and MU Presentation Grants, these uplifted me financially which was much needed. I must mention my sincere gratitude for Hina Tabassum from York University, Canada for her regular bits of advice and technical insight. Your input meant a lot to me and you are truly an inspiration. A very special thanks to Data Analyst team of Integrated Business Improvement Student System (IBISS) from Massey University, who was not directly involved in my research but was always involved in bucking me up morally and emotionally.

Words can't describe how grateful I am to my husband SS whose love and support have no bounds. He is the wind beneath my wings. The little ray of light during my dark study hours is my son Hadi who thinks that his mom is busy making a flying robot :D. I feel so proud to mention "Project Baby" which I finished along with my PhD research and its little outcome is my son Meer. Project Meer kept me motivated as I aligned my publication deadlines with his delivery time. Thank you SS, and my very own H&M, my success story is under your front cover.

Most of all, my parents who always believed in me and prayed day and night for my success. Thank you abbo and ammi, I need your prayers, always and forever. I cannot miss my siblings who always threw silly jokes on my PhD research and cracked

me up when I felt low. Their moral boost always pumped me up.

How can I forget some of my close friends, Ayesha, Saman, Shan, Ali, Abhipray, Van and Amardeep who listened to my endless stories, shared laughs and failures. Finally, I would like to express my thanks to everyone around me who motivated me directly or indirectly during my study tenure.

I dedicate this thesis to my abbo- who dreamt that I will be a PhD even when I was not aware what PhD is :)

Chapter 1

Introduction

Each generation of cellular technology progressed to meet the burgeoning connectivity demand. Coverage provision started at fixed locations for ground devices like phones and advanced to aerial devices like unmanned aerial vehicles (UAVs). The earlier analog first generation (1G) of mobile phone transited to the second generation (2G) with the characteristic features of digital technology that increased the number of users per channel and opened the way for basic data services. The changes in 2G began in earnest with the widespread use of internet. Mobile phone technology made a sharp move towards third generation (3G) which was not only capable of phone calls (voice data), but also delivered internet and video services to devices like hand-held phones, laptop, computers, and similar gadgets. In recent years, the purpose of the cell phone has shifted from a verbal communication tool to a multimedia tool, often adopting the name "smart phone" rather than being called a mobile phone. With the roll out of data hungry applications on smart phones, cellular-network providers announced fourth generation (4G) which delivered ten times faster broadband speed. Long term evolution (LTE), the standard technology of 4G, provides improved data rates to increased number of users than earlier generations of mobile communications. At present, availability of cellular data on smart phones is pervasive, albeit at varying speeds and with different cost levels. Quick technological advancements, the unveiling of increasingly intelligent consumer-friendly devices, and a marked acceleration in people using the internet and mobile devices worldwide provide compelling evidence that there is a significant need to support future wireless communications [3]. The proliferation of technology savvy devices has resulted in a deluge of digital traffic and there is an increased emphasis on ubiquitous internet, greater connectivity, increased coverage and faster communication between the devices which are expected to be delivered by fifth generation (5G). 5G has been launched in the UK [4] and some countries of the European Union like Germany, Spain and Italy by some telecommunication operators and is capable to handle 1000x

traffic than today's networks and it would be 10x faster than 4G LTE [5]. Fig. 1.1 illustrates the progress of cellular communication networks along with the key technologies introduced in each generation of mobile networks.

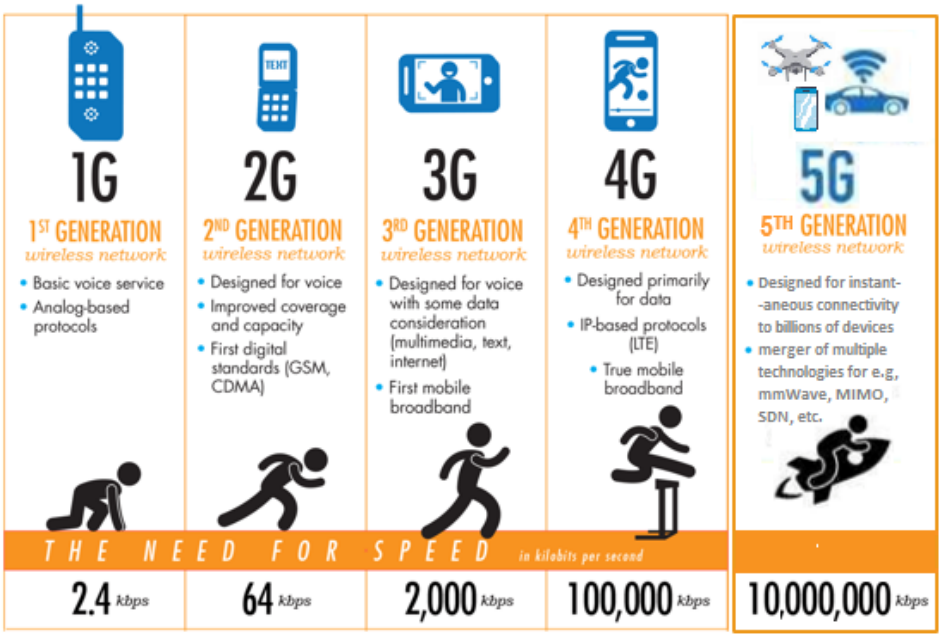

Figure 1.1: Generations of Wireless Communications [1].

There is need for faster, smarter, and more reliable data communication services due to the storm of devices and users, and the nascent developments in medical-care, industrial internet of things (IoT) applications, ground and aerial transport, agriculture and farming, media, and entertainment industry. To deliver ubiquitous coverage and support these use cases, 5G is expected to meet the challenge of peak data performance and consistent user experience throughout the network. For the initial deployment of 5G, shared spectrum in the range of low frequencies 3.3-4.2 GHz is being used globally. Below 6 GHz spectrum requires lower site density at the cost of narrower bandwidths of about 100MHz per channel, and consequently peak throughput in the order of Gbps. However to help realise 5G's full potential in demanding cases, the allocation of new spectrum in high frequency bands above 24GHz is necessary. High frequency spectrum results in extra capacity but at the cost of greater propagation limits, while jeopardizing the delivery of consistent coverage due to propagation characteristics.

Higher frequency bands deployment will not be able to provide same coverage as its low frequency counterpart, consequently omnipresent coverage will be a necessity which

will be obtained by network densification in future wireless networks. These dense networks with larger numbers of cells should maintain consistent user experience and the quality of service should not be compromised at the edge of cells. Existing cellular networks deploy relay nodes to improve the coverage of the cell which increases operational and capital expenditures of a cellular network operator. To lower the deployment cost, a way forward is to utilise existing network devices to cooperate and act as relays. This means that even after introducing new spectrum, there is a need to usher in improved infrastructure, access mechanisms, and radio interfaces for improved user experience. Hence not only new spectrum, but the synergies between different technologies, deployment approaches and modes will contribute towards ubiquitous connectivity and coverage in future networks. Nonetheless, when the devices communicate with each other, they access radio resources. Provision of radio resources in current wireless networks is done orthogonally in time or frequency domain which limits network capacity. The effective access mechanisms for a large number of devices with varied nature of communication not only improve network capacity but also provide new avenues for extending network coverage. In this work, we aim to exploit the effective schemes for spectrally efficient communication and improved user experience in future wireless networks.

The research methodology adopted in this work is widely practised in the discipline of communication engineering. At first, the related literature was studied to get the insights of the current state of the art. During the detailed study of the literature, research on the available simulation tools was also done. It then followed the well accepted practice of system modelling and theoretical analysis, supported by numerical simulation.

The remainder of this chapter is organised as follows. Section 1.1 presents a preamble and rationale of the research. In Section 1.2, motivation to study effective relaying mechanisms is explained, followed by Section 1.3 on the objectives we aim to achieve. We explain scope of work in Section 1.4. The research goals are then explained with an identification of the contributions in Section 1.5. Publications generated from this research work are listed in Section 1.6. Finally, the organisation of this dissertation is presented in Section 1.7.

1.1 Rationale of the Study

Current cellular networks suffer from the issue of inconsistent user experience and poor network coverage at the edge of a cell. In existing 4G LTE infrastructure, a concept of fixed term relaying is introduced which involves the deployment of low-power BSs, named as fixed relays, to assist the communication between a source and a destination [6]. To lower the deployment cost of these extra relay nodes, existing

network devices can be utilised for user cooperation, i.e, they can help BS in ferrying data to cell edge users. This communication between the devices is a kind of device-to-device (D2D) communication which helps in extension of cell coverage as well. D2D communication is currently a part of 4G-LTE advanced networks and is envisioned to evolve continuously into the future cellular networks to support a diverse range of devices and applications with better speed, improved capacity, low power consumption and stringent security [7]. D2D communication establishes link between digital devices independently, without the involvement of the BS, therefore proximate devices can directly communicate with each other. This short-range communication with nearby devices brought out the concept of device relaying. Device relaying makes it possible for devices in a network to function as transmission relays for each other and realize a massive adhoc mesh network [8].

Radio Spectrum is expensive and scarce and must be utilised efficiently. For serving a massive future networks with ever-increasing data traffic levels, it is important to provide superior spectral access mechanisms to accommodate a large number of devices thereby enhancing the spectral efficiency. Apart from invoking D2D technique to extend coverage of a wireless network, another emerging idea is non-orthogonal multiple access (NOMA), which is able to address the spectral efficiency enhancement issue, on the standpoint of realizing a new power dimension for multiple access [9]. NOMA is a channel access scheme which allows more than one user in a single time/frequency band by varying power levels to acquire channel for transmission [10]. In this scheme, users are paired together to access the channel after acquiring distinguished power levels or distinct codes from transmitter's end in downlink communication. However, in uplink communication maintaining distinct power levels for multiple users in a single band is also mandatory. Several researchers advocated the ability of NOMA in device relaying and proposed that one user from the NOMA pair can assist in delivering the messages to another user to improve signal diversity and increase reception reliability of the other user in the pair [11]. Nevertheless for increasing number of users, improved relaying mechanisms need to be formed to provide extended coverage to larger domains.

Despite the impressive progress achieved by the concept of user cooperation in NOMA, a major concern is the provision of energy to the nodes who are involved in relaying [12]. While, a fair volume of literature exists for cooperative relaying in wireless networks, for example [11, 13, 14], these works do not take into account the incentive mechanism in lieu of data ferrying relays. A number of researchers have proposed a range of incentive techniques for participating relays such as token allotment, bandwidth exchange, and reputation based mechanisms [15, 16], conversely methods can be derived for energy depletion in relay nodes. Thus, energy harvesting from radio frequency (RF) is gaining attention to recharge network nodes or devices [17]. Authors

in [18,19] proposed energy harvesting mechanisms from received radio signals to aid the relay node for data transmission. As the batteries of the smart phones are rechargeable from the power sources, the research community is trying hard to revolutionize the signal reception by extracting energy from the ambient RF sources. In D2D communication, the relay or participating nodes may have limited battery capacities and they need some external charging resources for communicating actively in network [20, 21]. Hence, providing energy to the user nodes while utilising spectrum efficiently for extending coverage is equally important for data relaying. Reliable connectivity to a large

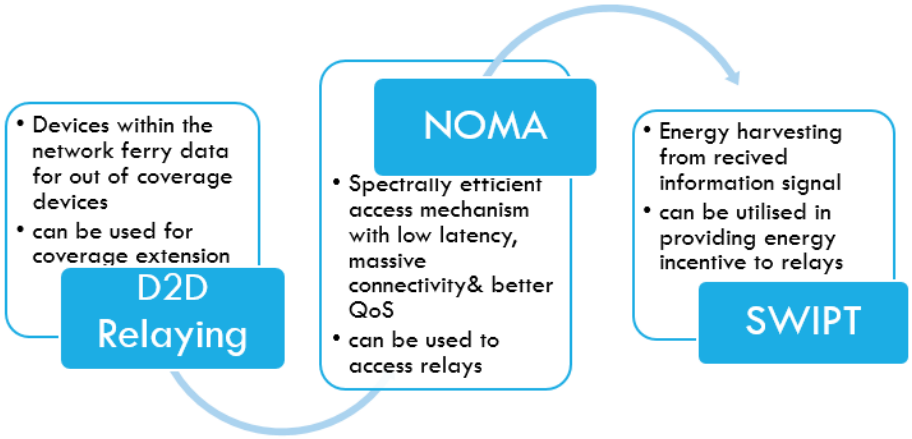

Figure 1.2: Key technologies.

number of heterogeneous users and coverage extension are major concerns for future networks with a diverse range of applications like weather forecasting, live video/audio streaming, digital farming. These networks are expected to incorporate UAVs for services from data-collection to delivery [22]. Sweeping applications of UAV technology attracts prominent attention to provide cellular connectivity to UAVs along with ground devices [23]. UAVs are different than ground users in terms of altitude, propagation characteristics and channel fading environment. Nonetheless, reviving the multiple access scheme is advantageous for 5G to improve spectral efficiency, the characteristic difference of ground devices and UAVs for connectivity provision cannot be ignored. With stringent requirements of the future communication networks, excessive cost and difficulty of setting up urban hotspots, UAVs stand as a potential candidate to provide connectivity solutions for the IoT networks, assistance in relaying data for network devices, and high-altitude assisted transmission because of their deployment flexibility and lower cost [24].

1.2 Research Motivation

Relaying helps to achieve performance improvements in wireless communication networks by assisting in the data transmission between nodes in a network [25]. It may be a dedicated relay station deployed explicitly in the network to forward the data to other users or an implicit user present to cooperate with BS in data transmission. In contrast to deploying extra relay nodes, cooperative relaying makes the use of existing users in relaying information between two devices and is also referred as D2D relaying. D2D relaying is appealing because it does not increase infrastructure costs for the network operator in contrast to infrastructure relay nodes, which are included as a part of the current LTE-Advanced standard [26,27]. D2D relaying to improve system capacity and coverage comes into consideration for future wireless networks as well [28,29]. The underlying idea is that there are a large number of devices that may act as relays, either infrastructure ultra-dense network access points without wired back-haul, or other devices such as user-deployed devices, nomadic nodes, drones, or mobile users, which may act as relay stations to help to convey user traffic to or from the network, see Fig. 1.3.

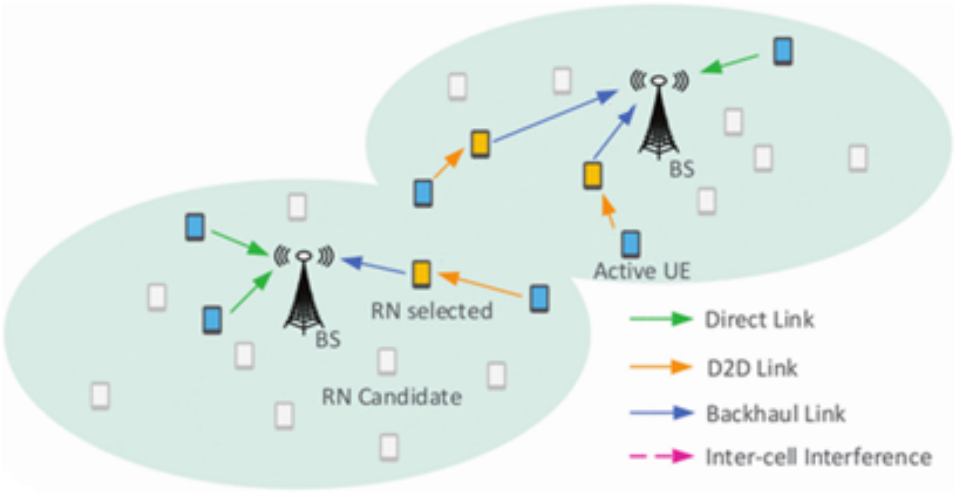

Figure 1.3: An Illustration of Device to Device Relaying [2].

Most of the research works which have been done to facilitate the concept of relaying are based on orthogonal multiple access scheme (OMA) of radio resources in wireless networks [30]. The emergence of beyond 5G (B5G) networks requires new radio access technologies that can provide relatively high speeds as compared to existing LTE networks for burgeoning spectral efficiency sector to satisfy the increasing demand of data traffic by the subscribers. In order to accomplish this, an increasing trend in technologies is to introduce an overhaul to the current network infrastructure, wider range of

software architectures, concepts of dense heterogeneous networks, and innovations in accessing radio resources. Access mechanism of radio resources is attracting widespread interest with the concept of NOMA. As mentioned earlier, NOMA is a relatively new technique for increasing spectral efficiency and reliability of transmission and stands as a candidate technique for channel access [31]. This access technique exploits the power domain to incorporate the messages of two users in a single frequency band in one time slot and applies successive interference cancellation techniques at the receiver end to extract the message of the particular user [32]. The non-orthogonality in power domain can be extremely useful in utilising the spectrum efficiently and in increasing the reliability of transmission as well. NOMA is gaining rapid attention, as it seems like a winning strategy to cope with the severe spectral availability problem. Hence it is important to study the application of relaying not only on the conventional multiple access schemes but also on the newly proposed NOMA scheme.

Relaying can be further improved if the relaying device is paid off for their relaying job by means such as extra spectral efficiency, bandwidth allocation, energy boost, etc. [33] or is provided with sufficient energy for relaying data. This issue is important and has attracted significant consideration from the researchers [34–36]. Although wireless networks can be provided energy from power sources such as, heat, wave and wind [17] but for low power nodes in short range D2D communication, energy harvesting from radio frequencies is the taking lead [37, 38]. Recharging batteries or replacing them with new ones sidelines energy harvesting but it is highly inconvenient for the relay nodes and incurs more cost and also is not possible/undesirable in many embedded devices or sensors (such as sensors within human, plant or animal body or embedded within a fixed place). Energy harvesting with radio frequency is a viable solution in cooperative networks as it allows devices to communicate and scavenge energy from the same radio source simultaneously [39]. In wireless networks, multi-hop communication is a realistic scenario in which the relays or the sensor nodes have limited battery capacity to carry out information processing and they rely on external sources to charge their batteries, hence energy harvesting could be utilised in relaying to replenish the battery of relay nodes. Most previous works either consider the NOMA based relaying for signal diversity or ignore the energy constraint imposed on the NOMA based node in small cell networks. Radio frequency energy harvesting is considered in OMA based relaying protocols mostly [40, 41] and is under research for NOMA based relaying schemes [42, 43]. According to the recent studies, there's no question that spectral efficiency is the primary beneficiary of NOMA [31, 44], there is still a need for realising its gains in cooperative data relaying together with mechanisms to furnish relays with energy for data transmission.

As stated earlier, spectral efficiency of NOMA based communication [9, 45, 46] is

beneficial for the future wireless networks which will comprise of a variety of cellular connected devices, such as sensors, mobile phones, IoT devices and drones [47]. While a significant number of research works utilises mobile nodes in a network to act as a relay [11, 14], a few have proposed to take advantage of aerial devices such as drones to participate in device relaying [48, 49]. So far research studies have grouped network devices located at ground level, in NOMA band [12, 46, 50] to reveal the superiority of NOMA in spectral efficiency. A few works have also explored NOMA with aerial devices, such as UAVs [51, 52] to deploy manifest abilities of NOMA. However,to date, no research work has explored the opportunity for an aerial and a ground device to access channel with NOMA.

1.3 Research Objectives

Particularly, we aim to achieve the following objectives from this research.

- The development of a network model where the users are able to communicate successfully to the BS with distinct power levels with the help of NOMA by harvesting energy from the downlink radio signals.
- Building on the proposed model, our objective is to exploit SWIPT for a unique relaying mechanism to provide coverage to cell-edge users in downlink and uplink communication.
- Further to extend cellular connectivity to aerial devices, we aim to pair an aerial and a ground user with the help of NOMA based on a novel user ranking scheme.

1.4 Scope and Limitations

It is important to clarify that energy harvesting from radio frequencies is not the primary domain of this research work. We rely on the existing literature to obtain the values of certain parameters related to energy harvesting efficiency. Another limitation is the ability of devices to harvest energy from radio frequency which depends on the internal electronic circuitry of the devices and hence is not covered in our work. Furthermore, whether or not harvesting energy from downlink radio signals is practical, is out of scope of this work. In this thesis, we consider network models and scenarios that have not been addressed in the literature before, and apply mathematical tools to evaluate network performance. More specifically, we will exploit two important performance metrics of a wireless network, i.e., outage probability and ergodic capacity or ergodic rate. Therefore, in this thesis, we are specifically interested in following key performance indicators of the proposed network models in the following chapters.

- **Outage Probability:** This is the probability that a received signal at a certain node goes below a specified threshold value required for the correct recovery of the message. In a typical wireless communication system, there are three important entities, i.e, a source or transmitter, a destination or a receiver and a communication channel in between them. Based on the information, the transmitter first modulates the electromagnetic signal and sends it through propagation medium where the power of electromagnetic signal decays along with an increase in the propagation distance. For correct recovery of the information, the power of the signal received needs to be greater than a particular threshold required for correct recovery of information. If the received power is less than the specified threshold, the outage is declared and the data transmission is declared as failed. Hence evaluating the probability of outage in data transmission is an important metric to study.

- **Ergodic Rate:** It is defined as the average data rate supported per channel per hertz in data transmission between a source and a destination. In wireless communications, frequency channels divide the available spectrum into multiple blocks. Multiple transmitters are allowed to transmit their data on these channels based on different multiple access mechanisms like OMA and NOMA. Based on the threshold requirement, the data is recovered at the receiving end for each frequency channel. Therefore, when data is transmitted over more frequency channels, a larger number of wireless links are established between transmitter and a receiver. The link capacity or data rate can be evaluated with the help of Shannon's formula: $\mathcal{C} = \mathcal{B}\log_2(1 + SNR)$ bits/sec, where, $\mathcal{C}$ is the data rate obtained for one transmission link and $\mathcal{B}$ is the available bandwidth of a channel. As in NOMA, when multiple signals are transmitted over the same channel to accommodate increasing number of devices, the signals may interfere with each other, causing interference. When such signal is received by the receiver, the interfering signal is treated as a noise and the signal to interference and noise ratio (SINR) is evaluated at receiver's end, hence Shannon's capacity formula is written as

$$\mathcal{C} = \mathcal{B}\log_2(1 + SINR) \quad bits/sec. \tag{1.1}$$

1.5 Research Contributions

This thesis aims at providing a new paradigm for improving the underlying basis of relaying mechanisms that overcome the spectral efficiency limitations and energy depletion issues of devices. In the following, we summarise the research contributions based on our objectives stated in previous section.

A Novel Uplink NOMA Scheme: We propose a novel scheme to establish uplink communication in a NOMA based network. This unique scheme provides distinct power to each user in a NOMA pair for uplink transmission to the source. The difference in the uplink power is achieved by harvesting energy from the received downlink signals from the source. Through our research work, we ensure that the devices have the opportunity of establishing communication with radio source without relying entirely on their own batteries. We evaluate the downlink and uplink ergodic rate achieved for each user node and provide mathematical derivation of the results. Here, we also reveal the superiority of power splitting energy harvesting protocol and also highlight the trade-off in achieving desired uplink or downlink data rate. Further details of this work are covered in Chapter 2 of the thesis.

A Unique Relaying Scheme with NOMA: We further extend the idea to initiate the concept of device relaying for overcoming the connectivity issues of users located at the edge of a cell. In this context, we propose the concept of wireless powered relays on the basis of NOMA to extend the coverage of a base station in uplink and downlink communication. These device relays are powered with RF energy harvesting. We perform mathematical modelling of the proposed model and evaluate the performance by deriving outage probabilities and system throughput in delay sensitive and delay tolerant transmission modes in downlink and uplink transmission. This study unveils the concept of overcoming double-near far problem in relaying networks. The explanation is covered in Chapter 3 of this thesis.

A Mechanism to Pair Ground and Aerial Devices using NOMA: To facilitate the cellular connectivity for a range of network devices which includes ground and aerial devices, we propose to apply NOMA based on a novel user ranking scheme. We argue that because of the difference in channel characteristics and environmental conditions of an aerial and a ground user, distance based ranking cannot be applied. Hence, we propose a parameter known as instantaneous distinct signal power (IDSP) to rank users in a NOMA pair consisting of an aerial and a ground user. By evaluating this, we designate signal power to both users in downlink transmission and decide the order of decoding in uplink transmission. We derive the mathematical expressions of the outage probabilities in uplink and downlink transmission for ground and aerial users to evaluate system performance. This research direction brings interesting insights that are discussed in Chapter 4 of this thesis.

1.6 Related Publications and Awards

Below is the list of journal and conference papers which are published as a result of this research.

- ***Journals***
  - S. K. Zaidi, S. F. Hasan, and X. Gui, "Outage Analysis of Ground-Aerial NOMA with Distinct Instantaneous Channel Gain Ranking", IEEE Transactions on Vehicular Technology, doi: 10.1109/TVT.2019.2938516, September 2019.
  - S. K. Zaidi, S. F. Hasan, X. Gui, "Two-way SWIPT-aided hybrid NOMA relaying for out-of-coverage devices", Journal of Wireless Networks, pp. 1-16, September 2019.
  - S. K. Zaidi, S. F. Hasan, and X. Gui, "Evaluating the ergodic rate in SWIPT-aided hybrid NOMA", IEEE Communication Letters, vol. 22, no. 9, pp.870–1873, September 2018.
- ***Conferences***
  - S. Jaffry, S. K. Zaidi, S. T. Shah, S. F. Hasan, and X. Gui, "D2D Neighborhood Discovery by a Mobile Device ", in IEEE International Conference on Communications (ICC) 2019, May 2019, pp. 1-6.
  - S. K. Zaidi, S. F. Hasan, and X. Gui, "SWIPT-aided uplink in hybrid non-orthogonal multiple access", in 2018 IEEE Wireless Communications and Networking Conference (WCNC), April 2018, pp. 1–6.

    Award: Massey University Conference Presentation Grant 2018.
  - S. K. Zaidi, S. F. Hasan, and X. Gui, "Wireless-powered NOMA relays for out-of-coverage devices", in IEEE 28th Annual International Symposium on Personal, Indoor, and Mobile Radio Communications (PIMRC), October 2017, pp. 1-5.

    Award: Massey University Conference Presentation Grant 2017.
  - S. K. Zaidi, S. F. Hasan, and X. Gui, "Time Switching Based Relaying for Coordinated Transmission Using NOMA", in 2018 Eleventh International Conference on Mobile Computing and Ubiquitous Network (ICMU), February 2019, pp. 1-6.
  - S. K. Zaidi, A. A. Adheem, S. F. Hasan, and X.Gui, "Connecting Makaraka - A Case Study to Provide Connectivity in the Rural Area of New Zealand", in SmartGIFT 2018: Smart Grid and Innovative Frontiers in Telecommunications, July 2018, pp. 145-154.
  - S. K. Zaidi, S. F. Hasan, X. Gui, N. Siddique, and S. Ahmad, "Exploiting UAV as NOMA based relay for coverage extension", in 2nd International Conference on Computer Applications Information Security (ICCAIS), May 2019, pp. 1–5.

– S. K. Zaidi, S. F. Hasan, and X. Gui, "A Novel Relaying Mechanism for Multi-Cast Transmission with Ground-Aerial NOMA", in International Telecommunication Networks and Application Conference, November 2019.

Award: Massey University Conference Presentation Grant 2019.

1.7 Thesis Structure and Outline

This thesis is organised as follows.

Chapter 2. In this chapter, a NOMA based network model is proposed to facilitate the uplink communication on the basis of harvested energy. The chapter first covers the existing techniques for establishing uplink communication for NOMA. Following this, the proposed strategy for uplink communication is explained, detailing how the nodes communicate with a designated source and utilise a portion of the received downlink energy in communicating back to the source. The performance evaluation is shown by evaluating the ergodic rates of both nodes in uplink and downlink communication in a two-node network. At last, the chapter is concluded by stating the highlights of the research and future research directions.

Chapter 3. This chapter highlights the concept of wireless powered NOMA relays. It proposes a relaying scheme in which relays sustain uplink and downlink communication with radio frequency energy harvesting. The mathematical analysis to derive outage probabilities and ergodic rates is presented, followed by the numerical results to evaluate the behaviour of the system which are further verified by the simulation. Lastly, the proof of the theorems presented in the chapter are provided in the appendices.

Chapter 4. This chapter explains the concept behind ground-aerial NOMA in detail. The key contributions of this research part are highlighted along with relevant literature review. The chapter then highlights the proposed network model followed by mathematical explanation of the important performance evaluation metrics. Then, the results obtained from the proposed schemes are explained with details on the superiority of the scheme. In the end, the chapter is concluded and appendices are presented to document the details of mathematical analysis.

Chapter 5. In this chapter, the summary of the contributions made by the author is included with an explanation of the key research directions of the proposed techniques.

Chapter 2

Evaluating the Ergodic Rate in SWIPT-Aided Hybrid NOMA

Authors : Syeda Kanwal Zaidi, Syed Faraz Hasan, and Xiang Gui

Abstract

This chapter studies a hybrid non-orthogonal multiple access (NOMA) based wireless system, in which the users harvest energy from the received downlink signals in order to transmit on the uplink. We argue that the use of energy harvesting helps in maintaining distinct power levels when the users commence uplink NOMA transmissions. To evaluate the performance of the proposed model, we derive closed-form mathematical expressions of the average ergodic rate of the system. The results illustrate that: 1) this scheme is capable of establishing NOMA based uplink communication solely on the basis of harvested energy and 2) power-splitting parameter shows positive correlation on the uplink rate performance whereas the choice of time-splitting parameter favours either uplink or downlink data rate.

Keywords: Non-orthogonal multiple access (NOMA), simultaneous wireless information and power transfer (SWIPT).

2.1 Introduction

Non-orthogonal multiple access (NOMA) has been proposed for the fifth-generation (5G) wireless networks to help deliver higher throughput, improved reliability, reduced latency and increased spectral efficiency. NOMA assigns different power levels to the users in order to allow them to transmit simultaneously using the same frequency/time resource. There have been several previous works that focus on downlink (DL) NOMA, in which a base station (BS) transmits a composite signal which is successively decoded by the users based on the power levels assigned to each of them [53]. This decoding

process is termed as successive interference cancellation (SIC). However, in the uplink (UL) NOMA, it is very challenging for the BS to distinguish between multiple user transmissions based on their power levels. Different approaches have been proposed to resolve the optimal power allocation issue in NOMA-based UL transmissions. A power back-off scheme has been introduced in [54], which assigns different transmit power levels to the NOMA users that are transmitting on the uplink. The power levels are assigned based on the path loss between the NOMA users and the BS. The value of power back-off parameter is more for users with a larger path loss and is gradually degraded for the users with smaller path loss, which helps BS in correctly decoding individual transmissions. In [55], the authors use fractional power control for decoding NOMA messages at BS, where proper setting of control parameter is crucial in keeping received power levels distinct. It has been pointed out in [53] that the conventional power control solutions is not a viable solution in a system that uses NOMA. All existing works, for example [53]- [55], incur additional processing overhead in assigning power levels to the users that can be easily distinguished at BS.

The idea proposed in this chapter is to harvest energy from DL NOMA signals (that carry information from BS), and assign distinct power levels to the users when they transmit using UL NOMA. This so-called simultaneous wireless information and power transfer (SWIPT) is employed using power splitting (PS) based approach [18]. SWIPT has been explored in recent literature. For example, the work in [56] optimizes wireless power transfer in UL NOMA and that reported in [57] jointly optimizes BS transmit power, and time durations for energy harvesting and data transmission. The impact of the use of harvested energy on outages in UL transmissions has been studied in [58]. However, the use of an additional time slot limits the achievable throughput of the system. On the contrary, we use PS-based SWIPT protocol and harvest energy from the signals received from BS to enable UL NOMA communication. The use of SWIPT in a system that employs UL and DL NOMA yields two benefits: it creates a self-sustained reverse channel and inherently provides difference in the power levels of the users transmitting in UL because of different harvested energy. In this chapter, we obtain verified analytical expressions of DL and UL ergodic rates of SWIPT-aided hybrid NOMA system, which to the best of the authors' knowledge have not been evaluated before. It is shown in the results that the UL rate of NOMA users is improved by providing more power to energy harvesting circuitry with a compromise on DL data rate. We also notice that while increasing DL transmission time allows more energy to be harvested, it does not correspondingly increase UL data rate.

The rest of the chapter is structured as follows. Section 2.2 introduces the system model while section 2.3 covers its ergodic rate analysis. Section 2.4 presents analytical and simulation results. This chapter is concluded in Section 2.5.

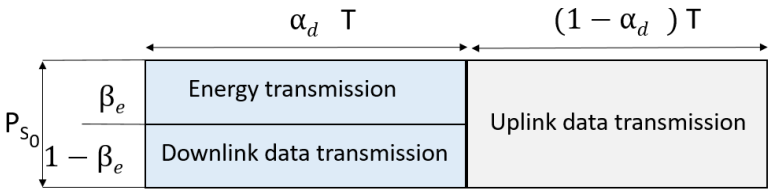

Figure 2.1: Transmission Block Structure.

2.2 Preliminaries

2.2.1 System Model

We consider a NOMA network, where two single-antenna nodes U_A and U_B with fixed locations $d_i \epsilon \mathbb{R}^2, i \epsilon \{U_A, U_B\}$ communicate bi-directionally with a source (S_0) located at centre of the cell, where ($||d_{U_A}|| < ||d_{U_B}||$). Both nodes are energy constrained with integrated resources to provide fixed transmit power and to eliminate randomness of instantaneous received power [18]. Bounded path loss model ($\varepsilon + ||d_i||$) is considered with a distance-dependant path loss at the rate of ($||d_i||^{-l_e}$) [59], where l_e is the path loss exponent, and ε is a fixed parameter to ensure finite path loss and finite harvested energy [58]. Transmission block time T (see Fig. 2.1) is divided into two phases by a time-split parameter α_d ($0 < \alpha_d < 1$). A fraction $\alpha_d T$ is used for DL transmission and the remaining $(1 - \alpha_d)T$ is used in UL transmission. The users receive power P_{S_0} from S_0, which is split by a power-split parameter β_e ($0 < \beta_e < 1$). A portion of split power $\beta_e P_{S_0}$ is used for energy harvesting while the remaining $(1 - \beta_e)P_{S_0}$ is used for information decoding. We assume quasi-static, independent and identically distributed Rayleigh fading channels $h_{S_0 i}$ ($h_{S_0 i} \sim \mathcal{CN}(0, 1)$) between users and S_0 [55]. These channels are assumed constant over one block. Additive white Gaussian noise (AWGN) is assumed for all wireless links and the channel state information is available at all nodes [60]. The nodes harvest a finite amount of energy for information transmission and the power utilised in information processing is negligible and ignored [18, 59].

2.2.2 SWIPT based Transmission Model

The aggregate energy harvested by each node is:

$$E_i^H = \frac{\eta_{e,i}\zeta_{e,i}P_{S_0}|h_{S_0 i}|^2\alpha_i}{(\varepsilon + ||d_i||^{l_e})}T, \tag{2.1}$$

where, $\zeta_{e,i}$ denotes efficiency factor specific to receiver architecture of *i-th* node, $\eta_{e,i}$ is the RF-to-DC power conversion efficiency of *i-th* node and $\alpha_i = \alpha_d \beta_e$ for integrated receiver architecture.

The downlink NOMA signal received by a user is given as:

$$Y_{DL} \longrightarrow U_i = \sqrt{P_{DL}} \sum_{i\epsilon(U_A,U_B)} m_i p_i \frac{|h_{S_0 i}|}{\sqrt{(\varepsilon + ||d_i||^{l_e})}} + n_i, \tag{2.2}$$

where, p_i and m_i are the transmit power coefficient and DL message for i_{th} user respectively. $n_i \sim \mathcal{CN}(0, \sigma_i^2)$ denotes AWGN at the i_{th} user with variance σ_i^2 and $P_{DL} = P_{S_0}(1 - \beta_e)$. The signal to interference plus noise ratio (SINR) at U_A and U_B for DL messages m_{U_A} and m_{U_B} respectively, is given by:

$$\gamma^{DL}_{U_A, m_{U_A}} = \frac{|h_{S_0 U_A}|^2 \rho_{U_A}}{(\varepsilon + ||d_{U_A}||^{l_e})}, \tag{2.3}$$

$$\gamma^{DL}_{U_B, m_{U_B}} = \frac{|h_{S_0 U_B}|^2 \rho_{U_B}}{\rho_{U_A}|h_{S_0, U_B}|^2 + (\varepsilon + ||d_{U_B}||^{l_e})}, \tag{2.4}$$

where $\rho_i = \dfrac{P_{DL} p_i^2}{\sigma_i^2}$ is the power to noise ratio at *i-th* user.

The power of the individual users for UL transmission is given by

$$P_i^T = \frac{\eta_{e,i}\zeta_{e,i} P_{S_0} |h_{S_0 i}|^2 \alpha_i}{(\varepsilon + ||d_i||^{l_e})(1 - \alpha_d)}, \tag{2.5}$$

Using the energy harvested from DL NOMA signal, the users transmit data to S_0 on the uplink. The user (U_A) with a higher channel gain, which is located closer to S_0, harvests more energy as compared to the user (U_B) with lower channel gain. Consequently, this difference in energy helps in making distinguishable transmissions to S_0 using UL NOMA. Since U_A transmits with more power, it does not interfere with U_B because of SIC [54] at S_0. Moreover, when U_A transmits with maximum harvested power, it significantly contributes to increasing throughput of the system. The combined UL NOMA signal received by S_0 is given as:

$$Y_{UL} \longrightarrow S_0 = \sum_{i\epsilon(U_A,U_B)} \frac{\sqrt{P_i^T} m_i' |h_{S_0 i}|}{\sqrt{(\varepsilon + ||d_i||^{l_e})}} + n_S, \tag{2.6}$$

where, m_i' is the UL message transmitted by *i-th* node and $n_S \sim \mathcal{CN}(0, \sigma_S^2)$ denotes AWGN at S_0 with variance σ_S^2. Using Eq. (2.5), the SINR of m'_{U_A} at S_0 is given by

$$\gamma^{UL}_{S_0, m'_{U_A}} = \frac{\varrho_{U_A}|h_{S_0 U_A}|^4}{\varrho_{U_B}|h_{S_0 U_B}|^4 + \sigma_S^2(1 - \alpha_d)}, \tag{2.7}$$

where, $\varrho_i = \eta_{e,i}\zeta_{e,i}\alpha_i P_{S_0}(\varepsilon + ||d_i||^{l_e})^{-2}$. After SIC of m'_{U_A}, S_0 will retrieve m'_{U_B} with

following SINR

$$\gamma^{UL}_{S_0,m'_{U_B}} = \frac{\varrho_{U_B}|h_{S_0U_B}|^4}{\sigma_S^2(1-\alpha_d)}. \tag{2.8}$$

2.3 Performance Analysis: Ergodic Rates

To evaluate the performance, here we investigate DL and UL ergodic rate of the system over independent Rayleigh fading channel. Ergodic rate is expressed on the basis of received SINR at *i-th* node during communication.

2.3.1 Downlink Ergodic Rate

The DL average ergodic rate of the model is written as

$$R^{DL} = \alpha_d \sum_{i\epsilon(U_A,U_B)} R_i^{DL}. \tag{2.9}$$

where R_i^{DL} represents the ergodic rate of DL message achieved by *i-th* node.

Proposition 1: The analytical expression of average rate R_{DL} achieved during DL phase is given by

$$R^{DL} = \frac{\alpha_d}{\ln 2}\Bigg(e^{\psi_{U_A}}E_i(\psi_{U_A}) + e^{\psi_{U_B}}E_i(\psi_{U_B}) - e^{\psi_{U_B,m_{U_A}}}E_i(\psi_{U_B,m_{U_A}})\Bigg). \tag{2.10}$$

where, $\psi_{U_A} = \rho_{U_A}^{-1}(\varepsilon + ||d_{U_A}||^{l_e})$, $\psi_{U_B} = \rho_{U_B}^{-1}(\varepsilon + ||d_{U_B}||^{l_e})p_{U_B}^2$ and $\psi_{U_B,m_{U_A}} = \rho_{U_A}^{-1}(\varepsilon + ||d_{U_B}||^{l_e})$.

Proof: In general, associated rate with symbol m_i is written as $R_i^{DL} = \log_2(1 + \gamma^{DL}_{U_i,m_i})$. $R_{U_A}^{DL}$ can be derived as

$$R_{U_A}^{DL} = \int_{\gamma_{U_A}^{DL}=0}^{\infty} \log_2(1+\gamma_{U_A}^{DL}) f_{\gamma^{DL}_{U_A,m_{U_A}}}(\gamma_{U_A}^{DL}) d\gamma_{U_A}^{DL}, \tag{2.11}$$

In Eq. (2.11) above, we can write $f_{\gamma^{DL}_{U_A,m_{U_A}}}(\gamma_{U_A}^{DL})$ as

$$f_{\gamma^{DL}_{U_A,m_{U_A}}}(\gamma_{U_A}^{DL}) = \frac{\partial}{\partial \gamma_{U_A}^{DL}}\Big(\Pr(\gamma^{DL}_{U_A,m_{U_A}} < \gamma_{U_A}^{DL})\Big), \tag{2.12}$$

Using Eq. (2.3) and after solving the differential equation $f_{\gamma^{DL}_{U_A,m_{U_A}}}(\gamma_{U_A}^{DL})$ can be written as

$$f_{\gamma^{DL}_{U_A,m_{U_A}}}(\gamma_{U_A}^{DL}) = \exp\left(-\frac{\gamma_{U_A}^{DL}(\varepsilon + d_{U_A}^{l_e})}{\rho_{U_A}}\right)\frac{(\varepsilon + ||d_{U_A}||^{l_e})}{\rho_{U_A}}, \tag{2.13}$$

By plugging the value of $f_{\gamma^{DL}_{U_A,m_{U_A}}}(\gamma^{DL}_{U_A})$ into Eq. (2.11) and applying [4.337.2, [61]], we can simplify $R^{DL}_{U_A}$ as

$$R^{DL}_{U_A} = \frac{1}{\ln 2} e^{\psi_{U_A}} E_i(\psi_{U_A}), \tag{2.14}$$

where, $E_i(x)$ is the exponential integral [8.2.11.1, [61]]. Since m_{U_B} is assigned higher power than m_{U_A} in combined NOMA signal, we can deduce $R^{DL}_{U_B}$ as

$$\begin{aligned} R^{DL}_{U_B} = &\int_{\gamma^{DL}_{U_B}=0}^{\infty} \log_2(1+\gamma^{DL}_{U_B}) f_{\gamma^{DL}_{U_B,m_{U_B}}}(\gamma^{DL}_{U_B}) d\gamma^{DL}_{U_B} - \\ &\int_{\gamma^{DL}_{U_A}=0}^{\infty} \log_2(1+\gamma^{DL}_{U_A}) f_{\gamma^{DL}_{U_B,m_{U_A}}}(\gamma^{DL}_{U_A}) d\gamma^{DL}_{U_A}, \end{aligned} \tag{2.15}$$

Following similar steps of $f_{\gamma^{DL}_{U_A,m_{U_A}}}(\gamma^{DL}_{U_A})$, we can write

$$R^{DL}_{U_B} = \frac{1}{\ln 2}\Big(e^{\psi_{U_B}} E_i(\psi_{U_B}) - e^{\psi_{U_B,m_{U_A}}} E_i(\psi_{U_B,m_{U_A}}) \Big), \tag{2.16}$$

By substituting the values of $R^{DL}_{U_A}$ and $R^{DL}_{U_B}$ in Eq. (2.9), we obtain Proposition 1.

2.3.2 Uplink Ergodic Rate

The UL average ergodic rate is written as

$$R^{UL} = (1-\alpha_d) \sum_{i\epsilon(U_A,U_B)} R^{UL}_i. \tag{2.17}$$

Proposition 2: The analytical expression of ergodic rate R_{UL} achieved during UL phase is given by

$$\begin{aligned} R_{UL} = \varkappa \Bigg(&\sum_{k=1}^{K} \Lambda_k \Big(\frac{\pi}{2} \sin(\Omega_k) - \sin(\Omega_k) Si(\Omega_k) - \cos(\Omega_k) \\ &Ci(\Omega_k) \Big) + \frac{\pi}{2} \sin(\Omega) - \sin(\Omega) Si(\Omega) - \cos(\Omega) Ci(\Omega) \Bigg). \end{aligned} \tag{2.18}$$

where, $\varkappa = \dfrac{2(1-\alpha_d)}{\ln 2}$, $\omega_K = \dfrac{\pi}{K}$, $\theta_k = \cos\Big(\dfrac{2k-1}{2K}\Big)\pi$, $\pi_k = \dfrac{\pi}{4}(\theta_k+1)$, $\Lambda_k = \omega_K \sqrt{1-\theta_k^2} e^{-tan(\pi_k)} sec^2(\pi_k)$, $\chi_1 = \dfrac{\varrho_{U_B}}{\varrho_{U_A}}$, $\chi_2 = \dfrac{\sigma_S^2(1-\alpha_d)}{\varrho_{U_A}}$, $\chi_3 = \dfrac{\sigma_S^2(1-\alpha_d)}{\varrho_B}$, $\lambda_k = \sqrt{tan^2(\pi_k) + \dfrac{\chi_2}{\chi_1}}$, $\Omega = \sqrt{\chi_3}$, $\Omega_k = \sqrt{\chi_1}\lambda_k$, $Si(.)$ is sine integral [8.230.1, [61]], $Ci(.)$ is cosine integral [8.230.2 , [61]] and K is cheybshev approximation parameter.

Proof: Like R_i^{DL}, $R_i^{UL} = \log_2(1+\gamma_{U_i,m_i'}^{UL})$. Starting with $R_{U_A}^{UL}$, we can write

$$R_{U_A}^{UL} = \int_{\gamma_{U_A}^{UL}=0}^{\infty} \log_2(1+\gamma_{U_A}^{UL}) f_{\gamma_{S_0,m_{U_A}'}^{UL}}(\gamma_{U_A}^{UL}) d\gamma_{U_A}^{UL}, \tag{2.19}$$

With the help of Eq. (2.7), we can write $f_{\gamma_{S_0,m_{U_A}'}^{UL}}(\gamma_{U_A}^{UL})$ as

$$f_{\gamma_{S_0,m_{U_A}'}^{UL}}(\gamma_{U_A}^{UL}) = \frac{\partial}{\partial \gamma_{U_A}^{UL}} \underbrace{\left[\Pr\left(\frac{\varrho_{U_A}|h_{S_0U_A}|^4}{\varrho_{U_B}|h_{S_0U_B}|^4 + \sigma_S^2(1-\alpha_d)} < \gamma_{U_A}^{UL} \right) \right]}_{\Xi}, \tag{2.20}$$

Based on Rayleigh fading, power of the channels ($|h_{S_0U_A}|^2$, $|h_{S_0U_B}|^2$) follows exponential distribution. Ξ can be simplified as

$$\Xi = 1 - \int_{b=0}^{\infty} \exp\Big(- \sqrt{b^2\chi_1\gamma_{U_A}^{UL} + \chi_2\gamma_{U_A}^{UL}} - b \Big) db \tag{2.21}$$

The integral in equation above cannot be solved with conventional integration techniques. After changing of variable and applying Gaussian cheybshev quadrature [61], we get

$$\Xi = 1 - \frac{\pi}{4} \sum_{k=1}^{K} \Lambda_k e^{-\sqrt{\chi_1\gamma_{U_A}^{UL}}\lambda_k}, \tag{2.22}$$

By plugging Ξ in Eq. (2.20) and solving differential equation we get $f_{\gamma_{S_0,m_{U_A}'}^{UL}}(\gamma_{U_A}^{UL})$ which is placed in Eq. (2.19) to get,

$$R_{U_A}^{UL} = \frac{\pi}{8\ln 2} \left(\sum_{k=1}^{K} \omega_K' \int_{\gamma_{U_A}^{UL}=0}^{\infty} \Lambda_k' e^{-\sqrt{\chi_1\gamma_{U_A}^{UL}}\lambda_k} \ln(1+\gamma_{U_A}^{UL}) d\gamma_{U_A}^{UL} \right), \tag{2.23}$$

where, $\Lambda_k' = \dfrac{\sqrt{\chi_1}\lambda_k\Lambda_k}{2\sqrt{\gamma_{U_A}^{UL}}}$, $\omega_K' = \omega_K\sqrt{1-\theta_k^2}$. In order to solve Eq. (2.23), we have applied Laplace transform of $\ln(1+\gamma^{2}{}_{U_A}^{UL})$ and integration by parts on above integral, and with the help of partial fraction decomposition, we can write $R_{U_A}^{UL}$ as

$$R_{U_A}^{UL} = \frac{2}{\ln 2} \sum_{k=1}^{K} \Lambda_k \Big(\frac{\pi}{2}\sin(\Omega_k) - \sin(\Omega_k) Si(\Omega_k) - \cos(\Omega_k) Ci(\Omega_k) \Big). \tag{2.24}$$

Moving to $R_{U_B}^{UL}$ in Eq. (2.17), we can write

$$R_{U_B}^{UL} = \int_{\gamma_{U_B}^{UL}=0}^{\infty} \log_2(1+\gamma_{U_B}^{UL}) f_{\gamma_{S_0,m_{U_B}'}^{UL}}(\gamma_{U_B}^{UL}) d\gamma_{U_B}^{UL}, \tag{2.25}$$

With the help of Eq. (2.8), we can write $f_{\gamma^{UL}_{S_0,m'_{U_B}}}(\gamma^{UL}_{U_B})$ as

$$f_{\gamma^{UL}_{S_0,m'_{U_B}}}(\gamma^{UL}_{U_B}) = \frac{\partial}{\partial \gamma^{UL}_{U_B}} \underbrace{\left[\Pr\left(\frac{\varrho_{U_B}|h_{S_0U_B}|^4}{\sigma_S^2(1-\alpha_d)} < \gamma^{UL}_{U_B} \right) \right]}_{\Xi_B}, \tag{2.26}$$

Since $|h_{S_0U_B}|^2$ follows exponential distribution, Ξ_B is simplified as $\Xi_B = 1 - \exp\big(-\sqrt{\chi_3 \gamma^{UL}_{U_B}}\big)$. We substitute Ξ_B in Eq. (2.26) and solve differential equation to get $f_{\gamma^{UL}_{S_0,m'_{U_B}}}(\gamma^{UL}_{U_B})$. After substituting it in (2.25) we write $R^{UL}_{U_B}$ as,

$$R^{UL}_{U_B} = \frac{1}{2\ln 2} \int_{\gamma^{UL}_{U_B}=0}^{\infty} \left(\sqrt{\frac{\chi_3}{\gamma^{UL}_{U_B}}} e^{-\sqrt{\gamma^{UL}_{U_B}\chi_3}} \right) \ln(1+\gamma^{UL}_{U_B}) d\gamma^{UL}_{U_B}, \tag{2.27}$$

Applying similar techniques as before, we simplify $R^{UL}_{U_B}$ as:

$$R^{UL}_{U_B} = \frac{2}{\ln 2}\left(\frac{\pi}{2}\sin(\Omega) - \sin(\Omega)Si(\Omega) - \cos(\Omega)Ci(\Omega)\right). \tag{2.28}$$

Substituting the values of $R^{UL}_{U_A}$ and $R^{UL}_{U_B}$ in Eq. (2.17) completes the proof of Proposition 2.

2.4 Observations

This section provides numerical results averaged over 10K simulation runs to evaluate the performance of proposed system model. The locations of users from S_0 are such that $||d_{U_A}||/||d_{U_B}|| = 0.5$. $\eta_{e,i} = 80\%$, $\zeta_{e,i} = 0.9$, $\varepsilon = 1$, l_e is 2 or 2.8, and approximation parameter K is 500. $p^2_{U_A} = 1/5$ and $p^2_{U_B} = 1 - p^2_{U_A}$. Fig. 2.2 plots R_{DL} and R_{UL} obtained from Eqs. (2.10) and (2.18) vs. signal to noise ratio (SNR), which are well matched with the simulation results. It follows that the proposed scheme performs well in less lossy environments. Fig. 2.3 evaluates the impact of β_e on the UL and DL ergodic rates of the system. It is clear from the figure that providing more power to energy harvesting circuitry improves UL data rate sharply in the high SNR region. Secondly, the variation in β_e results in an increase in UL data rate at the expense of the DL data rate. This can be useful in future low data rate applications, where users will be able to transmit high priority UL messages to the source even if the system needs to compromise on DL data rate. This means that an appropriate selection of β_e can adjust the data rate in DL and UL communication as per system requirements.

In Fig. 2.4, we illustrate the impact of β_e and α_d on UL data rate. With equal DL and UL transmission phases ($\alpha_d = 0.5$), if β_e increases from 50% to 60%, UL rate is improved, demonstrating the benefits of introducing SWIPT. However, when

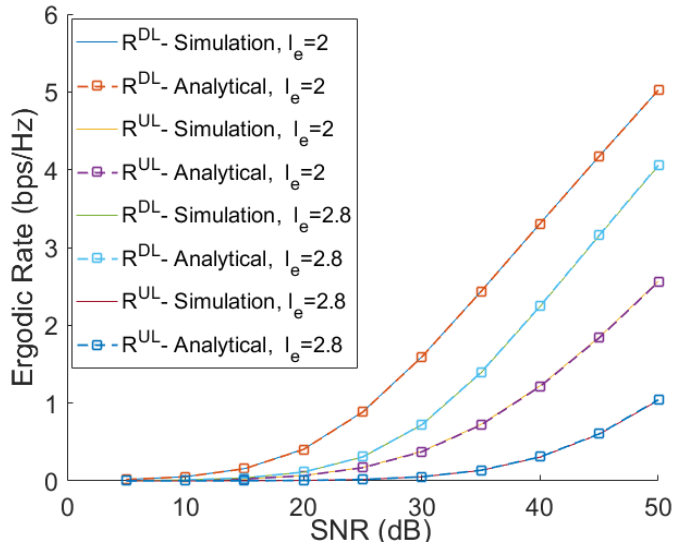

Figure 2.2: System Ergodic Rate vs SNR, $\beta_e = \alpha_d = 0.5$.

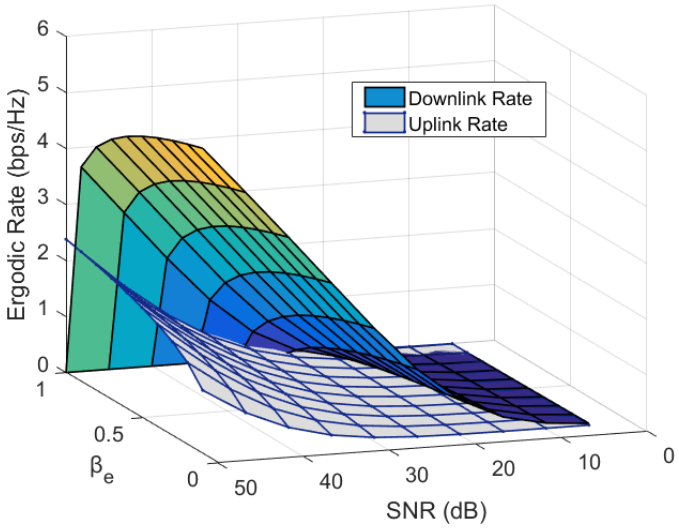

Figure 2.3: Downlink and Uplink Rate with variable β_e.

DL transmission phase is given more time ($\alpha_d > 0.5$) for harvesting more energy, UL data rate starts to fall. The reason of this decline is the reduction in UL transmission time. It follows that with a careful choice of β_e and α_d, wireless powered low data-rate uplink NOMA communication can be established successfully in SWIPT-aided wireless networks.

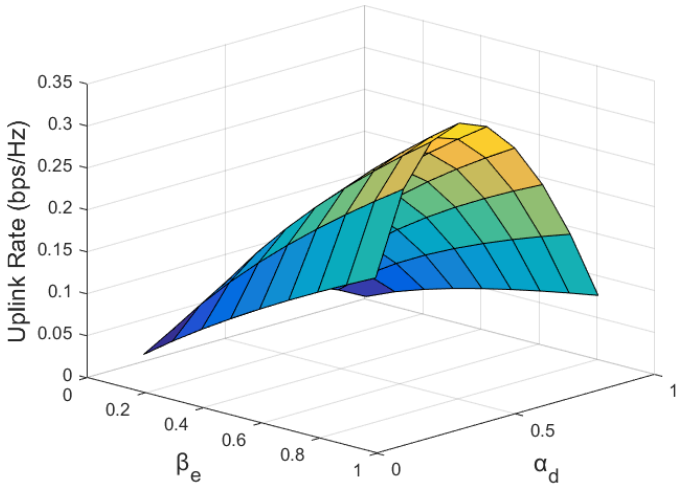

Figure 2.4: Uplink Rate with variable β_e and α_d, SNR= 30 dB.

2.5 Conclusion

This research work has used PS based SWIPT protocol to enable NOMA communication between a source and its nodes with energy harvesting. We have obtained closed-form expressions for DL and UL ergodic rates to demonstrate the performance of the proposed system. Our analytical and simulation results show that utilising larger portion of received DL power in energy harvesting results in improved UL rate of the NOMA users. Data rates in hybrid NOMA system also depend on how the transmission resources are split between UL and DL. A future research direction is to study the application of multi-antenna techniques with SWIPT in NOMA-based UL communication.

Appendices

A DRC 16 Form

DRC 16

MASSEY UNIVERSITY
GRADUATE RESEARCH SCHOOL

STATEMENT OF CONTRIBUTION
DOCTORATE WITH PUBLICATIONS/MANUSCRIPTS

We, the candidate and the candidate's Primary Supervisor, certify that all co-authors have consented to their work being included in the thesis and they have accepted the candidate's contribution as indicated below in the *Statement of Originality*.

Name of candidate:	Syeda Kanwal Zaidi
Name/title of Primary Supervisor:	Syed Faraz Hasan
Name of Research Output and full reference:	
S. K. Zaidi, S. F. Hasan, and X. Gui, "Evaluating the ergodic rate in SWIPT-aided hybrid NOMA", IEEE Communication Letters, vol. 22, no. 9, pp.870–1873, September 2018.	
In which Chapter is the Manuscript /Published work:	Chapter 2
Please indicate:	
• The percentage of the manuscript/Published Work that was contributed by the candidate:	90%
and	
• Describe the contribution that the candidate has made to the Manuscript/Published Work:	
The candidate has proposed the system model, conducted model simulations and mathematical analysis. Illustration and interpretation of the results has also been done by the candidate. Related manuscript has been written by the candidate majorly. The supervisors were throughout involved in the review of the work.	
For manuscripts intended for publication please indicate target journal:	
Candidate's Signature:	Syeda Kanwal Zaidi Digitally signed by Syeda Kanwal Zaidi Date: 2020.01.06 08:53:08 +13'00'
Date:	06/Jan/2020
Primary Supervisor's Signature:	Faraz Hasan Digitally signed by Faraz Hasan Date: 2020.01.06 10:48:11 +13'00'
Date:	6 Jan 2020

(This form should appear at the end of each thesis chapter/section/appendix submitted as a manuscript/ publication or collected as an appendix at the end of the thesis)

GRS Version 4– January 2019

Figure A.1: DRC 16 -Chapter 2.

Chapter 3

Two-Way SWIPT-Aided Hybrid NOMA Relaying for Out-of-Coverage Devices

Authors : Syeda Kanwal Zaidi, Syed Faraz Hasan, and Xiang Gui

Abstract

Relaying is a tool to solve basic problem of poor coverage and low capacity at the cell border due to low signal to interference and noise ratio (SINR). In this paper, we propose a novel non-orthogonal multiple access (NOMA) based relaying mechanism to extend the coverage of a source for bi-directional communication with some users in an out-of-coverage area by exploiting two users from a NOMA pair to act as relays for remote devices. A combination of multiple access schemes is used, source-relay communication is established with NOMA while relay-device communication is orthogonal multiple access (OMA) based. To avoid battery consumption of the relay nodes, power-switching based simultaneous wireless information and power transfer (SWIPT) protocol is used for relaying uplink and downlink data between source and the users. Potentially, the scheme provides parallel coverage to multiple disconnected users with the help of wireless-powered NOMA relays (WPNRs). To characterise the performance gains of proposed system, two important metrics outage probability and ergodic rate are discussed. Specifically, analytical expressions for outage probabilities and delay-limited throughput in downlink (DL) and uplink (UL) communications are derived, which are also verified with simulations. Additionally, we also obtain closed-form expressions for the DL and UL asymptotic ergodic rates. Our results demonstrate that: 1) WPNRs establish bi-directional communication link between the source and remotely located users solely on the basis of scavenged energy; 2) WPNR based relaying network is superior in performance than OMA based relaying network in high SNR region; 3) Orientation of WPNRs contributes in improved system throughput.

3.1 Introduction

Spectral efficiency, energy efficiency, low latency processing, and wider connectivity are the key performance pillars of fifth-generation (5G) wide spreading wireless networks' deployment and implementation [62]. 5G not only aims to take forward some prior technologies like relaying, small-cells, heterogeneous networks, massive antenna systems [63] etc. but also welcomes cutting-edge techniques like multi-user multiple-in-multiple-out (MIMO), device-to-device communication [64, 65], energy harvesting and non-orthogonal multiple access (NOMA) to foster the aim of future wireless communication [12, 66]. The apparent aim of relaying is to offload traffic of the base station (BS) with the help of intermediate nodes so that communication is realised between remotely located devices and BS or between two devices. Relaying plays a vital role in ever growing dense networks to serve cell-edge users for improved throughput and better quality of service (QoS). For prolonged communication, the relays can be powered with radio frequency energy harvesting (RFEH) refraining them to utilize their own energy for relaying purposes. RFEH is on boom these days as it exploits available radio signals to recharge devices enabling simultaneous wireless information and power transfer (SWIPT) so that the devices self sustain without counting on any extra energy sources within the network [67].

3.1.1 Related Works and Motivation

With expected sharp rise in future wireless network devices, cell phones, sensors etc., NOMA has gained substantial attention to improve spectral efficiency and reduce latency [68]. In general NOMA is classified into two brackets, power-domain NOMA and code-domain NOMA [12]. Specifically, power-domain NOMA, recently proposed to 3GPP LTE [69] multiplexes users on account of power i.e., the information of two users, hereafter referred as NOMA pair, is clubbed in a single frequency/time block with varying power levels. A comprehensive study on NOMA for 5G is presented in [69] with insights on real world deployment. So far, NOMA has been examined in uplink (UL) and downlink (DL) communication from various points of views in [9, 58]. In recent research works, concept of cooperative NOMA (CNOMA) is proposed in which one of the user in NOMA pair serves as a relay to forward the information to other user [13]. In a conventional CNOMA scheme, only one user from the NOMA pair contributes as a relay to increase signal diversity, improve reception reliability and extend coverage of the network [13]. In DL communication, a coordinated two-point system based on superposition coding (SC) was investigated in [70] exploiting the use of NOMA in cooperative communications. The authors in [11] used decode-and-forward (DF) relaying while the authors in [14] applied amplify and forward (AF) relaying with NOMA

over different fading channels and analysed outage probability and sum rates of the system. Lately, two cooperative user relaying scenarios with near user in half duplex (HD) or full duplex (FD) mode are studied in [71] to compare the performance gain of HD or FD relaying in CNOMA. It is important to realise that both of the NOMA users can also act as relays to forward the information to some devices which are not in the proper coverage range of the source. Such situations can occur practically in internet of things (IoT) or machine-to-machine (M2M) communications. For example, in smart automotive networks, two cars moving away from the source towards a low connectivity area may require some assistance or emergency signals from the source. Therefore, it is possible to exploit two users in a NOMA pair to act as relays and assist two or more out-of-coverage devices. Albeit the use of relay nodes helps to improve coverage, reception reliability and QoS of a network, but at the cost of relay's own energy, hence the need of sufficient energy supply to relay information cannot be ignored. It has been recognised already that SWIPT allows relays to scavenge from the wireless signals carrying information [72,73] with the help of two key relaying protocols: i) time switching (TS) and ii) power splitting (PS) [19]. SWIPT has been adopted in HD as well as FD relaying schemes [74, 75]. A research work in [59] used PS relaying scheme to harvest energy at near user in CNOMA for improved DL communication of far user. Most recently, a user selection scheme with the use of TS and PS relaying protocol is proposed for CNOMA netwoks using SWIPT in DL transmission only [76]. While aforementioned research works have already used CNOMA in DL relaying with or without SWIPT for enhanced signal diversity, the use of NOMA based relaying for extension of coverage in two-way communication is in infancy. A novel work to foster this concept is introduced in [77] where, the authors utilized NOMA pair as relays with TS protocol to serve two disconnected users simultaneously for DL communication. However, only outage performance of end users in DL communication was analysed. To the best of our knowledge, the use of NOMA pair based relaying in both DL and UL communication considering energy incentive for relaying information has not been investigated yet. Not quite the same as past works, we aim to derive relaying benefits from a NOMA pair with SWIPT for extending coverage of a network in DL and UL transmissions. More specifically, we explore the potential capacity of NOMA pair in user relaying in a NOMA-OMA based network with identifying the following key impact factors.

- Will two users in a NOMA pair be able to act as relays for remote users for two-way communication solely on the basis of harvested energy? If yes, then what would be the impact on the signal outages and what would be the systems performance in delay-limited and delay tolerant modes in terms of throughput?
- Will NOMA based relaying contributes towards improved system throughput

than conventional OMA based network along with the use of SWIPT?
- What are the significant factors that may impact the system performance in this hybrid NOMA-OMA network?

3.1.2 Contributions

We propose a concept of intermediate wireless powered NOMA relays (WPNR) in a NOMA based network where a source utilizes both users in a NOMA pair to act as relays for remotely located cell-edge users. Based on the proposed system, the main contributions of this paper are summarised as follows:

- We investigate two-way hybrid WPNR based communication scheme for UL and DL transmission enabling the source to establish bi-directional communication with users which may not be accessed via single relay.
- To highlight the behaviour of proposed system, we derive analytical expressions for the outage probabilities of UL and DL information symbols and system throughput in delay-limited transmission mode based on these outages. Furthermore we obtain closed form expressions for ergodic sum rate to extract key insights on the performance.
- Our findings reveal that compared to the conventional OMA based network with SWIPT, the proposed system provides improved performance in terms of overall system throughput.
- We further investigate the impact of some key factors for e.g, relay's distance, power splitting factor and orientation of relay on the system throughput and symbol outage. The results reflect the fact that WPNR based relaying is beneficial in providing energy incentive to intermediate relays and in terms of spectral efficiency.

In the end, we also verified our analytical model with the help of numerical simulations to validate the mathematical derivations of outage probabilities and ergodic sum rates of the proposed system. The approach followed in this paper provides following benefits: 1) the use of SWIPT in a NOMA pair eliminates doubly near-far effect [78], 2) two disconnected users which are far from each other are simultaneously served by the source in UL and DL communication, 3) relays do not need to utilize their own energy in transferring the information to the end users.

3.1.3 Organisation and Notations

The rest of the chapter is organised as follows: In section 3.2, system model and important notations are outlined. The detailed explanation of operation modes is in section 3.3. In section 3.4, performance analysis is reported with remarks on important

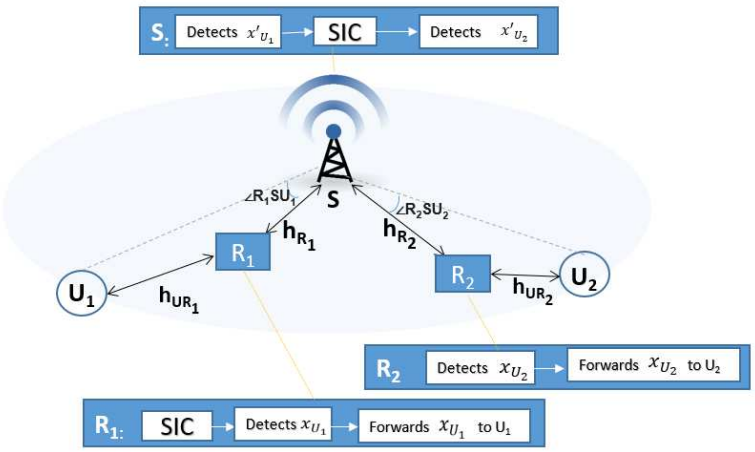

Figure 3.1: Proposed System Model for Hybrid NOMA with SWIPT.

results. Numerical explanation and verification of analytical results is done in section 3.5, while the conclusion is given in section 3.6 with future research directions.

The notations used in the paper are as follows: $\mathbb{E}[.]$ represents expectation operator and $\Pr(.)$ shows the probability of an event; $f_X(x)$ and $F_X(x)$ denote the probability density function (PDF) and the cumulative density function (CDF) of a random variable (RV) X respectively; $\mathcal{CN}(\mu, \sigma^2)$ denotes a circularly symmetric complex Gaussian RV with mean μ and variance σ^2.

3.2 The System Model

3.2.1 Wireless Powered NOMA Relays (WPNR)

We assume a scenario as illustrated in Fig.1, where a source S communicates with two users U_1 and U_2 that are far from each other and are located in a poorly covered area. As in [77], there is no direct link between each of these users and the source due to heavy shadowing. Since these users lie far part from each other, one common relay is not able to establish individual communication links between the users and source at the same time. Hence, source exploits two relays R_1 and R_2 in the form of a NOMA pair to establish simultaneous communication paths to the users. The users in NOMA pair, referred as WPNR, employ PS based SWIPT protocol and scavenge energy from the received wireless signals for relaying information. The following transmission protocol and channel model further explain the proposed system in detail.

Table 3.1: Communication Slots

Time Slot	**Link**	**Access Mode**
t_1	$S \rightarrow R_j$	NOMA
t_2	$R_j \rightarrow U_i$	OMA
t_3	$U_i \rightarrow R_j$	OMA
t_4	$R_j \rightarrow S$	NOMA

3.2.2 Channel Model Description

A dual-hop wireless network with a source S, user U_i and WPNR R_j is assumed, where $i = j\epsilon\{1, 2\}, \forall i = j$, shown in Fig. 3.1 . All nodes are assumed to be single antenna nodes [18] and relays employ DF protocol. Euclidean distance between users and relays is denoted by $d_{U_iR_i}$ while d_{U_i}, d_{R_j} represents distance between S and users, and S and relays respectively, where $d_{R_1} < d_{R_2}$. Assuming that S is located at the center of the cell, $\angle U_iSR_j$ represents the angle U_i, S and R_j thus $d_{U_iR_j} = \sqrt{d_{U_i}^2 + d_{R_j}^2 - 2d_{U_i}d_{R_j}\cos(\angle U_iSR_j)}$, where $-\pi \leq \angle U_iSR_j \leq +\pi$. For a realistic communication model, we assume that the communication links exhibit large-scale path loss effects and experience small scale fading. Under the premise of perfect channel state information (CSI) at all nodes [79], all channels are quasi-static Rayleigh fading channels which means that each element of the channel coefficients is circularly symmetric complex Gaussian variable and channel power gains are exponentially distributed. The complex channel coefficients for the links $S \longleftrightarrow R_j$, $S \longleftrightarrow U_i$, $U_i \longleftrightarrow R_j$ are denoted as $h_{R_j} \sim \mathcal{CN}(0, 1)$, $h_{U_i} \sim \mathcal{CN}(0, 1)$ and $h_{U_iR_j} \sim \mathcal{CN}(0, 1)$ respectively.

3.3 Operation Modes

Table 3.1 shows that the UL and DL communication between S and the two users U_i via relays R_j respectively happens in four time slots due to HD constraint. During $t_{1,3}$, the received power by R_j is split by a power-splitting factor called ρ based on PS architecture for decoding information and the remaining power is utilized in harvesting energy [19]. Energy harvested in these time slots is utilized by R_j for relaying DL/UL data between S and U_i. Table 3.2 lists the important notations used hereafter in this paper.

3.3.1 Downlink Transmission

During t_1, S transmits DL NOMA message $\sum_{i=j=1}^{2} x_{U_i}\sqrt{p_{R_j}}$ to relay R_j with fixed power allocation coefficient p_{R_j} for message x_{U_i}, where x_{U_i} is normalised unit power signal with $\mathbb{E}\{|x_{U_i}|^2\}$=1. To state fairness among relays $p_{R_1} < p_{R_1}$ and $\sum_{j=1}^{2} p_{R_j} = 1$

Table 3.2: Important Symbols

Symbol	Meaning
x_{U_i}	DL message for U_i from S
x'_{U_i}	UL message for S from U_i
$\mathcal{P}_S$	Transmit power of S
p_{R_j}	Power allocation coefficient for R_j
$\mathcal{P}_U$	Transmit power of U_i
α	Path loss exponent for a channel
η_{e,R_j}	Energy conversion efficiency[1] of R_j
ζ_{e,R_j}	Circuit efficiency of R_j
$\sigma^2_{U_i/R_j/S}$	Noise power at U_i, R_j or S
$\gamma^o_{x_{U_i}}$	Threshold SINR for message x_{U_i}
$\gamma^o_{x'_{U_i}}$	Threshold SINR for message x'_{U_i}

[9]. Power corresponding to harvested energy by R_j is expressed as

$$P^H_{R_j,t_1} = \frac{\mathcal{P}_S(1-\rho)\eta_{e,R_j}\zeta_{e,R_j}|h_{R_j}|^2}{(\varepsilon + d^\alpha_{R_j})}, \tag{3.3.1}$$

where, ε is the reference parameter for bounded path-loss model to ensure finite path loss and finite harvested energy [77]. With $p_{R_2} > p_{R_1}$, R_1 invokes successive interference cancellation (SIC) of x_{U_2} i.e. it subtracts x_{U_2} from the received signal first and then decodes x_{U_1} [9]. Therefore, received signal to interference and noise ratio (SINR) of x_{U_2} and x_{U_1} at R_1 is given by

$$\gamma^{R_1}_{x_{U_2}} = \frac{\Omega_{R_2}|h_{R_1}|^2}{\Omega_{R_1}|h_{R_1}|^2 + \sigma^2_{R_1}(\varepsilon + d^\alpha_{R_1})}, \tag{3.3.2}$$

$$\gamma^{R_1}_{x_{U_1}} = \frac{\Omega_{R_1}|h_{R_1}|^2}{\sigma^2_{R_1}(\varepsilon + d^\alpha_{R_1})}, \tag{3.3.3}$$

where $\Omega_{R_j} = \mathcal{P}_S p_{R_j}\rho$. On the other hand, R_2 is not required to perform SIC because of lower transmit power allocation to x_{U_1}. Therefore received SINR of x_{U_2} at R_2 is given by

$$\gamma^{R_2}_{x_{U_2}} = \frac{\Omega_{R_2}|h_{R_2}|^2}{\Omega_{R_1}|h_{R_2}|^2 + \sigma^2_{R_2}(\varepsilon + d^\alpha_{R_2})}, \tag{3.3.4}$$

After decoding the messages, R_1 and R_2 transmit x_{U_1} and x_{U_2} to U_1 and U_2 respectively using the energy harvested in t_1. Received SINR of x_{U_1} at U_1 is expressed as

$$\gamma^{U_1}_{x_{U_1}} = \frac{P^H_{R_1,t_1}|h_{U_1R_1}|^2}{\sigma^2_{U_1}(\varepsilon + d^\alpha_{U_1R_1})}, \tag{3.3.5}$$

and SINR of x_{U_2} at U_2 is written as

$$\gamma_{x_{U_2}}^{U_2} = \frac{P_{R_2,t_1}^H |h_{U_2R_2}|^2}{\sigma_{U_2}^2(\varepsilon + d_{U_2R_2}^{\alpha})}, \tag{3.3.6}$$

3.3.2 Uplink Transmission

During t_3, U_i transmits x'_{U_i} to R_j with transmit power $\mathcal{P}_U$, where x'_{U_i} is normalised unit power signal with $\mathbb{E}\{|x'_{U_i}|^2\}$=1. Similar to DL approach, a portion ρ of the received power is consumed in decoding information while remaining is utilized in harvesting energy. Power corresponding to harvested energy by each relay in this time slot is expressed as

$$P_{R_j,t_3}^H = \frac{\mathcal{P}_U(1-\rho)\eta_{e,R_j}\zeta_{e,R_j}|h_{U_iR_j}|^2}{(\varepsilon + d_{U_iR_j}^{\alpha})}, \tag{3.3.7}$$

As stated in Table 1, this transmission is OMA based hence the relays do not need to perform SIC. Thus, SINR at R_1 to decode x'_{U_1} is given by

$$\gamma_{x'_{U_1}}^{R_1} = \frac{\mathcal{P}_U\rho|h_{U_1R_1}|^2}{\sigma_{U_1}^2(\varepsilon + d_{U_1R_1}^{\alpha})}, \tag{3.3.8}$$

and SINR of x'_{U_2} at R_2 is written as

$$\gamma_{x'_{U_2}}^{R_2} = \frac{\mathcal{P}_U\rho|h_{U_2R_2}|^2}{\sigma_{U_2}^2(\varepsilon + d_{U_2R_2}^{\alpha})}, \tag{3.3.9}$$

After decoding UL messages, R_1 and R_2 send UL NOMA signal to S, which ranks relays based on their channel conditions. The geographical separation of these relays from their end users is the basis of difference in their harvested energy which in turn leads to different transmit powers in UL NOMA signal. At this moment, it can be observed that our proposed system coherently eliminates doubly-near far problem and power allocation issue in UL NOMA communication. In order to detect individual user's message, SIC is carried out at S and messages (x'_{U_1} and x'_{U_2}) are decoded one by one, starting with the message received with higher power first. Received SINR at S for x'_{U_1} is given by

$$\gamma_{x'_{U_1}}^{S} = \frac{|h_{R_1}|^2 P_{R_1,t_3}^H}{(\varepsilon + d_{R_1}^{\alpha})(|h_{R_2}|^2 P_{R_2,t_3}^H(\varepsilon + d_{R_2}^{\alpha})^{-1} + \sigma_S^2)}, \tag{3.3.10}$$

Since R_1 is closer to S as compared to R_2, S subtracts higher power symbol x'_{U_1} from the received UL signal and continues to decode x'_{U_2}, hence the SINR at S to decode

x'_{U_2} is given as:

$$\gamma^S_{x'_{U_2}} = \frac{|h_{R_2}|^2 P^H_{R_2,t_3}}{\sigma^2_S(\varepsilon + d^\alpha_{R_2})}, \tag{3.3.11}$$

This completes one transmission cycle and the UL and DL information is relayed by WPNRs between S and the serviced users.

3.4 Performance Analysis of the system

The performance of our proposed model is characterised by evaluating two important metrics: outage probability and ergodic rate.

3.4.1 Outage Analysis

Outage probability is defined as the probability of effective end-to-end SINR at receiver node (γ_R) falls below a certain threshold (γ^o), due to channel fading or interferences, and is denoted by P^{out} below. Mathematically, we can write

$$P^{out} = \Pr(\gamma_R < \gamma^o). \tag{3.4.1}$$

Outage in Downlink Transmission

The outage in downlink transmission of x_{U_i} occurs if it is not decoded by U_i or by its WPNR R_j.

$$P^{out}_{x_{U_i}}(R_{x_{U_i}}) = \mathbb{E}\Big[\Pr\big(\log_2(1+\gamma^{U_i/R_j}_{x_{U_i}}) < R^o_{x_{U_i}}\big)\Big] = \mathbb{E}\Big[\Pr\big(\gamma^{U_i/R_j}_{x_{U_i}} < \gamma^o_{x_{U_i}}\big)\Big]. \tag{3.4.2}$$

where, $R^o_{x_{U_i}}$ is the target rate to detect x_{U_i}, and

$$\gamma^o_{x_{U_i}} = 2^{R^o_{x_{U_i}}} - 1. \tag{3.4.3}$$

Proposition 1: *The analytical expression of outage probability at U_1 for x_{U_1} is expressed as:*

$$P^{out}_{x_{U_1}} = 1 - (\breve{\varrho}_{x_{U_1}} \times \varrho_{x_{U_1}}), \tag{3.4.4}$$

where, $\gamma^o_{x_{U_1}}$ is defined in (3.4.3), $\gamma^o_{x_{U_2}} < \frac{p_{R_2}}{p_{R_1}}$, $\breve{\mathcal{A}}_{U_1} = \max(\breve{a}_1, \breve{a}_2)$, $\breve{a}_1 = \frac{\gamma^o_{x_{U_1}}}{\Omega_{R_1}}$, $\breve{a}_2 = \frac{\gamma^o_{x_{U_2}}}{\Omega_{R_2} - \gamma^o_{x_{U_2}}\Omega_{R_1}}$, $\Psi_{x_{U_1}} = \frac{\sigma^2_{U_1}(\varepsilon + d^\alpha_{U_1R_1})(\varepsilon + d^\alpha_{R_1})}{\mathcal{P}_S(1-\rho)\eta_{e,R_1}\zeta_{e,R_1}}$, $\breve{\varrho}_{x_{U_1}} = \exp\big(-\breve{\mathcal{A}}_{U_1}\sigma^2_{R_1}(\varepsilon + d^\alpha_{R_1})\big)$, $\varrho_{x_{U_1}} = 1 - 2\sqrt{\Psi_{x_{U_1}}\gamma^o_{x_{U_1}}}K_v\big(\sqrt{4\Psi_{x_{U_1}}\gamma^o_{x_{U_1}}}\big)$, $K_v(.)$ represents the modified Bessel function of second kind with *v-th* order [8.432.6, [61]]. If in above proposition, $\gamma^o_{x_{U_2}} \geq \frac{p_{R_2}}{p_{R_1}}$ then

$P^{out}_{x_{U_1}}$=1.

Proof: see Appendix A.

Remark 1: *R_1 needs to decode both of the messages for successful relaying. However the successful decoding at user's end is also dependent on the received power at R_1 which in turn relies on its channel condition with S.*

Proposition 2: *The analytical expression of outage probability at U_2 for x_{U_2} is given by*

$$P^{out}_{x_{U_2}} = 1 - \varrho_{x_{U_2}} \times \breve{\varrho}_{x_{U_2}}, \tag{3.4.5}$$

where, $\gamma^o_{x_{U_2}}$ is defined in (3.4.3), $\Psi_{x_{U_2}} = \dfrac{\sigma^2_{U_2}(\varepsilon + d^{\alpha}_{U_2R_2})(\varepsilon + d^{\alpha}_{R_2})}{\mathcal{P}_S(1-\rho)\eta_{e,R_2}\zeta_{e,R_2}}$, $\breve{\varrho}_{x_{U_2}} = \exp\big(-\breve{a}_2\sigma^2_{R_2}(\varepsilon + d^{\alpha}_{R_2})\big)$, $\varrho_{x_{U_2}} = 2\sqrt{\Psi_{x_{U_2}}\gamma^o_{x_{U_2}}}K_v\big(\sqrt{4\Psi_{x_{U_2}}\gamma^o_{x_{U_2}}}\big)$.

Proof: With the help of (3.3.4) and (3.3.6), we obtain Proposition 2 following same steps as of Proposition 1. The details are omitted here for the sake of brevity.

Remark 2: *As can be observed that the outage in DL transmission is dependent on the power allocation factors of WPNR and on the joint channel distribution between source with WPNRs, and between WPNRs and the users.*

Outage in Uplink Transmission

The outage in uplink transmission of x'_{U_i} occurs if the message sent by U_i is either not decoded by its WPNR R_j or by S.

$$P^{out}_{x'_{U_i}}(R_{x'_{U_i}}) = \mathbb{E}\Big[\Pr\big(\log_2(1+\gamma^{R_j/S}_{x'_{U_i}}) < R^o_{x'_{U_i}}\big)\Big] = \mathbb{E}\Big[\Pr\big(\gamma^{R_j/S}_{x'_{U_i}} < \gamma^o_{x'_{U_i}}\big)\Big]. \tag{3.4.6}$$

where, $R^o_{x'_{U_i}}$ is the threshold rate to detect x'_{U_i} and is expressed as

$$\gamma^o_{x'_{U_i}} = 2^{R^o_{x'_{U_i}}} - 1. \tag{3.4.7}$$

Proposition 3: *The outage at S for x'_{U_1} is derived as*

$$P^{out}_{x'_{U_1}} \approxeq 1 - \varrho_{x'_{U_1}} \times \tilde{\varrho}_{x'_{U_1}} \tag{3.4.8}$$

where, $\varrho_{x'_{U_1}} = \exp\Big(-\dfrac{\tilde{\mathcal{A}}_S(\varepsilon + d^{\alpha}_{U_1R_1})}{\mathcal{P}_U}\Big)$, $\tilde{\mathcal{A}}_S = \dfrac{\gamma^o_{x'_{U_1}}\sigma^2_{U_1}}{\rho}$, $\delta_n = \cos\Big(\dfrac{2n-1}{2\mathcal{N}}\pi\Big)$, $\tilde{\varrho}_{x'_{U_1}} \approx \sum_{n=1}^{\mathcal{N}}\sum_{m=1}^{\mathcal{M}} \chi_n\chi_m\sqrt{\gamma^o_{x'_{U_1}}\tilde{\chi_{mn}}}K_v\Big(2\sqrt{\gamma^o_{x'_{U_1}}\tilde{\chi_{mn}}}\Big)$, $\omega_n = \tan\Big(\dfrac{\pi}{4}(\delta_n+1)\Big)$, $\tilde{\delta_n} = \dfrac{\pi^2}{2\mathcal{N}}\sqrt{1-\delta_n^2}\sec^2(\arctan\omega_n)$, $\xi_1 = \dfrac{(\varepsilon + d^{\alpha}_{R_1})(\varepsilon + d^{\alpha}_{U_1R_1})}{(\varepsilon + d^{\alpha}_{R_2})(\varepsilon + d^{\alpha}_{U_2R_2})}$, $\tilde{\chi_{mn}} = \xi_1\omega_n\omega_m + \xi_2$, $\xi_2 = \dfrac{\sigma^2_S(\varepsilon + d^{\alpha}_{R_1})(\varepsilon + d^{\alpha}_{U_1R_1})}{\mathcal{P}_U\eta_{e,R_1}\zeta_{e,R_1}(1-\rho)}$, $\delta_m =$

$\cos\left(\frac{2m-1}{2\mathcal{M}}\pi\right)$, $\omega_m = \tan\left(\frac{\pi}{4}(\delta_m{+}1)\right)$, $\chi_n = \tilde{\delta_n} e^{-(\omega_n+\omega_m)}$, $\chi_m = \frac{\pi^2}{4\mathcal{M}}\sqrt{1-\delta_m^2}\sec^2(\arctan\omega_m)$, and $\mathcal{N}$ and $\mathcal{M}$ are the Gauss-Cheybshev approximation parameters.

Proof: Appendix B.

Remark 3: *Outage of UL transmission is computationally complex because of the fact that transmitted power of WPNR is dependent on the harvested energy from received power sent by the user and WPNR uses NOMA in relaying UL message as compared to conventional OMA in relaying DL message.*

Proposition 4: The outage at S for x'_{U_2} is expressed

$$P^{out}_{x'_{U_2}} \approx 1 - \varrho_{x'_{U_2}} \times \tilde{\varrho}_{x'_{U_2}} \times \tilde{\varrho}_{x'_{U_1}}, \tag{3.4.9}$$

where, $\varrho_{x'_{U_2}} = \exp\left(-\frac{\tilde{\mathcal{B}}_S(\varepsilon + d^{\alpha}_{U_2R_2})}{\mathcal{P}_U}\right)$, $\tilde{\varrho}_{x'_{U_2}} = 1 - 2\sqrt{\varpi\gamma^o_{x'_{U_2}}}K_v(\sqrt{4\varpi\gamma^o_{x'_{U_2}}})$, $\tilde{\mathcal{B}}_S = \frac{\gamma^o_{x'_{U_2}}\sigma^2_{U_2}}{\rho}$, $\varpi = \frac{\sigma^2_S(\varepsilon + d^{\alpha}_{R_2})(\varepsilon + d^{\alpha}_{U_2R_2})}{\eta_{e,R_2}\zeta_{e,R_2}\mathcal{P}_U(1-\rho)}$, and $\tilde{\varrho}_{x'_{U_1}}$ is defined in Proposition 1.

Proof: Steps follows Appendix B and are omitted here to avoid longevity.

Remark 5: *The analytical form of the outage probability of x'_{U_2} has extra product term which corresponds to the successful decoding of x'_{U_1} at S. One can observe that the decoding of x'_{U_2} by S is dependent on the joint channel distribution of R_2 and U_2 and on the successful decoding of x'_{U_2} at R_2.*

Remark 6: *The results in Proposition 1 to 4 are consistent with the intuition that by employing WPNR in a wireless system, S can establish successful communication link with the two remote service deprived users.*

3.4.2 System Throughput

System throughput in delay-limited transmission mode [19] is dependant on the outages of the symbols x_{U_i} and x'_{U_i}.

Downlink system throughput

In this case, S transmits x_{U_i} at a constant rate of $R^o_{x_{U_i}}$ in a wireless fading channel, which is under the effect of outage probability. The system throughput in downlink communication is written as

$$R^{dlim}_{DL} = (1 - P^{out}_{x_{U_1}})R^o_{x_{U_1}} + (1 - P^{out}_{x_{U_2}})R^o_{x_{U_2}}, \tag{3.4.10}$$

where, $P^{out}_{x_{U_1}}$ and $P^{out}_{x_{U_2}}$ are given in (3.4.4) and (3.4.5) respectively.

Uplink system throughput

For uplink communication, U_i transmits x'_{U_i} at a threshold rate of $R^o_{x'_{U_i}}$ which is also subject to outage. We obtain uplink system throughput on the basis of outage probabilities as below

$$R^{dlim}_{UL} = (1 - P^{out}_{x'_{U_1}})R^o_{x'_{U_1}} + (1 - P^{out}_{x'_{U_2}})R^o_{x'_{U_2}}, \tag{3.4.11}$$

where, $P^{out}_{x'_{U_1}}$ and $P^{out}_{x'_{U_2}}$ are expressed in (3.4.6) and (3.4.7) respectively.

3.4.3 Rate Analysis

Here we analyse ergodic rate of the proposed system which is also an important performance metric if system is working under delay tolerant transmission mode [19]. Ergodic rate is the data rate achieved by a communication link averaged over all the fading states of wireless channel and is expressed with the help of effective SINR as:

$$R^{erg} = \int_0^\infty B \log_2(1 + \gamma_R) f_{\gamma_R}(\gamma) d\gamma_R, \tag{3.4.12}$$

where, B is the received signal bandwidth.

Downlink Ergodic Rate

$R^{erg}_{x_{U_i}}$ represents the ergodic rate achieved for x_{U_i} over the communication link $S \to R_j \to U_i$.

Proposition 5: *The closed-form expression for downlink ergodic rate is expressed as follows*

$$R^{erg}_{DL} = \frac{1}{\ln 2} \sum_{l=0}^{k} \sum_{q=0}^{l} \Bigg(\sum_{g=0}^{\mathcal{G}} \lambda_{\mathcal{G}} \sqrt{1 - \Theta_g^2} \Upsilon_g \Phi_g e^{-\tau_{1_g}} \Big(e^{-\beta \Upsilon_g} \Lambda(v, l, q) \cdot (\beta \Upsilon_g)^{q-v} + \mathcal{T}_\epsilon \Big) + \sum_{f=0}^{\mathcal{F}} \psi_{\mathcal{F}} \sqrt{1 - \mu_f^2} \mathcal{W}_f \Big(e^{-\beta \varsigma_f} \Lambda(v, l, q) \cdot (\beta \varsigma_f)^{q-v} + \mathcal{T}_\epsilon \Big) \Bigg) \tag{3.4.13}$$

where, $\lambda_{\mathcal{G}} = \frac{\pi^2}{4\mathcal{G}}, \Theta = \cos\left(\frac{2g-1}{2\mathcal{G}}\pi\right), \Upsilon_g = \sqrt{4\Psi_{x_{U_1}} \tan \mathcal{X}_g}, \Phi_g = \frac{\sec^2 \mathcal{X}_g}{1 + \tan \mathcal{X}_g}, \tau_{1_g} = (-\frac{\tan \mathcal{X}_g (\varepsilon + d^\alpha_{R_1}) \sigma^2_{R_1}}{\Omega_{R_1}})$, $\mathcal{X}_g = \frac{\pi}{4}(\Theta_g + 1)$, $\psi_{\mathcal{F}} = \frac{\pi p_{R_2}}{2\mathcal{F} p_{R_1}}$, $\mu_f = \cos\left(\frac{2f-1}{2\mathcal{F}}\pi\right)$, $\beta = 1$, $\mathcal{W}_f = \frac{\sqrt{4\Psi_{x_{U_2}} \mathcal{Y}_f}}{1 + \mathcal{Y}_f}$, $\mathcal{Y}_f = \frac{p_{R_2}}{2p_{R_1}}(\mu_f + 1)$, $\varsigma_f = \sqrt{4\Psi_{x_{U_2}} \mathcal{Y}_f}$, q, l, and k are accuracy parameters, and $\mathcal{G}$ and $\mathcal{F}$ are Gaussian-Cheybshev approximation parameters.

Proof: See Appendix C.

Uplink Ergodic Rate

$R^{erg}_{x'_{U_i}}$ represents the ergodic rate achieved for x'_{U_i} over the communication link $U_i \rightarrow R_j \rightarrow S$.

Proposition 6: *The closed-form expression for uplink ergodic rate of x'_{U_2} is expressed as follows*

$$\begin{aligned} R^{erg}_{UL} = \frac{1}{\ln 2}\Bigg[\sum_{l'=1}^{\mathcal{L}'} \sum_{m=1}^{\mathcal{M}} \sum_{n=1}^{\mathcal{N}} \frac{\pi \beth_{l'} \chi_n \chi_m}{\mathcal{L}'} \sqrt{\frac{1+\wp_{l'}}{1-\wp_{l'}}} \exp\left(\frac{\wp_{l'}+1}{\wp_{l'}-1}\nu\right) \\ \left(e^{-\beta 2\beth_{l'}} \sum_{n=0}^{k}\sum_{q=0}^{l} \Lambda(v,l,q)\cdot(\beta 2\beth_{l'})^{q-v} + \mathcal{T}_\epsilon\right) + \\ \sum_{z=1}^{\mathcal{Z}} \frac{\pi^2\sqrt{(1-\varphi_z^2)(\varpi\tan\mathcal{V}_z)}}{2\mathcal{Z}(1+\tan\mathcal{V}_z)} \exp(-\digamma\tan\mathcal{V}_z)\sec^2\mathcal{V}_z \\ \left(e^{-2\beta\sqrt{\varpi\tan\mathcal{V}_z}} \sum_{n=0}^{k}\sum_{q=0}^{l} \Lambda(v,l,q)\cdot(2\beta\sqrt{\varpi\tan\mathcal{V}_z})^{q-v} + \mathcal{T}_\epsilon\right)\Bigg], \end{aligned} \tag{3.4.14}$$

where, $\beth_{l'} = \dfrac{1+\wp_{l'}}{1-\wp_{l'}}(\chi_1\omega_m\omega_n + \chi_2)$, $\wp_{l'} = \cos\left(\dfrac{2l'-1}{2\mathcal{L}'}\pi\right)$, $\varphi_z = \cos\left(\dfrac{2z-1}{2\mathcal{Z}}\pi\right)$, $\nu = \dfrac{\sigma^2_{U_1}(\varepsilon + d^{\alpha}_{U_1R_1})}{\rho\mathcal{P}_U}$, $\digamma = \dfrac{\sigma^2_{U_2}(\varepsilon + d^{\alpha}_{U_2R_2})}{\rho\mathcal{P}_U}$ $\mathcal{V}_z = \dfrac{\pi}{4}(\varphi_z+1)$, and $\mathcal{L}'$ and $\mathcal{Z}$ are Gaussian Cheybshev approximation parameters.

3.5 Numerical Results and Discussion

This section presents the numerical results of our proposed system along with corroboration of analytical results obtained in section 3.4. We verify our analytical results with numerical simulations as follows. We simulate a source S at the centre of a cell with users U_1 and U_2 located 10m away from S. $\angle R_jSU_i$ is kept variable and is mentioned in the corresponding figures. We model the channel fading gain between S and users, and WPNR and its respective user with exponential random variable. We execute 10K channel realisations, and for each realisation in the downlink and uplink transmission, outage is evaluated. Outage occurs if the signal to noise ratio at each node in every realisation is less than the threshold signal to noise ratio. Table 3.3 shows the simulation parameters. The antenna and receiver conversion noise variances at all nodes are unit normalised for generality but can be altered to evaluate performance.

3.5.1 Effect of Transmit Power

We evaluate the impact of the transmit power of source and users on the outages of downlink and uplink messages. $P^{out}_{x_{U_1}}$ and $P^{out}_{x_{U_2}}$ from (3.4.4) and (3.4.5) respectively is

Table 3.3: Simulation Parameters

Parameters	**Settings**
η_{e,R_j}	90% [77]
ζ_{e,R_j}	100%
p_{R_1}, p_{R_2}	0.3, 0.7
α	2 (free space), 3 (shadowed-urban area)
Cheybshev Approximation Parameters	500

first verified via Monte Carlo simulations and the results are shown in Fig. 3.2a for different value of $R^o_{x_{U_i}}$ and $\rho = 0.5$. The precise agreement between simulated and analytical results verify our derivation of outage. The figure clearly shows that outage of x_{U_i} is inversely proportional to the SNR. And also, when the requirement of DL data rate for U_1 is increased, signals reception is decreased leading to more outage at U_1. The deterioration of the received signals is because of the presence of second user's symbol at relay node which is decoded a prior by R_1. Fig. 3.2b shows a plot of the outages of x_{U_1} and x_{U_2} vs. SNR for a varying value of ρ. It is obvious from the results that an increasing the value of ρ increases the outage of the downlink symbols which is consistent with the system description mentioned in section 3.2. For instance, $\rho = 0.8$ results in more outage than the outage achieved with $\rho = 0.4$. This demonstrates that providing less energy to energy harvesting circuitry will increase the outage in relaying link, resulting in increased outage at user's end.

It is to be noted that the outage at U_2 is similar to outage at U_1 despite the fact that the distance between R_1 and U_1 is more, and that between R_2 and U_2 is less. The main reason behind this is that the relay located near S harvests more energy and transmits with higher power as the intended user is far. However, R_2 harvests less energy because it requires less power to transmit to a closer user. This indicates the fairness for the serviced users in our proposed scheme and it also shows that the proposed model ignores doubly-near-far problem [13]. The expressions in (3.4.8) and (3.4.9) are also verified with simulations and the results are depicted in Fig. 3.3a where dashed/dotted lines represent analytical results while solid lines are used to show Monte Carlo simulations. Outage of x'_{U_i} symbol has an inverse relationship with transmit SNR which is consistent with the downlink transmission results. It is to be noted that the outage probability reveals an error floor in high SNR region which increases with the increase in uplink transmission rate. This is because of the interference caused by one user towards other user's message in a single frequency/time domain which is an inherent property of uplink NOMA transmissions [80]. To verify the effect of power split ratio ρ on uplink transmissions, Fig. 3.3b illustrates impact of varying value of ρ on uplink outage. By comparing it with Fig. 3.2b, it can be demonstrated that the effect of ρ is same as explained earlier in this section for downlink transmission

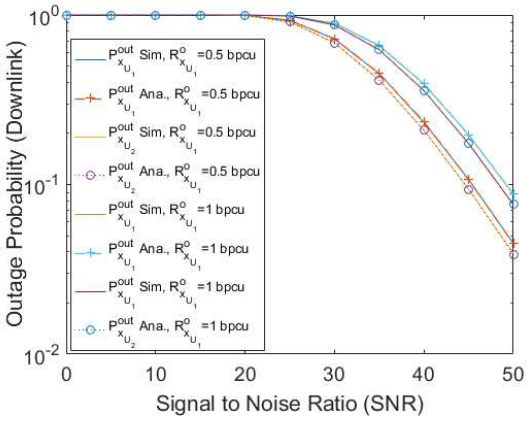

(a) Outage Probability of x_{U_1} and x_{U_2} with varying DL data rate.

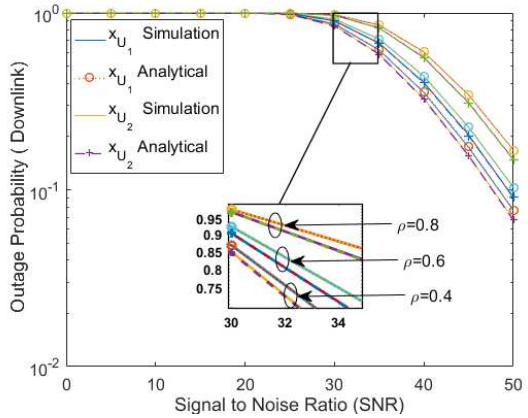

(b) Outage Probability of x_{U_1} and x_{U_2} with varying value of ρ.

Figure 3.2: Downlink Outage Probability

Fig. 3.2 and Fig. 3.3 illustrate that with the help of the WPNR pair, two remote users can be serviced adequately with nearly equal probabilities of reception at both ends. This scheme is highly useful in time-critical situations as well. For example, if an emergency signal needs to be transmitted to remote devices and a single relay is unable to communicate to both of them, then the use of a WPNR pair can serve the purpose effectively.

The results of Fig. 3.4a and 3.4b depict the delay-limited system throughput which is plotted with the help of expressions of the outage probabilities of the users. It is interesting to see that proposed relaying with NOMA offers superior uplink and downlink throughput as compared to OMA[1] based transmission. At $\mathcal{P}_S$=40 dB and $\mathcal{P}_U$=30 dB with a target threshold of unit bps, there's a 40% percentage gain achieved

[1]OMA uses more resource blocks (time/frequency) as compared to NOMA

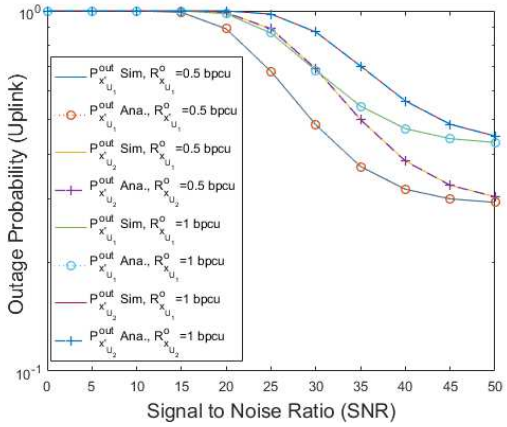

(a) Outage Probability of x'_{U_1} and x'_{U_2} with varying UL data rate.

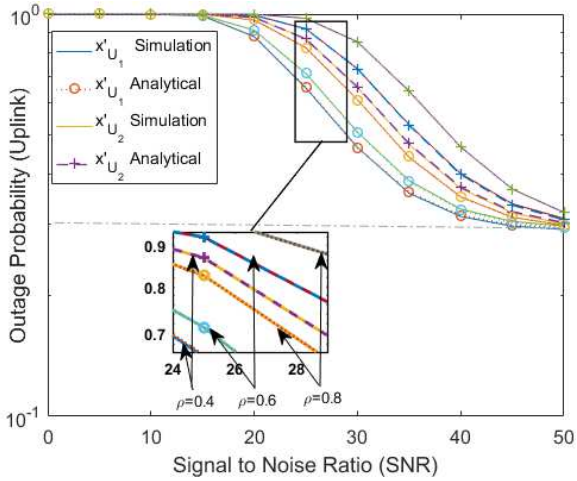

(b) Outage Probability of x'_{U_1} and x'_{U_2} with varying value of ρ.

Figure 3.3: Uplink Outage Probability

with WPNRs than OMA based relaying in UL and DL transmission. Fig. 3.5a and 3.5b plot the ergodic rate of the proposed system which corresponds to system throughput in delay tolerant transmission mode. The dashed curves are obtained from (3.4.13) and (3.4.14) which are well matched with the solid lines representing Monte Carlo simulations. This verifies the closed form expressions of R_{DL}^{erg} and R_{UL}^{erg} derived in Proposition 5 and 6. It can be seen that ergodic rate of downlink transmission is fairly equal to ergodic rate achieved in uplink transmission, because of the fact that in uplink transmission user to relay transmission is OMA based where the relays harvest energy more as compared to downlink transmission where individual relay receives a portion of the transmit power because of NOMA.

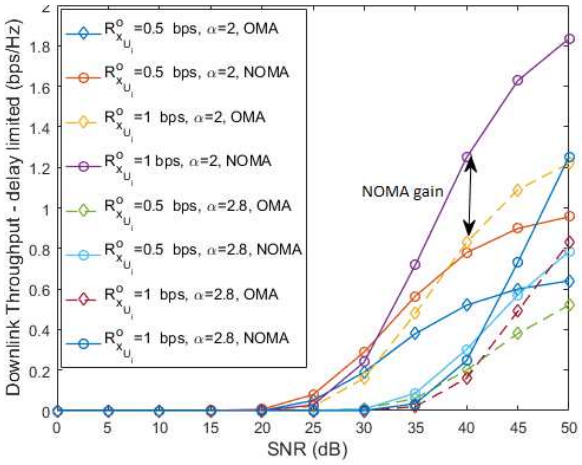

(a) Downlink throughput in delay-limited transmission mode vs. SNR

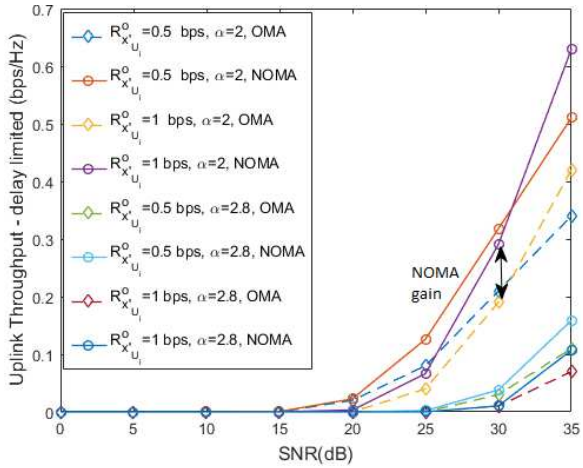

(b) Uplink throughput in delay-limited transmission mode vs. SNR

Figure 3.4: System Throughput-delay-limited transmission mode.

3.5.2 Effect of distance and transmission angle

The graph in Fig. 3.6a illustrates the impact of geographical orientation of relays with respect to users and source. It is to be noted that average uplink and downlink rate of a NOMA pair degrades as the angular distance between users and relays increases. One important observation which this figure reflects is, if two relays are present at the similar distance then it is important for BS to consider the relay which lies in the line of sight of BS and relays. Another important insight is that, equal transmission rates can be achieved in the proposed model, when downlink transmit power is more than uplink transmit power. The reason behind this is the partial allocation of power to different NOMA users in downlink which leads to less harvested energy and reduced transmission rate. However, uplink NOMA assigns equal transmit power to both of the

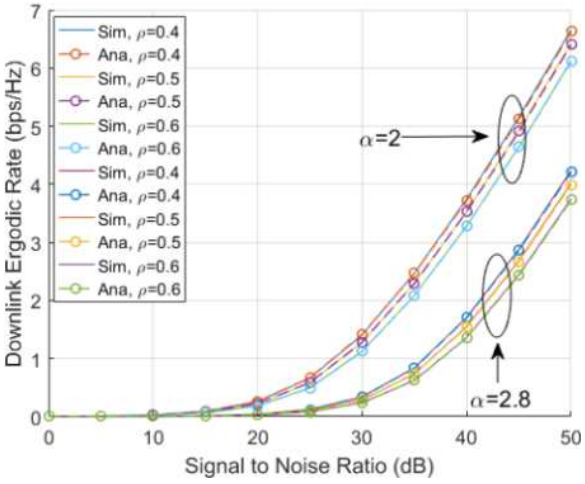

(a) Downlink Ergodic Rate vs. SNR.

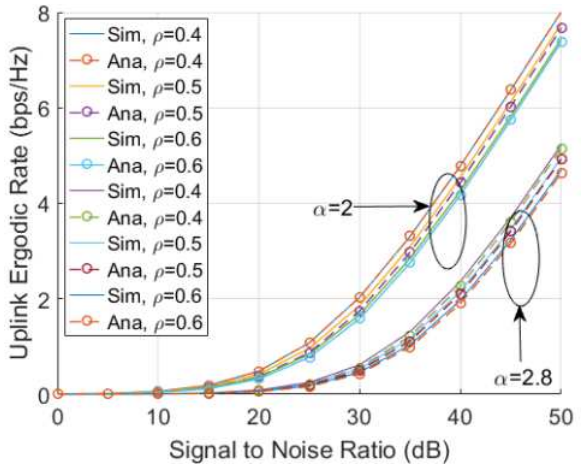

(b) Uplink Ergodic Rate vs. SNR.

Figure 3.5: Ergodic Rate- Delay-tolerant transmission mode

users while each user experience additional interference caused by other user's message in the same assigned resource. To further elaborate systems performance, we plotted ergodic rate with respect to the ratio of relays' distance from source in Fig 3.6b. It is witnessed that when $d_{R_2} \gg d_{R_1}$, ergodic rate in DL and UL transmission is high and for instance, it decrease by 28% and 40% respectively when the distance between the relays is kept equal with $\mathcal{P}_S = 40$ dB and $\mathcal{P}_U = 30$ dB. The explanatory reason is due to the basic concept of NOMA transmission [9]. When the two NOMA users are significantly a part, it becomes easier for the receiver to extract both messages successfully due to a difference of channel conditions.

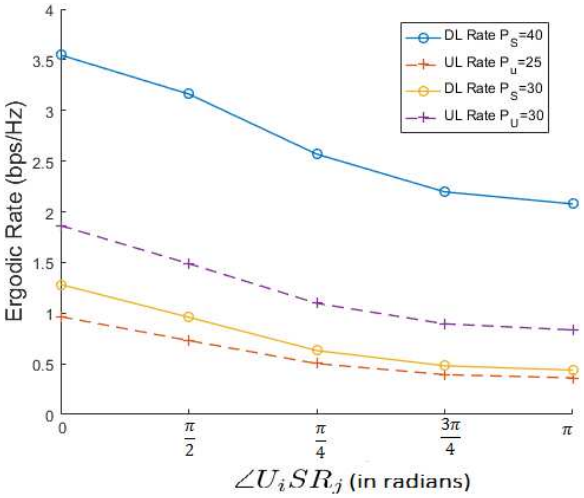

(a) Ergodic Rate versus $\angle U_i SR_j$ with varying $\mathcal{P}_S$ and $\mathcal{P}_U$.

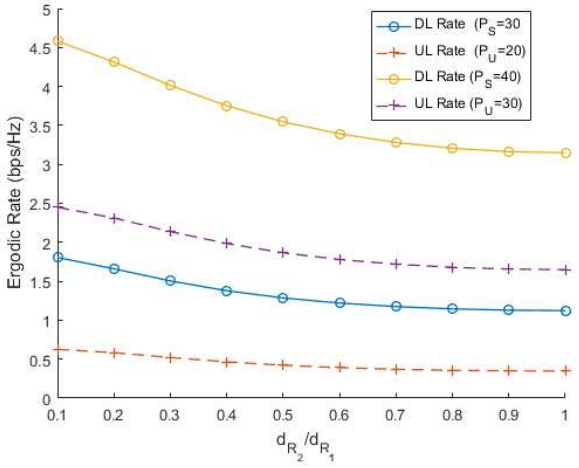

(b) Ergodic Rate versus distance of relays.

Figure 3.6: Effect of distance and transmission angle on rate

3.5.3 Uplink and Downlink Transmission

Fig. 3.7a plots the downlink throughput achieved by the system vs. the data rate of both users in downlink transmission. One can observe that the system throughput is increased more when the data rate of R_2 is increased as compared to the situation when data rate of R_1 is increased owing to the fact that R_1 decodes message of R_2 first and then decodes the message intended for U_1. If the data rate of R_1 is increased, it leads to outage of x_{U_1} which in turn reduces the system throughput. However, for the higher data rate of R_2, system throughput shows a bit sharp rise because only one message is decoded at R_2's end. To clearly demonstrate the impact of user data rates on uplink transmission, Fig. 3.7b illustrates the uplink throughput versus the uplink data rate required for x'_{U_1} and x'_{U_2}. Comparing Fig. 3.7a and Fig. 3.7b, it is apparent that the

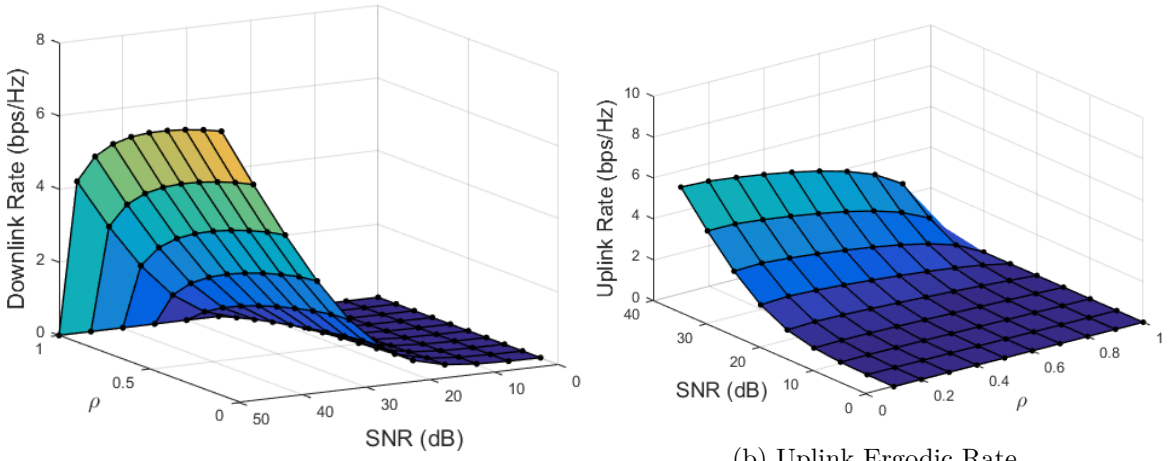

(a) Downlink Ergodic Rate.

(b) Uplink Ergodic Rate.

Figure 3.7: Ergodic Rate with varying SNR and ρ.

surface plot of downlink throughput has different slope than the uplink throughput. On the uplink, throughput increases sharply with increased data rate of R_1 which is closer to the source. When the NOMA uplink message is sent by WPNRs, the message sent by R_1 is decoded first hence its data rate contributes more towards the increased throughput. However, when data rate of R_2 is increased, the outage at source increases which leads to reduction in the achieved throughput. Hence, it is important to choose the data rates appropriately to achieve the desired performance.

3.6 Conclusion

In this chapter, the concept of WPNR is applied on hybrid NOMA system to sustain communication with remotely located devices. A novel idea of using SWIPT in NOMA-based HD[2] relays is proposed which extends the coverage of the source for the isolated users. Specifically, we derived outage probabilities of the downlink and uplink transmission between the source and the remote devices. For our proposed scheme, Monte Carlo runs validated by the analytical model are executed. The system offers acceptable extension for the out-of-coverage devices with the aid of NOMA relays powered by the signals received from the source and the users. It can be concluded that with appropriate choice of uplink and downlink data rates along with careful consideration of WPNRs geographical location, this system model is adequate and satisfactory. A future extension of this study is to deploy WPNRs on a larger scale network with optimised system throughput via adequate relay selection method for multiple users. Another aspect is to employ FD WPNR to reduce the extra time slots used in this

[2]An extension of this scheme with Time Division Duplex (TDD) full-duplex relays is our future work, which will reduce the overhead of additional time slots of this scheme.

system for information transfer which in turn may improve the system throughput at the cost of extra complexity.

Appendices

A Proof of Proposition 1

Proof. The outage of x_{U_1} at U_1 is dependant on the successful decoding of x_{U_1} at R_1 and U_1. We can write outage of x_{U_1} at $U_1(P^{out}_{x_{U_1}})$ as

$$P^{out}_{x_{U_1}} = 1 - \Big(\underbrace{\Pr(\gamma^{R_1}_{x_{U_2}} > \gamma^{o}_{x_{U_2}}, \gamma^{R_1}_{x_{U_1}} > \gamma^{o}_{x_{U_1}})}_{E^{R_1}_{x_{U_1}}} \cap \underbrace{\Pr(\gamma^{U_1}_{x_{U_1}} > \gamma^{o}_{x_{U_1}})}_{E^{U_1}_{x_{U_1}}} \Big), \tag{A.1}$$

Based on the condition, $p_{R_1}\gamma^{o}_{x_{U_2}} < p_{R_2}$, and with the help of (3.3.2) and (3.3.3), we can express $E^{R_1}_{x_{U_1}}$ as

$$E^{R_1}_{x_{U_1}} = \Pr\left(|h_{R_1}|^2 > \breve{\mathcal{A}}_{U_1}\sigma^2_{R_1}(\varepsilon + d^{\alpha}_{R_1})\right) = \exp\left(-\breve{\mathcal{A}}_{U_1}\sigma^2_{R_1}(\varepsilon + d^{\alpha}_{R_1})\right) \tag{A.2}$$

With the help of (3.3.5), $E^{U_1}_{x_{U_1}}$ is expressed as

$$E^{U_1}_{x_{U_1}} = 1 - \Pr\left(|h_{U_1}|^2|h_{R_1}|^2 < \frac{\gamma^{o}_{x_{U_1}}\sigma^2_{U_1}(\varepsilon + d^{\alpha}_{U_1R_1})(\varepsilon + d^{\alpha}_{R_1})}{\mathcal{P}_S(1-\rho)p^2_{R_1}\eta_{e,R_1}\zeta_{e,R_1}}\right), \tag{A.3}$$

Considering exponential distribution for power of channel gains, we compute (A.3) as

$$E^{U_1}_{x_{U_1}} = 1 - \int_0^{\infty} \Big(e^{-t} - \exp\big(\frac{\gamma^{o}_{x_{U_1}}\Psi_{x_{U_1}}}{t} - t\big)\Big)dt \overset{(a)}{=} 1 - 2\sqrt{\Psi_{x_{U_1}}\gamma^{o}_{x_{U_1}}}K_v\big(\sqrt{4\Psi_{x_{U_1}}\gamma^{o}_{x_{U_1}}}\big). \tag{A.4}$$

where, (a) is obtained with the help of (3.324, [61]). Substituting (A.2 and (A.4) into (A.1), we obtain $P^{out}_{x_{U_1}}$ as expressed in Proposition 1 and this completes the proof. ■

B Proof of Proposition 3

Proof. The outage probability of x'_{U_1} at S can be expressed as

$$P^{out}_{x'_{U_1}} = 1 - \underbrace{\Big(\Pr(\gamma^{R_1}_{x'_{U_1}} > \gamma^{o}_{x'_{U_1}})\Big)}_{E^{R_1}_{x'_{U_1}}} \cap \underbrace{\Big(1 - \Pr(\gamma^{S}_{x'_{U_1}} < \gamma^{o}_{x'_{U_1}})\Big)}_{E^{S}_{x'_{U_1}}}, \tag{B.1}$$

With the help of (3.3.8), $E^{R_1}_{x'_{U_1}}$ is written as

$$E^{R_1}_{x'_{U_1}} = \Pr\Big(|h_{U_1R_1}|^2 > \frac{\tilde{\mathcal{A}}_S(\varepsilon + d^{\alpha}_{U_1R_1})}{\mathcal{P}_U}\Big) \overset{(a)}{=} \exp\Big(-\frac{\tilde{\mathcal{A}}_S(\varepsilon + d^{\alpha}_{U_1R_1})}{\mathcal{P}_U}\Big), \tag{B.2}$$

(a) follows that $|h_{U_1}|^2$ is exponentially distributed. Using (3.3.10), we can write $E^S_{x'_{U_1}}$ as:

$$E^S_{x'_{U_1}} = 1 - \Pr\Big(|h_{R_1}|^2 < \frac{\gamma^o_{x'_{U_1}}(\varepsilon + d^{\alpha}_{R_1})(|h_{R_2}|^2 P^H_{R_2,t_3}(\varepsilon + d^{\alpha}_{R_2})^{-1} + \sigma^2_S)}{P^H_{R_1,t_3}}\Big), \tag{B.3}$$

Substituting the value of $P^H_{R_i,t_3}$ from (3.3.7) and after some algebraic manipulations, we write

$$E^S_{x'_{U_1}} = 1 - \Pr\left(|h_{U_1R_1}|^2|h_{R_1}|^2 < (\xi_1|h_{U_2R_2}|^2|h_{R_2}|^2 + \xi_2)\gamma^o_{x'_{U_1}}\right), \tag{B.4}$$

Furthermore, we simplify (B.4) as

$$E^S_{x'_{U_1}} = 1 - \int_0^{\infty}\int_0^{\infty}\int_0^{\infty} 1 - \exp\left(-\frac{(\xi_1 vw + \xi_2)\gamma^o_{x'_{U_1}}}{u} - u\right) f_{|h_{U_2R_2}|^2}(v) f_{|h_{R_2}|^2}(w) du dv dw, \tag{B.5}$$

With the help of [3.324, [61]] and some algebraic simplification, we write

$$E^S_{x'_{U_1}} = \int_0^{\infty}\int_0^{\pi/2} \underbrace{2\sqrt{(w\xi_1 \tan\theta + \xi_2)\gamma^o_{x'_{U_1}} \sec^4\theta} \times K_v\left(\sqrt{4(w\xi_1 \tan\theta + \xi_2)\gamma^o_{x'_{U_1}}}\right) e^{-\tan\theta} d\theta}_{\Delta_v} \Delta_w, \tag{B.6}$$

Note that trigonometric substitution has also been used in (B.6), where $\Delta_w = f_{|h_{R_2}|^2}(w)dw$ According to the features of Eq. above, conventional integration techniques may not be applied, so we use Gauss-Cheybshev quadrature [81] to simplify Δ_v as

$$\Delta_v \approxeq \hat{\delta_n} \sum_{n=1}^{\mathcal{N}} \sqrt{\gamma^o_{x'_{U_1}}(\xi_1\omega_n w + \xi_2)} \times K_v\left(2\sqrt{\gamma^o_{x'_{U_1}}(\xi_1\omega_n w + \xi_2)}\right) \times \exp(-\omega_n), \tag{B.7}$$

Substituting the value of Δ_v in (B.6), following equation is obtained

$$E^S_{x'_{U_1}} \approxeq \sum_{n=1}^{\mathcal{N}} \hat{\delta_n} \int_0^{\infty} \sqrt{\gamma^o_{x'_{U_1}}(\xi_1\omega_n w + \xi_2)} \times K_v\left(2\sqrt{\gamma^o_{x'_{U_1}}(\xi_1\omega_n w + \xi_2)}\right) \times \exp(-\omega_n - w) dw, \tag{B.8}$$

It is difficult to solve the complex integral in (B.8) so we replace integration variable with trigonometric substitution and again apply Gauss-Cheybshev Quadrature [81] to simplify $E^S_{x'_{U_1}}$ as below

$$E^S_{x'_{U_1}} \approxeq \sum_{n=1}^{\mathcal{N}} \sum_{m=1}^{\mathcal{M}} \chi_n \chi_m \sqrt{\gamma^o_{x'_{U_1}} \tilde{\chi_{mn}}} K_v\left(2\sqrt{\gamma^o_{x'_{U_1}} \tilde{\chi_{mn}}}\right), \tag{B.9}$$

Finally, substituting the value of $E^{R_1}_{x'_{U_1}}$ from (B.3) and $E^{S}_{x'_{U_1}}$ from (B.9) in (B.1), the proof of Proposition 3 is complete. ■

C Proof of Proposition 5

Proof. The achievable capacity of x_{U_1} is written as

$$R^{erg}_{x_{U_1}} = \mathbb{E}\Big[\log_2(1+\min(\gamma^{R_1}_{x_{U_1}}, \gamma^{U_1}_{x_{U_1}})\Big], \tag{C.1}$$

Let $\tilde{\mathcal{A}} \triangleq \gamma^{R_1}_{x_{U_1}}$ and $\tilde{\mathcal{B}} \triangleq \gamma^{U_1}_{x_{U_1}}$, then the CDF of $\tilde{\mathcal{A}}$ and $\tilde{\mathcal{B}}$ is expressed as

$$F_{\tilde{\mathcal{A}}}(\tilde{a}) = 1 - \exp\Big(-\frac{\tilde{a}(\varepsilon + d^{\alpha}_{R_1})\sigma^2_{R_1}}{\Omega_{R_1}}\Big), \tag{C.2}$$

$$F_{\tilde{\mathcal{B}}}(\tilde{b}) = 1 - 2\sqrt{\Psi_{x_{U_1}}\tilde{b}}K_v\Big(\sqrt{4\Psi_{x_{U_1}}\tilde{b}}\Big), \tag{C.3}$$

Let $\tilde{\mathcal{C}} = \min(\tilde{\mathcal{A}}, \tilde{\mathcal{B}})$, and by using CDF of minimum of two exponential variables, we express

$$F_{\tilde{\mathcal{C}}}(\tilde{c}) = 1 - \Big(\exp\big(-\frac{\tilde{c}(\varepsilon + d^{\alpha}_{R_1})\sigma^2_{R_1}}{\Omega_{R_1}}\big) \times \sqrt{4\Psi_{x_{U_1}}\tilde{c}}K_v(\sqrt{4\Psi_{x_{U_1}}\tilde{c}})\Big), \tag{C.4}$$

As, $R^{erg}_{x_{U_1}} = \int_0^{\infty} \log_2(1+\tilde{c}) f_{\tilde{\mathcal{C}}}(\tilde{c}) d\tilde{c} = \frac{1}{\ln 2}\int_0^{\infty} \frac{1 - F_{\tilde{\mathcal{C}}}(\tilde{c})}{1+\tilde{c}} d\tilde{c}$. Thus, we express $R^{erg}_{x_{U_1}}$ as

$$R^{erg}_{x_{U_1}} = \frac{1}{\ln 2}\int_0^{\infty}\Big(\frac{1}{1+\tilde{c}}\sqrt{4\Psi_{x_{U_1}}\tilde{c}}\exp\big(-\frac{\tilde{c}(\varepsilon + d^{\alpha}_{R_1})\sigma^2_{R_1}}{\Omega_{R_1}}\big)K_v(\sqrt{4\Psi_{x_{U_1}}\tilde{c}})\Big)d\tilde{c}, \tag{C.5}$$

For different communication scenarios when ρ is variable and $\alpha > 0$, the integral above becomes challenging to solve. In this case, we find approximation using Gauss-Cheybshev quadrature [81] as

$$R^{erg}_{x_{U_1}} \approx \frac{\lambda_{\mathcal{G}}}{\ln 2}\sum_{g=0}^{\mathcal{G}} \sqrt{1-\Theta^2_g}\Upsilon_g \Phi_g e^{-\tau_{1_g}} K_v(\beta\Upsilon_g), \tag{C.6}$$

In (C.6), $K_v(x)$ is a modified Bessel function of the second kind and *v-th* order, with *v>0* and it can be represented by the infinite series [82] as

$$K_v(\beta x) = e^{-\beta x}\sum_{l=0}^{k}\sum_{q=0}^{l}\Lambda(v,l,q)\cdot(\beta x)^{q-v} + \mathcal{T}_{\epsilon}, \tag{C.7}$$

where truncation error $\mathcal{T}_\epsilon$ is given in [82] with coefficient as

$$\Lambda(v,l,q)=\frac{(-1)^q\sqrt{\pi}\Gamma(2\nu)\Gamma(\frac{1}{2}+l-\nu)L(l,q)}{2^{\nu-q}\Gamma((\frac{1}{2}-v)\Gamma(\frac{1}{2}+l+\nu)l!}, \tag{C.8}$$

involving Gamma function ($\Gamma(.)$) and Lah numbers (for e.g. [83])

$$L(l,q)=\binom{l-1}{q-1}\frac{l!}{q!}\quad \text{for } l,q>0, \tag{C.9}$$

and the conventions $L(0,0)$=1; $L(n,0)$=0 and $L(l,1)=l!$ for $l>0$. Substituting equivalent of $K_v(\beta x)$ from (C.7) into (C.6), we obtain

$$R^{erg}_{x_{U_1}}\approx\frac{\lambda_{\mathcal{G}}}{\ln 2}\sum_{l=0}^{k}\sum_{q=0}^{l}\sum_{g=0}^{\mathcal{G}}\sqrt{1-\Theta_g^2}\Upsilon_g\Phi_g e^{-\tau_{1_g}}\left(e^{-\beta\Upsilon_g}\Lambda(v,l,q)\cdot(\beta\Upsilon_g)^{q-v}+\mathcal{T}_\epsilon\right), \tag{C.10}$$

Similarly, $R^{erg}_{x_{U_2}}$ is expressed as

$$R^{erg}_{x_{U_2}}=\mathbb{E}\Big[\log_2(1+\min(\gamma^{R_2}_{x_{U_2}},\gamma^{U_2}_{x_{U_2}})\Big], \tag{C.11}$$

Let $\tilde{\mathcal{X}}=\gamma^{R_2}_{x_{U_2}}$, $\tilde{\mathcal{Y}}=\gamma^{U_2}_{x_{U_2}}$, and $\tilde{\mathcal{Z}}=\min(\tilde{\mathcal{X}},\tilde{\mathcal{Y}})$, then CDF of $\tilde{\mathcal{Z}}$ is given as

$$F_{\tilde{\mathcal{Z}}}(\tilde{z})=\begin{cases}1-\Big(\exp\big(-\frac{\tilde{z}(\varepsilon+d^{\alpha}_{R_2})\sigma^2_{R_2}}{\Omega_{R_2}-\tilde{z}\Omega_{R_1}}\big)\times\sqrt{4\Psi_{x_{U_2}}\tilde{z}}K_v\big(\sqrt{4\Psi_{x_{U_2}}\tilde{z}}\big)\Big) & \text{for } \tilde{z}<\frac{p_{R_2}}{p_{R_1}},\\ 1 & \text{otherwise.}\end{cases} \tag{C.12}$$

We can compute $R^{erg}_{x_{U_2}}=\int\limits_0^\infty\log_2(1+\tilde{z})f_{\tilde{\mathcal{Z}}}(\tilde{z})d\tilde{z}=\frac{1}{\ln 2}\int\limits_0^\infty\frac{1-F_{\tilde{\mathcal{Z}}}(\tilde{z})}{1+\tilde{z}}d\tilde{z}$ as

$$R^{erg}_{x_{U_2}}=\frac{1}{\ln 2}\int\limits_0^{q'}\frac{\sqrt{4\Psi_{x_{U_2}}\tilde{z}}K_v(\sqrt{4\Psi_{x_{U_2}}\tilde{z}})}{1+\tilde{z}}\qquad\text{where } q'=\frac{p_{R_2}}{p_{R_1}}, \tag{C.13}$$

Integral in (C.13) does not admit closed form, so we again apply Gaussian Cheybshev Quadrature [81] to simplify $R^{erg}_{x_{U_2}}$ as

$$R^{erg}_{x_{U_2}}=\frac{\psi_{\mathcal{F}}}{\ln 2}\sum_{f=0}^{\mathcal{F}}\sqrt{1-\mu_f^2}\mathcal{W}_f K_v(\beta\varsigma_f) \tag{C.14}$$

Applying equivalent representation of $K_v(\beta x)$ from (C.7) above, we get

$$R_{x_{U_2}}^{erg} = \frac{\psi_{\mathcal{F}}}{\ln 2} \sum_{f=0}^{\mathcal{F}} \sum_{l=0}^{k} \sum_{q=0}^{l} \sqrt{1-\mu_f^2} \mathcal{W}_f \Big(e^{-\beta \varsigma_f} \Lambda(v,l,q) \cdot (\beta \varsigma_f)^{q-v} + \mathcal{T}_\epsilon \Big), \tag{C.15}$$

Proposition 5 is obtained as (24) by using (C.10) and (C.15). This completes the proof. ■

D Proof of Proposition 6

Proof. The achievable capacity of x'_{U_1} is written as

$$R_{x'_{U_1}}^{erg} = \mathbb{E}\Big[\log_2(1 + \min(\gamma_{x'_{U_1}}^{R_1}, \gamma_{x'_{U_1}}^{S}) \Big], \tag{D.1}$$

Using the similar approach of downlink rate, let $\mathcal{A}' \triangleq \gamma_{x'_{U_1}}^{S}$ and $\mathcal{B}' \triangleq \gamma_{x'_{U_1}}^{R_1}$. For finding CDF of $\mathcal{A}'$, we obtain

$$F_{\mathcal{A}'}(a') = 1 - \sum_{n=1}^{\mathcal{N}} \sum_{m=1}^{\mathcal{M}} \chi_n \chi_m \sqrt{a'(\xi_1 \omega_n \omega_m + \xi_2)} K_v \Big(2\sqrt{a'(\xi_1 \omega_n \omega_m + \xi_2)} \Big), \tag{D.2}$$

The CDF of $\mathcal{B}'$ is obtained with the help of (B.3) as:

$$F_{\mathcal{B}'}(b') = 1 - \exp\Big(- \frac{b' \sigma_{U_1}^2 (\varepsilon + d_{U_1 R_1}^{\alpha})}{\mathcal{P}_U \rho} \Big), \tag{D.3}$$

Let $\mathcal{C}' = \min(\mathcal{A}', \mathcal{B}')$, by using CDF of minimum of two exponential variables, we can write

$$\begin{aligned} F_{\mathcal{C}'}(c') = 1 - \Big(\sum_{n=1}^{\mathcal{N}} \sum_{m=1}^{\mathcal{M}} \exp\Big(- \frac{c' \sigma_{U_1}^2 (\varepsilon + d_{U_1 R_1}^{\alpha})}{\mathcal{P}_U \rho} \Big) \times \\ \chi_n \chi_m \sqrt{c'(\xi_1 \omega_n \omega_m + \xi_2)} K_v \Big(2\sqrt{c'(\xi_1 \omega_n \omega_m + \xi_2)} \Big) \Big), \end{aligned} \tag{D.4}$$

We now represent $R_{x'_{U_1}}^{erg}$ as

$$R_{x'_{U_1}}^{erg} = \int_0^{\infty} \sum_{n=1}^{\mathcal{N}} \sum_{m=1}^{\mathcal{M}} \frac{\Big(\chi_n \chi_m \sqrt{c'(\xi_1 \omega_n \omega_m + \xi_2)} K_v \Big(2\sqrt{c'(\xi_1 \omega_n \omega_m + \xi_2)} \Big) \Big) \exp(-\nu c')}{\ln 2 (1 + c')} dc', \tag{D.5}$$

The complicated integral in (D.5) needs to be solved to obtain closed form expression of $R_{x'_{U_1}}^{erg}$, which is not possible with tralatitious integration. We assume $t' = \dfrac{1}{1+c'}$ and

apply numerical integration using Gaussian quadrature to simplify above

$$R^{erg}_{x'_{U_1}} = \frac{1}{\ln 2}\sum_{l'=1}^{\mathcal{L}'}\sum_{m=1}^{\mathcal{M}}\sum_{n=1}^{\mathcal{N}}\frac{\pi\chi_n\chi_m}{\mathcal{L}'}\sqrt{\frac{1+\wp_{l'}}{1-\wp_{l'}}}\exp\left(\frac{\wp_{l'}+1}{\wp_{l'}-1}\nu\right)\beth_{l'}K_v(2\beth_{l'}), \tag{D.6}$$

where $\beth_{l'} = \sqrt{\frac{(\wp_{l'}+1)(\xi_1\omega_n\omega_m+\xi_2)}{(1-\wp_{l'})}}$. To obtain closed form expression of $R^{erg}_{x'_{U_1}}$, we apply approximation of $K_v(.)$ from (C.7) and obtain final expression as shown below .

$$\begin{aligned} R^{erg}_{x'_{U_1}} = \frac{1}{\ln 2}\sum_{l'=1}^{\mathcal{L}'}\sum_{m=1}^{\mathcal{M}}\sum_{n=1}^{\mathcal{N}}\frac{\pi\beth_{l'}\chi_n\chi_m}{\mathcal{L}'}\sqrt{\frac{1+\wp_{l'}}{1-\wp_{l'}}}\exp\left(\frac{\wp_{l'}+1}{\wp_{l'}-1}\nu\right) \\ \left(e^{-\beta 2\beth_{l'}}\sum_{n=0}^{k}\sum_{q=0}^{l}\Lambda(v,l,q)\cdot(\beta 2\beth_{l'})^{q-v}+\mathcal{T}_\epsilon\right), \end{aligned} \tag{D.7}$$

Similar to the argument from (D.1) to (D.7), $R^{erg}_{x'_{U_2}}$ is obtained as

$$\begin{aligned} R^{erg}_{x'_{U_2}} = \frac{1}{\ln 2}\sum_{z=1}^{\mathcal{Z}}\frac{\pi^2\sqrt{(1-\varphi_z^2)(\varpi\tan\mathcal{V}_z)}}{2\mathcal{Z}(1+\tan\mathcal{V}_z)}\exp(-\digamma\tan\mathcal{V}_z)\sec^2\mathcal{V}_z \\ \left(e^{-2\beta\sqrt{\varpi\tan\mathcal{V}_z}}\sum_{n=0}^{k}\sum_{q=0}^{l}\Lambda(v,l,q)\cdot(2\beta\sqrt{\varpi\tan\mathcal{V}_z})^{q-v}+\mathcal{T}_\epsilon\right), \end{aligned} \tag{D.8}$$

Summing the values of $R^{erg}_{x'_{U_1}}$ and $R^{erg}_{x'_{U_2}}$, we obtain Proposition 6. This completes the proof. ■

E DRC 16 Form

DRC 16

MASSEY UNIVERSITY
GRADUATE RESEARCH SCHOOL

STATEMENT OF CONTRIBUTION
DOCTORATE WITH PUBLICATIONS/MANUSCRIPTS

We, the candidate and the candidate's Primary Supervisor, certify that all co-authors have consented to their work being included in the thesis and they have accepted the candidate's contribution as indicated below in the *Statement of Originality*.

Name of candidate:	Syeda Kanwal Zaidi
Name/title of Primary Supervisor:	Syed Faraz Hasan
Name of Research Output and full reference:	
S. K. Zaidi, S. F. Hasan, X. Gui, "Two-way SWIPT-aided hybrid NOMA relaying for out-of-coverage devices", Journal of Wireless Networks, pp. 1-16, September 2019.	
In which Chapter is the Manuscript /Published work:	Chapter 3
Please indicate:	
• The percentage of the manuscript/Published Work that was contributed by the candidate:	90%
and	
• Describe the contribution that the candidate has made to the Manuscript/Published Work:	
The candidate has proposed the system model, conducted model simulations and mathematical analysis. Illustration and interpretation of the results has also been done by the candidate. Related manuscript has been written by the candidate majorly. The supervisors were throughout involved in the review of the work.	
For manuscripts intended for publication please indicate target journal:	
Candidate's Signature:	Syeda Kanwal Zaidi Digitally signed by Syeda Kanwal Zaidi Date: 2020.01.06 08:53:08 +13'00'
Date:	06/Jan/2020
Primary Supervisor's Signature:	Faraz Hasan Digitally signed by Faraz Hasan Date: 2020.01.06 10:48:55 +13'00'
Date:	6 Jan 2020

(This form should appear at the end of each thesis chapter/section/appendix submitted as a manuscript/ publication or collected as an appendix at the end of the thesis)

GRS Version 4– January 2019

Figure E.1: DRC 16 -Chapter 3.

Chapter 4

Outage Analysis of Ground-Aerial NOMA with Distinct Instantaneous Channel Gain Ranking

Authors : Syeda Kanwal Zaidi, Syed Faraz Hasan, and Xiang Gui

Abstract

Future wireless networks envision to provide seamless connectivity to a multitude of devices including unmanned aerial vehicles (UAVs). This paper investigates a unique case where we aim to serve ground users and a UAV, with distinct channel characteristics and access environments in three-dimensional (3D) space, based on non-orthogonal multiple access (NOMA). Unlike traditional distance-based ranking or channel-gain-based ranking, we apply NOMA in uplink and downlink transmissions by evaluating instantaneous channel gain and distance-dependant path-loss together. The communication links of ground and aerial users have different fading environments and path losses which make it crucial to analyse instantaneous channel gain before applying NOMA. To this end, we derive new mathematical expressions of outage probabilities in downlink and uplink transmissions based on instantaneous distinct signal power (IDSP) for each user, verified by simulations. Next, we investigate the impact of different system parameters, e.g. data rate, path loss exponent, channel fading characteristics and UAV height, on outage behaviour. The results confirm that ground-aerial NOMA can be successfully employed in future wireless networks to provide cellular connectivity with improved spectral efficiency to a broader range of devices with individual data rate requirements.

4.1 Introduction

The storm of wireless devices is on the rise with nearly twenty-billion devices to be deployed by 2020 [84]. Unmanned aerial vehicles (UAVs), commonly referred to as drones, have become popular in the recent years with a variety of usuage in a range of applications including live audio/video streaming, package delivery, road traffic monitoring, network provision in catastrophic scenarios, farm monitoring and other agriculture applications, etc. Rapid advancements in drone technology are deriving research interests towards UAVs as aerial base stations (BSs) to deliver on demand and reliable service to desired users, or as relays [85] to help regular terrestrial networks in extending the network coverage, or as cellular-connected UAVs for data delivery or surveillance, etc. In beyond 5G (B5G) cellular networks, fully autonomous or remotely operated UAVs stand as a potential candidate of acquiring communication link with BS [47, 86]. While the drones are present in the air, they need to be served like a conventional cellular user and require distinct uplink and downlink data traffic pattern based on their usage in an application.

B5G networks are likely to adopt more promising multiple access schemes like non-orthogonal multiple access (NOMA) to provide reliable connectivity with higher spectral efficiency and required quality of service (QoS) to a multitude of devices. NOMA serves multiple users by sharing the same resource block (called as sub-bands) at a time by altering power levels or assigning codes to users [9]. When power domain is utilised to realise multiple access, NOMA is referred as power-domain NOMA [87] while if codes are used to share the resource among users, NOMA is referred as code-domain NOMA [88]. Power-domain downlink NOMA utilises power allocation mechanism where low transmission power is used for a user with good channel conditions and vice versa [89] in a band. In power-domain uplink NOMA, the users with sufficiently distinct channel conditions utilise their maximum battery power for transmission [54] in a single-band. Here-after, we refer to the users clubbed in a single band as a NOMA pair. In [9]- [12], the concept and key attributes of NOMA are discussed. Authors in [10] debate on signalling overhead, error propagation and multi-user power allocation. A combination of multiple-input-multiple-output (MIMO) and NOMA is explored in [90], [91]. So far recent literature has investigated the application of NOMA on ground users specifically where the devices share the similar communication and multipath fading environment, see [92] and references therein. Some research works exploited NOMA's applicability in UAV based communications as well. In [86], a UAV in the form of aerial BS is deployed to serve ground users under NOMA with a power allocation scheme to achieve maximum sum-rate of the communication system with reduced energy expense for the UAV. Furthermore, the authors presented a methodology to render expansion of the aerial cell coverage, which is facilitated by NOMA user-rate

gains. Along the similar lines, to leverage the strength of line-of-sight connections and effectively support the coverage and throughput of wireless communication, a max-min rate optimization problem is formulated under total power, total bandwidth, UAV altitude, and antenna beam-width constraints for a multi-user communication system, in which a single-antenna UAV-BS serves ground users by employing NOMA [93]. The application of MIMO UAV-BS providing NOMA access to ground users is investigated in [94], where the performance of the network is evaluated by deriving analytical expressions for the outage probability and the ergodic rate of MIMO-NOMA enhanced UAV networks. Different to previous works, the interference management problem between a UAV BS serving NOMA users and underlying device-to-device users is studied in [95]. The works [86], [93]- [95] deployed aerial BSs with single or multi-antenna UAVs to serve ground users by NOMA. Multi-antenna mmWaves drones are deployed to provide coverage to a group of users with NOMA in [96] for spectrally efficient UAV-BS based communication. Moreover, the authors in [48, 49] have investigated the placement of UAVs as relays to improve network coverage and performance. A few of the research works have focused on connectivity of UAVs as cellular users, e.g. Wang et. al. studied NOMA based UAV satellite network, where multiple satellites served UAV and a mobile terminal cooperatively under rain fading with Ku-band [97]. The authors conducted outage analysis and proposed a power allocation scheme for user fairness.

The application of NOMA on network users requires ordering of users on the basis of certain characteristics. It has been demonstrated that NOMA improves throughput and spectral efficiency of a wireless communication system by serving users non-orthogonally based on their ranking. The ranking or ordering of users plays an important role in deriving the performance of a NOMA-based system and is done on the basis of communication link quality. In general, weak to strong users are ranked based on the ascending values of mean signal power (MSP), instantaneous signal power (ISP) or instantaneous-signal-to-noise ratio (ISNR) [9,45,46]. In downlink (DL) communication, distance-based ranking of users has been considered in [9, 87], [46, 50, 53, 98] to evaluate different performance metrics such as coverage probability, ergodic rates, and user fairness in NOMA-based systems. Similarly in uplink (UL) communication, [58, 79, 99] also assumed that users present close to BS are strong while the ones located far away from BS are weak users and hence BS decodes the signals of weak users after decoding the message of strong users first. With UAVs, there are several characteristics which are different from ground users, including:

- Height of UAVs from the ground or BS, which may vary depending upon the flight and regulatory requirement of the drone zone
- Distance-dependant path loss of UAVs may be different to ground users based on the communication environment, as explained by field experiments [100]

- Channel fading characteristics of UAVs- small-scale fading effects often contribute more than shadowing in UAVs for example when UAVs are flying higher, actual shadowing is not present but variation in small-scale fading still happens [101]

The above mentioned features of UAVs make them unique in accessing a cellular network[1]. When a network has a range of devices including aerial devices like UAVs and ground devices like cell phones and vehicles, etc., it is not fair to evaluate transmission link quality using only the distance metric. It is possible that an aerial user which is far from the BS experiences a strong communication link as compared to a near user from BS which suffers from severe shadowing in a multipath environment. Therefore, it is crucial to identify the conditions of the communication link not only based on path loss or channel gain but also on the instantaneous channel power of the link to apply NOMA effectively. The focus of our work is to apply NOMA on a pair of aerial and ground NOMA users which are exclusive in terms of channel fading and path loss characteristics but require cellular connectivity at the same time. Research on cellular-connected UAVs is not well established and to the best of authors' knowledge there is no research work which has considered cellular-connectivity of aerial and ground users together in three-dimensional (3D) space using NOMA in UL and DL transmissions. To-date, literature considers NOMA for ground users only and has not examined the non-orthogonal access of aerial and ground devices as cellular connected devices. Research studies [50]- [53] have used distance based ranking and [45]- [46] considered ISNR for terrestrial NOMA wireless networks, however the ranking of an aerial and ground user in a NOMA pair based on instantaneous channel gain and distance-dependant path-loss is still unexplored. Motivated to support NOMA for aerial and ground users, we analytically study a multi-user system that takes into account the instantaneous channel gains of aerial and ground users, i.e., the product of their channel fading gain and distance-dependant path loss, to assign power levels to the users in a NOMA pair. The authors in [102] have analysed the accuracy of the ranking method in NOMA-based system where users are ranked according to their distances from BS considering ground users in NOMA pair and highlighted that with this method, the coverage results are closely matched to instantaneous-channel-based ranking only when i) network is interference or noise limited, ii) unsuccessful SIC is very probable, or iii) the assumption of ranking on the basis of instantaneous channel gain based ranking is correct [102] . The authors in [102] have considered distance-based approximation valid for ground users experiencing Nakagami-m or Rayleigh fading. Different to the approaches in [45]- [99], we have a UAV and a ground user as candidates for NOMA transmissions and we discuss the application of variable power levels to each user by

[1]Cellular networks use down-tilted BS antennas but small UAVs may be served by the side-lobes of BS antennas [47]

scrutinising the fading environment of aerial and ground user, 3D distance from BS, individual path loss exponent of each user (which is different for both users) and target data rate in downlink transmissions. Further in this context, we analyse UL NOMA transmission with aerial-ground pairing considering all the parameters enumerated for DL transmissions. We also show that though the aerial user is located far from the BS, there is a possibility of attaining better instantaneous channel gain than closely located ground user based on environmental and spatial characteristics. This possibility shows that it is not necessary that a far user is always considered as weak user and a near user is always a strong user. Contrary to the conventional NOMA assumption, we show that ranking of aerial and ground users is not only distance-dependant. To elucidate the benefits of our system, conventional orthogonal multiple access (OMA) is considered as benchmark and simulation results are provided to reveal the accuracy of our outage analysis.

4.1.1 Contributions

We summarise the contributions of this paper as follows:

- This paper characterises the performance of a NOMA-based system where a ground user and an aerial user are paired together in a single NOMA band for improved spectral efficiency. Due to the unique environments of aerial and ground users, NOMA in DL and UL transmission is applied by ranking users based on the product of their channel fading gain and distance-dependant path loss together, referred to as instantaneous distinct signal power (IDSP).

- We show that ranking of the users in a ground-aerial NOMA is not dependant on distance only but also on several other important factors, for example, path loss exponent of aerial user, path loss exponent of ground users, height of the aerial user and fading severity.

- In particular, we derive the outage probabilities of an aerial user and a ground user in DL and UL transmissions by analysing two cases together, i) when the instantaneous channel gain of ground user is greater than that of aerial user, and ii) when the instantaneous channel gain of aerial user is greater than that of ground user. This approach of applying NOMA based on the significant environment characteristics on an aerial user and a ground user is novel and has not been considered in the literature before.

- We obtain following insights based on the derived expressions: i) The probability of instantaneous channel gain of aerial user being greater than that ground users has a direct relationship with large scale fading of ground users and it increases

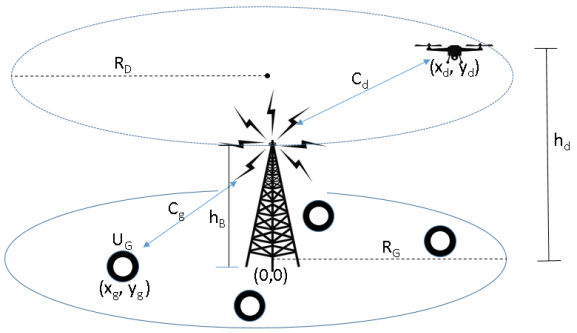

Figure 4.1: System Model.

with the path loss exponent of the ground user. Hence it is important to evaluate IDSP before applying ground-aerial NOMA; ii) The outage behaviour of aerial user is impacted by changes in the path-loss exponent of ground user while changes in fading environment of drone user has a little impact on the outage of ground user in DL and UL transmissions; iii) The height of aerial user impacts its outage behaviour in UL and DL transmissions, hence it is crucial to keep the height of aerial user within limits to achieve desired performance; iv) Ground-aerial NOMA outperforms OMA transmissions in high SNR region in terms of system throughput.

The rest of the paper is organised as follows: Section 4.2 describes the system model and related assumptions. The information theoretics of NOMA-based DL and UL transmissions is introduced in Section 4.3. In Section 4.4, detailed analysis is conducted. Section 4.5 presents the results and comparisons with the benchmark system, while Section 4.6 concludes the paper along with future directions.

Notation:

$\mathbb{E}[.]$ represents the expectation operator while $\mathbb{P}(X)$ represents probability of an event X. $f_X(x)$ and $F_X(x)$ represent probability density function (PDF) and cumulative density function (CDF) of a random variable X respectively.

4.2 System Model and Assumptions

We consider a single-tier network with a BS $\mathcal{B}$ situated at $O' \equiv (0, 0, 0)$ with antenna height $h_{\mathcal{B}}$. In a disc of radius $\mathcal{R}_{\mathcal{G}}$, which is centred at $(0, 0, h_g)$, $\mathcal{N}_{\mathcal{G}}$ devices are uniformly distributed at height h_g in Euclidean space. The devices are distributed according to homogeneous Poisson point process (HPPP) $\Phi_{\mathcal{G}}$ with a density of $\lambda_{\mathcal{G}}$. Each device is situated at location $\{l_g\}_{g=1:\mathcal{N}_{\mathcal{G}}} \equiv \Phi_{\mathcal{G}} \subset \mathbb{R}^2$, where the distance between any arbitrary device from centre of the disc $\mathcal{R}_{\mathcal{G}}$ [103] is denoted by u_g with PDF given as

$$f_{u_g}(x) = \frac{2x}{\mathcal{R}_{\mathcal{G}}^2}, x < \mathcal{R}_{\mathcal{G}}, \tag{4.1}$$

We also assume a quasi-stationary cellular-connected UAV d at a random location l_d in a disc of radius $\mathcal{R}_{\mathcal{D}}$ around O' centred at height h_d as shown in Fig. 4.1, such that its centre is $(0, 0, h_d)$. The UAV is present at any random location within $\mathcal{R}_{\mathcal{D}}$ and the PDF of its distance r_d from $\mathcal{R}_{\mathcal{D}}$'s centre is given by [104]

$$f_{r_d}(y) = \frac{2y}{\mathcal{R}_{\mathcal{D}}^2}, y < \mathcal{R}_{\mathcal{D}}, \tag{4.2}$$

$\mathcal{B}$ serves one random ground user g and the aerial user d having enough disparity among them (in terms of communication environment) in one frequency-time resource block by multiplexing signals with distinct power level based on the ranking explained in the next section. The communication links between $\mathcal{B}$ and all devices exhibit statistically independent small-scale frequency non-selective quasi-static fading and large scale path-loss. Owing to limited literature studies on cellular-connected UAVs [100] large-scale fading which depends on altitude, distance and elevation angle[2] between $\mathcal{B}$ and d [100], for communication link $\mathcal{B} \leftrightarrow d$, we adopt the working assumption of power-law path-loss model $\mathcal{L}_d = \left(\sqrt{r_d^2 + (h_d - h_{\mathcal{B}})^2}\right)^{-\alpha_d}$, where α_d is the path loss exponent for user d [49]. Nakagami-m fading, which mimics various environments, is exhibited by $\mathcal{B} \leftrightarrow d$ link, referred as $|C_d|$ and hence the channel gain follows Gamma distribution [100] with PDF given as

$$f_{|\mathcal{C}_d|^2}(x; m_d, \Omega_d) = \frac{{m_d}^{m_d} x^{m_d - 1}}{{\Omega_d}^{m_d} \Gamma(m_d)} e^{-\frac{m_d}{\Omega_d} x}, \forall x > 0, \tag{4.3}$$

where, m_d and Ω_d are Nakagami shape and spread control parameters respectively, and $\Gamma(m_d)$ is the Gamma function. A Rayleigh fading environment is assumed for link $g \leftrightarrow \mathcal{B}$, referred to as $|C_g|$ where channel gain follows exponential distribution with PDF expressed as

$$f_{|\mathcal{C}_g|^2}(x; \mu_g) = \frac{1}{\mu_g} e^{-\frac{x}{\mu_g}}, \quad \forall x \geq 0, \tag{4.4}$$

where μ_g is the mean parameter. The path loss for ground devices is also distance-dependant $\mathcal{L}_g = \left(\sqrt{u_g^2 + (h_g - h_{\mathcal{B}})^2}\right)^{-\alpha_g}$ with path loss exponent α_g, which is different from α_d [100].

[2]Elevation angle is the angle between horizontal plane and the line of sight between BS and the UAV. It has been used in the experimental studies to determine path loss for the communication link between BS and UAV [100].

4.3 Transmission Theoretic Model

Here, we explain the proposed model for ground-aerial NOMA transmissions in UL and DL and the benchmark OMA model used for comparison.

4.3.1 NOMA-based Model

Downlink Transmission

In DL NOMA transmissions, power allocation of users and the transmission rate are assigned such that the stronger user is able to decode the message of the weaker user. Consequently, successive interference cancellation (SIC) is employed to decode the messages of the users [9]. The strong and weak user are identified on the basis of transmission link quality between BS and user. Ranking of users in the current literature consider ground users only which are present in the same fading environment with same effect of path loss on distance. However, in case of an aerial user and a ground user, the path loss and channel fading environment of two users are distinct. We consider this fundamental difference and analyse the rank of users based on the IDSP which is determined by $|C_g|^2\mathcal{L}_g$ for ground user and $|C_d|^2\mathcal{L}_d$ for aerial user. This means that when IDSP of drone is greater than IDSP of user, drone is considered as strong user, and vice versa. To perform DL NOMA transmission, as stated earlier, we assume that $\mathcal{B}$ selects one random ground user g and pairs it with UAV d to serve on the same channel and time slot. Selecting a ground user randomly creates a fair opportunity for each user to access $\mathcal{B}$ along with user d. This pairing and ranking scheme together for an aerial and ground user is novel and unique. Based on the details above, there are two possible scenarios, either i) $|C_g|^2\mathcal{L}_g$ is greater than $|C_d|^2\mathcal{L}_d$, and g is a strong user or ii)$|C_g|^2\mathcal{L}_g$ is less than $|C_d|^2\mathcal{L}_d$, and d is a strong user, depending on the values of $|C_g|^2$, $|C_d|^2$, α_d, α_g, r_d, u_g, h_d and h_g. Following NOMA, $\mathcal{B}$ transmits with power $P_{\mathcal{B}}$ and assigns a portion of the total power $p_{\mathcal{W}}$ and $p_{\mathcal{S}}$ to weak and strong user respectively, where $p_{\mathcal{W}} + p_{\mathcal{S}} = 1$, and $p_{\mathcal{W}} > p_{\mathcal{S}}$. The signal received by a receiver is given as

$$\mathcal{S}_{i\epsilon\{d,g\}} = \sqrt{P_{\mathcal{B}}\mathcal{L}_i}|\mathcal{C}_i|(\sqrt{\omega_d}x_{dl}^d + \sqrt{\omega_g}x_{dl}^g) + \mathcal{Z}_i, \tag{4.5}$$

where x_{dl}^d and x_{dl}^g are transmitted messages for d and g respectively with $\mathbb{E}\{|x_{dl}^d|^2\} = \mathbb{E}\{|x_{dl}^g|^2\} = 1$. $\mathcal{Z}_i \sim \mathcal{CN}(0, \sigma_i^2)$ denotes Additive White Gaussian Noise (AWGN) with mean 0 and variance σ_i^2. ω_d and ω_g are power allocation factors for user d and g respectively. Order of decoding of x_{dl}^d and x_{dl}^g depends on the ω_d and ω_g at $\mathcal{B}$ which in turn depends on IDSP of d and g respectively. As per NOMA [9], if g is a strong user, i.e., IDSP of g is greater than d then $\omega_g = p_{\mathcal{S}}$, $\omega_d = p_{\mathcal{W}}$, $\omega_g < \omega_d$, and g cancels x_{dl}^d after decoding before extracting x_{dl}^g. On the the other hand, if IDSP of g is less

than d then $\omega_d = p_{\mathcal{S}}$, $\omega_g = p_{\mathcal{W}}$, $\omega_g > \omega_d$, and g decodes x_{dl}^g in the presence of x_{dl}^d. In practice, perfect SIC is an ideal case, we consider $0 \leq \beta_{SIC} \leq 1$ as residual interference from the weak user to strong user, similar to [45,105]. By taking $\beta_{SIC} = 0$, perfect SIC is assumed while $\beta_{SIC} = 1$ corresponds to failed SIC scenario. Therefore, with IDSP ranking at $\mathcal{B}$, we express received SINR (γ_{dl}^i) of x_{dl}^i at device i as follows.

If ($|C_g|^2\mathcal{L}_g > |C_d|^2\mathcal{L}_d$),

$$\gamma_{dl}^g = \frac{P_{\mathcal{B}}\omega_g|C_g|^2\mathcal{L}_g}{P_{\mathcal{B}}\omega_d|C_g|^2\mathcal{L}_g\beta_{SIC} + \sigma_g^2}, \tag{4.6}$$

$$\gamma_{dl}^d = \frac{P_{\mathcal{B}}\omega_d|C_d|^2\mathcal{L}_d}{P_{\mathcal{B}}\omega_g|C_d|^2\mathcal{L}_d + \sigma_d^2}, \tag{4.7}$$

else

$$\gamma_{dl}^g = \frac{P_{\mathcal{B}}\omega_g|C_g|^2\mathcal{L}_g}{P_{\mathcal{B}}\omega_d|C_g|^2\mathcal{L}_g + \sigma_g^2}, \tag{4.8}$$

$$\gamma_{dl}^d = \frac{P_{\mathcal{B}}\omega_d|C_d|^2\mathcal{L}_d}{P_{\mathcal{B}}\omega_g|C_d|^2\mathcal{L}_d\beta_{SIC} + \sigma_d^2}, \tag{4.9}$$

Uplink Transmission

In UL NOMA transmissions, users in a NOMA pair share the same frequency block by superimposing their distinct messages [54]. $\mathcal{B}$ applies SIC by decoding the signal of user with higher IDSP first by treating the signal with lower IDSP as noise. Therefore in ground-aerial UL NOMA transmission, the uplink signal received by $\mathcal{B}$ is written as

$$\mathcal{S}_{\mathcal{B}} = \sqrt{P_d\mathcal{L}_d}|\mathcal{C}_d|x_{ul}^d + \sqrt{P_g\mathcal{L}_g}|\mathcal{C}_g|x_{ul}^g + \mathcal{Z}_{\mathcal{B}}, \tag{4.10}$$

where, P_g and x_{ul}^g, P_d and x_{ul}^d are the transmit powers and transmitted messages of g and d respectively, where $P_g = P_d$ is considered throughout the paper. $\mathcal{Z} \sim \mathcal{CN}(0, \sigma_{\mathcal{B}}^2)$ denotes AWGN at $\mathcal{B}$.

Based on the IDSP ranking in UL transmissions, we can deduce SINR (γ_{ul}^i) of x_{ul}^i at $\mathcal{B}$ in UL as follows

If ($|C_g|^2\mathcal{L}_g > |C_d|^2\mathcal{L}_d$)

$$\gamma_{ul}^g = \frac{P_g|C_g|^2\mathcal{L}_g}{P_d|C_d|^2\mathcal{L}_d + \sigma_{\mathcal{B}}^2}, \tag{4.11}$$

$$\gamma_{ul}^d = \frac{P_d|C_d|^2\mathcal{L}_d}{P_g|C_g|^2\mathcal{L}_g\beta_{SIC} + \sigma_{\mathcal{B}}^2}, \tag{4.12}$$

else

$$\gamma_{ul}^g = \frac{P_g|C_g|^2\mathcal{L}_g}{P_d|C_d|^2\mathcal{L}_d\beta_{SIC} + \sigma_{\mathcal{B}}^2}, \tag{4.13}$$

$$\gamma_{ul}^{d} = \frac{P_d |C_d|^2 \mathcal{L}_d}{P_g |C_g|^2 \mathcal{L}_g + \sigma_{\mathcal{B}}^2}, \tag{4.14}$$

Current literature [57, 79] assesses UL NOMA assuming that the user closer to the BS has higher instantaneous channel power and hence only one case is considered in deriving the outage or coverage probabilities of the users. However, in applying uplink NOMA for a ground-aerial user pair it is crucial to consider IDSP, which may vary based on environment and positions of ground and aerial users as stated earlier in this section.

4.3.2 OMA-based Model

We compare our proposed ground-aerial NOMA model with a conventional OMA-based model where ground and aerial users are served by $\mathcal{B}$ in a single frequency-time resource block with time-division multiple access (TDMA) in UL and DL. Each message is transmitted with power $P_{\mathcal{B}}$ for a time duration $T/2$ in DL transmission by $\mathcal{B}$, while P_g and P_d are used as transmit powers of g and d in UL . We also assume similar time duration T for NOMA transmission for a fair comparison.

4.4 Performance Analysis

We investigate the outage probability of received messages to characterise the link level performance and measure if this pairing satisfies the data rate requirements in DL and UL transmissions. Outage probability is defined as the probability of instantaneous data rate $R_{a\to b}$ of message x sent by a to b being lower than a pre-defined threshold data rate $R_{\mathcal{T}}^{x}$.

We first obtain the probability $IDSP_g = \mathbb{P}(|C_g|^2\mathcal{L}_g > |C_d|^2\mathcal{L}_d)$ by deriving over the expectation of fading channel power and distance distribution of d and g.

Corollary 1: We express $IDSP_g$ as

$$IDSP_g = \sum_{k=0}^{K}\sum_{j=0}^{J}\sum_{t=0}^{m_d} \Lambda \sqrt{(1-\phi_j^2)(1-\phi_k^2)} \left(\frac{s_j s_k}{\binom{m_d}{t} \mathcal{Y}^t \mathcal{X}^{m_d - t}} \right), \tag{4.15}$$

where, $\Lambda = \dfrac{\pi^2 \mathcal{R}_{\mathcal{D}} \mathcal{R}_{\mathcal{G}} \Delta}{4JK}$, $\phi_j = \cos\left(\dfrac{2j-1}{2J}\right)$, $\phi_k = \cos\left(\dfrac{2k-1}{2K}\right)$, $s_j = \dfrac{\mathcal{R}_{\mathcal{G}}}{2}(\phi_j + 1)$, $s_k = \dfrac{\mathcal{R}_{\mathcal{D}}}{2}(\phi_k + 1)$, $s_j' = \left(\sqrt{s_j + (h_g - h_{\mathcal{B}})^2}\right)^{\alpha_g} \mu_g$, $s_k' = \left(\sqrt{s_k + (h_d - h_{\mathcal{B}})^2}\right)^{\alpha_d}$, $\mathcal{X} = \dfrac{s_k'}{s_j'}$ $\mathcal{Y} = \dfrac{m_d^{m_d}}{\Omega_d^{m_d}}$, and J, K are the Cheybshev approximation parameters.

Proof: See Appendix A.

It can be seen from Corollary 1 that the probability of IDSP of user g being greater than that of user d does not depend only on the distance of users from $\mathcal{B}$, but also on

the fading environment of aerial user, path loss exponents of aerial and ground users which are different from each other as communication environments are different and height of the aerial user from the ground. $IDSP_g$ evaluation in our model helps $\mathcal{B}$ to correctly assign power levels to both users in downlink transmission and apply SIC to extract signals in UL transmission.

Based on Corollary 1 above, we evaluate $IDSP_d$ as

$$IDSP_d = 1 - \sum_{k=0}^{K}\sum_{j=0}^{J}\sum_{t=0}^{m_d} \Lambda\sqrt{(1-\phi_j^2)(1-\phi_k^2)}\left(\frac{s_j s_k}{\binom{m_d}{t}\mathcal{Y}^t\mathcal{X}^{m_d-t}}\right), \tag{4.16}$$

4.4.1 Downlink Transmission

In this section, we evaluate the outage probability of a ground user and an aerial user which are paired together in a NOMA band based on IDSP ranking.

The outage probability of Aerial User

Based on IDSP of user d, we obtain outage of aerial user in DL transmission as in Theorem 1 for an arbitrary choice of α_d and α_g.

Theorem 1. The outage probability of user d in DL transmission is approximated as follows:

$$\begin{aligned} P_{\mathcal{O}}^{x_{dl}^d} \approx \Bigg(& \sum_{k=0}^{K}\sum_{j=0}^{J}\sum_{t=0}^{m_d}\sum_{a=0}^{A}\sum_{s=0}^{m_d-1} \nabla_s \zeta_a \mathcal{J}_a^s \Lambda\sqrt{(1-\phi_j^2)(1-\phi_k^2)} \\ & \left(\frac{s_j s_k}{\binom{m_d}{t}\mathcal{Y}^t\mathcal{X}^{m_d-t}} \exp\left(-\delta_d m_d \mathcal{J}_a\right)\right)\Bigg) + \\ & \left(\sum_{b=0}^{B}\sum_{s'=0}^{m_d-1} \ddagger_{s'}\zeta_b \mathcal{J}_b^{s'} \exp\left(-\delta'_d m_d \mathcal{J}_b\right)\right) \\ & \left(1 - \sum_{k=0}^{K}\sum_{j=0}^{J}\sum_{t=0}^{m_d} \Lambda\sqrt{(1-\phi_j^2)(1-\phi_k^2)}\left(\frac{s_j s_k}{\binom{m_d}{t}\mathcal{Y}^t\mathcal{X}^{m_d-t}}\right)\right), \end{aligned} \tag{4.17}$$

where, $\nabla_s = \dfrac{\pi\sqrt{1-\varphi_a^2}}{s!}$, $\zeta_a = \dfrac{m_d^s \delta_d^s \S_a}{\Omega_d{}^s A\mathcal{R}_\mathcal{D}}$, $\varphi_a = \cos\left(\dfrac{2a-1}{2A}\pi\right)$, $\S_a = \dfrac{\mathcal{R}_\mathcal{D}}{2}(\varphi_a + 1)$, $\mathcal{J}_a = \sqrt{\S_a + (h_d - h_\mathcal{B})^2}^{\alpha_d}$, $\delta_d = \dfrac{\gamma_\mathcal{T}^{x_{dl}^d}}{\varrho_d(p_\mathcal{W} - \gamma_\mathcal{T}^{x_{dl}^d} p_\mathcal{S})}$, $\varrho_d = P_\mathcal{B}\sigma_d^{-2}$, $\ddagger_{s'} = \dfrac{\pi\sqrt{1-\varphi_b^2}}{s'!}$, $\zeta_b = \dfrac{m_d^{s'}\delta_d^{s'}\dagger_b}{\Omega_d^{s'} B\mathcal{R}_\mathcal{D}}$, $\varphi_b = \cos\left(\dfrac{2b-1}{2B}\pi\right)$, $\dagger'_b = \dfrac{\mathcal{R}_\mathcal{D}}{2}(\varphi_b + 1)$, $\mathcal{J}_b = \sqrt{\dagger'_b + (h_d - h_\mathcal{B})^2}^{\alpha_d}$, $\delta'_d = \dfrac{2^{R_\mathcal{T}^{x_{dl}^d}} - 1}{\varrho_d(p_\mathcal{S} - (2^{R_\mathcal{T}^{x_{dl}^d}} - 1)\varrho_d\beta_{SIC}p_\mathcal{W})}$, A, B are the Cheybshev approximation parameter.

Proof: See Appendix B.

Corollary 2: For the special case where SIC is ideal, i.e., $\beta_{SIC} = 0$, the outage probability of user d can be simplified as follows

$$P_{\mathcal{O}}^{x_{dl}^{d}}|_{\beta_{SIC}=0} \approx \left(\sum_{a=0}^{A}\sum_{s=0}^{m_d-1} \nabla_s \zeta_a \mathcal{J}_a^s \exp\left(-\delta_d m_d \mathcal{J}_a\right)\right) \times IDSP_g + \left(\sum_{b=0}^{B}\sum_{s'=0}^{m_d-1} \ddagger_{s'} \zeta_b \mathcal{J}_b^{s'} \exp\left(-\frac{m_d \mathcal{J}_b (2^{R_{\mathcal{T}}^{x_{dl}^{d}}} - 1)}{\varrho_d p_{\mathcal{S}}}\right)\right) \times IDSP_d \tag{4.18}$$

Proof: Based on (4.17), after some algebraic manipulations with $\beta_{SIC} = 0$, Corollary 2 is obtained.

The outage probability of Ground User

The outage probability of a ground user g is approximated as follows.

Theorem 2. The outage probability of a ground user g is expressed as

$$\begin{aligned} P_{\mathcal{O}}^{x_{dl}^{g}} \approx & \left(1 - \frac{1}{\tilde{\alpha_g} \mathcal{R}_{\mathcal{G}}^2 \tau^{\tilde{\alpha_g}-1}}\left[\Gamma\left(\frac{1}{\tilde{\alpha_g}}, \tau \tilde{h}_g^{\tilde{\alpha_g}}\right) - \Gamma\left(\frac{1}{\tilde{\alpha_g}}, (\tilde{h}_g + \mathcal{R}_{\mathcal{G}}^2)^{\tilde{\alpha_g}} \tau\right)\right]\right) \\ & \times \left(1 - \sum_{k=0}^{K}\sum_{j=0}^{J}\sum_{t=0}^{m_d} \Lambda \sqrt{(1-\phi_j^2)(1-\phi_k^2)}\left(\frac{s_j s_k}{\binom{m_d}{t} \mathcal{Y}^t \mathcal{X}^{m_d - t}}\right)\right) + \\ & \left(1 - \frac{1}{\tilde{\alpha_g} \mathcal{R}_{\mathcal{G}}^2 \hat{\tau}^{\tilde{\alpha_g}-1}}\left[\Gamma\left(\frac{1}{\tilde{\alpha_g}}, \hat{\tau} \tilde{h}_g^{\tilde{\alpha_g}}\right) - \Gamma\left(\frac{1}{\tilde{\alpha_g}}, (\tilde{h}_g + \mathcal{R}_{\mathcal{G}}^2)^{\tilde{\alpha_g}} \hat{\tau}\right)\right]\right) \times \\ & \left(\sum_{k=0}^{K}\sum_{j=0}^{J}\sum_{t=0}^{m_d} \Lambda \sqrt{(1-\phi_j^2)(1-\phi_k^2)}\left(\frac{s_j s_k}{\binom{m_d}{t} \mathcal{Y}^t \mathcal{X}^{m_d - t}}\right)\right), \end{aligned} \tag{4.19}$$

where, $\tau = \left(\frac{\gamma_{\mathcal{T}}^{x_{dl}^{g}}}{\varrho_g (p_{\mathcal{W}} - p_{\mathcal{S}} \gamma_{\mathcal{T}}^{x_{dl}^{g}})}\right)$, $\tilde{\alpha_g} = \frac{\alpha_g}{2}$, and $\tilde{h}_g = (h_g - h_{\mathcal{B}})^2$, $\hat{\tau} = \left(\frac{\gamma_{\mathcal{T}}^{x_{dl}^{g}}}{\varrho_g (p_{\mathcal{S}} - p_{\mathcal{W}} \beta_{SIC} \gamma_{\mathcal{T}}^{x_{dl}^{g}})}\right)$, $\varrho_g = P_{\mathcal{B}} \sigma_g^{-2}$.

Proof: See Appendix C.

Corollary 3: For the special case where SIC is ideal, i.e., $\beta_{SIC} = 0$, the outage

probability of a user g can be simplified as follows

$$P_{\mathcal{O}}^{x_{dl}^{g}}|_{\beta_{SIC}=0} \approx \Bigg(1-\frac{1}{\tilde{\alpha_g}\mathcal{R}_{\mathcal{G}}^{2}\tau^{\tilde{\alpha_g}-1}}\Bigg[\Gamma\Big(\frac{1}{\tilde{\alpha_g}},\tau\tilde{h}_{g}^{\tilde{\alpha_g}}\Big)-\Gamma\Big(\frac{1}{\tilde{\alpha_g}},(\tilde{h}_g+ \mathcal{R}_{\mathcal{G}}^{2})^{\tilde{\alpha_g}}\tau\Big)\Bigg]\Bigg)\times IDSP_d + \Bigg(1-\frac{(\gamma_{\mathcal{T}}^{x_{dl}^{g}})^{\tilde{\alpha_g}-1}}{\tilde{\alpha_g}\mathcal{R}_{\mathcal{G}}^{2}(\varrho_g p_{\mathcal{S}})^{\tilde{\alpha_g}-1}}\Bigg[\Gamma\Big(\frac{1}{\tilde{\alpha_g}},\frac{\tilde{h}_{g}^{\tilde{\alpha_g}}}{\varrho_g p_{\mathcal{S}}}\Big)- \Gamma\Big(\frac{1}{\tilde{\alpha_g}},\frac{(\tilde{h}_g+\mathcal{R}_{\mathcal{G}}^{2})^{\tilde{\alpha_g}}(\gamma_{\mathcal{T}}^{x_{dl}^{g}})}{\varrho_g p_{\mathcal{S}}}\Big)\Bigg]\Bigg)\times IDSP_g, \tag{4.20}$$

Proof: Based on (4.19), after some algebraic manipulations with $\beta_{SIC}=0$, Corollary 3 is obtained.

System Throughput in Downlink Transmission

The DL system throughput in the delay-sensitive transmission mode, based on the outage probabilities of aerial and ground users in NOMA pair [59] is given by

$$R_{DL} = (1-P_{\mathcal{O}}^{x_{dl}^{d}})R_{\mathcal{T}}^{x_{dl}^{d}} + (1-P_{\mathcal{O}}^{x_{dl}^{g}})R_{\mathcal{T}}^{x_{dl}^{g}}, \tag{4.21}$$

where, $P_{\mathcal{O}}^{x_{dl}^{d}}$ and $P_{\mathcal{O}}^{x_{dl}^{g}}$ are given in Theorem 1 and 2 respectively.

4.4.2 Uplink Transmission

Here, we evaluate the outage probabilities of aerial and ground users conditioned on the decoding of the highest IDSP signal first by $\mathcal{B}$.

The outage probability of Ground User

Theorem 3 shows the outage probability of a ground user in NOMA pair in uplink transmission.

Theorem 3. The outage probability of a ground user g present in a radius $\mathcal{R}_{\mathcal{G}}$ is

approximated as follows:

$$P_{\mathcal{O}}^{x_{ul}^{g}} \approx \Bigg(1-\sum_{v_1=0}^{\mathcal{V}_1}\sum_{w_1=0}^{\mathcal{W}_1}\varkappa_{v_1}\varkappa_{w_1}\sqrt{(1-\mho_{v_1}^2)(1-\vartheta_{w_1}^2)}\Bigg(e^{-\kappa\tilde{}_{v_1}}-\sum_{n=0}^{m_d-1}\frac{\aleph^n}{n!}\beth\Bigg)\Bigg)\times \\ \Bigg(\sum_{k=0}^{K}\sum_{j=0}^{J}\sum_{t=0}^{m_d}\Lambda\sqrt{(1-\phi_j^2)(1-\phi_k^2)}\Bigg(\frac{s_j s_k}{\binom{m_d}{t}\mathcal{Y}^t\mathcal{X}^{m_d-t}}\Bigg)\Bigg)+ \\ \Bigg(1-\sum_{v_2=0}^{\mathcal{V}_2}\sum_{w_2=0}^{\mathcal{W}_2}\varkappa_{v_2}\varkappa_{w_2}\sqrt{(1-\mho_{v_2}^2)(1-\vartheta_{w_2}^2)}\times\Bigg(e^{-\tilde{\kappa}_{\breve{v}}}-\sum_{n=0}^{m_d-1}\frac{\digamma^n}{n!}\tilde{\beth}\Bigg)\Bigg)\times \\ \Bigg(1-\sum_{k=0}^{K}\sum_{j=0}^{J}\sum_{t=0}^{m_d}\Lambda\sqrt{(1-\phi_j^2)(1-\phi_k^2)}\Bigg(\frac{s_j s_k}{\binom{m_d}{t}\mathcal{Y}^t\mathcal{X}^{m_d-t}}\Bigg)\Bigg), \tag{4.22}$$

where, $\varkappa_{v\epsilon\{v_1,v_2\}}=\dfrac{\pi p_v}{\mathcal{V}\mathcal{R}_{\mathcal{G}}}$,$\mho_v=\cos\left(\dfrac{2v-1}{2\mathcal{V}}\pi\right)$, $p_v=\dfrac{\mathcal{R}_{\mathcal{G}}(\mho_v+1)}{2}$, $\breve{p_v}=\left(\sqrt{p_v^2+(h_g-h_{\mathcal{B}})^2}\right)^{\alpha_g}$, $\kappa\tilde{}_v=\dfrac{(2^{R_{\mathcal{T}}^{x_{ul}^g}}-1)\breve{p_v}}{\mu_g\hat{\varrho}_g}$, $\varkappa_{w\epsilon\{w_1,w_2\}}=\dfrac{\pi q_w}{\mathcal{W}\mathcal{R}_{\mathcal{D}}}$, $q_w=\dfrac{\mathcal{R}_{\mathcal{D}}(\vartheta_w+1)}{2}$, $\breve{q_w}=\left(\sqrt{q_w^2+(h_d-h_{\mathcal{B}})^2}\right)^{\alpha_d}$, $\aleph=\dfrac{m_d\hat{\varrho}_g\breve{q_w}}{\gamma_{\mathcal{T}}^{x_{ul}^g}\hat{\varrho}_d\breve{p_v}}$, $\vartheta_w=\cos\left(\dfrac{2w-1}{2\mathcal{W}}\pi\right)$, $\beth=e^{-\kappa\tilde{}_{v_1}}\Gamma(n+1)\left(\dfrac{\aleph}{m_d}+\dfrac{1}{\mu_g}\right)^{-n-1}$,$\hat{\varrho}_{i\epsilon\{d,g\}}=P_i\sigma_{\mathcal{B}}^{-2}$, $\digamma=\dfrac{m_d\hat{\varrho}_g\breve{q_w}}{\gamma_{\mathcal{T}}^{x_{ul}^g}\hat{\beta_{SIC}}\varrho_d\breve{p_v}}$, $\tilde{\beth}=e^{-\kappa\tilde{}_{v_2}}\Gamma(n+1)\left(\dfrac{\digamma}{m_d}+\dfrac{1}{\mu_g}\right)^{-n-1}$, and $\mathcal{V}\epsilon\{\mathcal{V}_1,\mathcal{V}_2\}$, $\mathcal{W}\epsilon\{\mathcal{W}_1,\mathcal{W}_2\}$ are Cheybshev-approximation parameters.

Proof: See Appendix D.

Corollary 4: For the special case where SIC is ideal at $\mathcal{B}$, i.e., $\beta_{SIC}=0$, the outage probability of a user g in UL can be simplified as follows

$$P_{\mathcal{O}}^{x_{ul}^{g}} \approx \Bigg(1-\sum_{v_1=0}^{\mathcal{V}_1}\sum_{w_1=0}^{\mathcal{W}_1}\varkappa_{v_1}\varkappa_{w_1}\sqrt{(1-\mho_{v_1}^2)(1-\vartheta_{w_1}^2)}\Bigg(e^{-\kappa\tilde{}_{v_1}}-\sum_{n=0}^{m_d-1}\frac{\aleph^n}{n!}\beth\Bigg)\Bigg)\times \\ IDSP_g+ \\ \Bigg(1-\frac{2}{\alpha_g\mathcal{R}_{\mathcal{G}}}\Bigg(\frac{\hat{\varrho}_g}{2^{R_{\mathcal{T}}^{x_{ul}^g}}-1}\Bigg)^{2\alpha_g^{-1}}\Bigg)\Bigg(\sum_{k=0}^{\tilde{m}}\exp(-\tilde{h}_g^{\alpha_g}\tilde{\gamma}_g)\frac{(\tilde{h}_g^{\alpha_g}\tilde{\gamma}_g)^k}{k!}- \\ \sum_{k=0}^{\tilde{m}}\exp(-\sqrt{\mathcal{R}_{\mathcal{G}}^2+\tilde{h}_g^2}^{\alpha_g}\tilde{\gamma}_g)\frac{\sqrt{\mathcal{R}_{\mathcal{G}}^2+\tilde{h}_g^2}^{\alpha_g}\tilde{\gamma}_g}{k!}\Bigg)\times IDSP_d, \tag{4.23}$$

where, $\tilde{m}=2\alpha_g^{-1}-1$, $\tilde{\gamma}_g=\dfrac{\gamma_{\mathcal{T}}^{x_{ul}^g}}{\hat{\varrho}_g}$.

Proof: Substituting $\beta_{SIC}=0$ in simplifying (D.7) and after some algebraic manipulations, we obtain (4.23).

The outage probability of Aerial User

The outage probability of user d in UL transmission is expressed in Theorem 4.

Theorem 4. The outage probability of aerial user d in ground-aerial NOMA is given as follows

$$P_{\mathcal{O}}^{x_{ul}^{d}} \approx \Bigg(1-\sum_{k=0}^{m_d-1}\sum_{\hat{k}=0}^{k}\sum_{e_1=0}^{\mathcal{E}_1}\sum_{f_1=0}^{\mathcal{F}_1}\frac{\exp(-\chi_{e_1})\beta_{SIC}^{k}\Lambda_*}{\hat{k}!}\left(\frac{\beta_{SIC}\hat{\varrho}_g\chi_{e_1}}{\tilde{s}_{f_1}^{\alpha_g}}+\frac{1}{\mu_g}\right)^{-k-1}$$
$$\left(\chi_{e_1}+\frac{\tilde{s}_{f_1}^{\alpha_g}}{\hat{\varrho}_g\beta_{SIC}\mu_g}\right)^{\hat{k}}\Bigg)\Bigg(\sum_{k=0}^{K}\sum_{j=0}^{J}\sum_{t=0}^{m_d}\Lambda\sqrt{(1-\phi_j^2)(1-\phi_k^2)}$$
$$\left(\frac{s_j s_k}{\binom{m_d}{t}\mathcal{Y}^t\mathcal{X}^{m_d-t}}\right)\Bigg)+\Bigg(1-\sum_{k=0}^{m_d-1}\sum_{\hat{k}=0}^{k}\sum_{e_2=0}^{\mathcal{E}_2}\sum_{f_2=0}^{\mathcal{F}_2}\frac{\exp(-\chi_{e_2})\Lambda_*}{\hat{k}!} \tag{4.24}$$
$$\left(\frac{\hat{\varrho}_g\chi_{e_2}}{\tilde{s}_{f_2}^{\alpha_g}}+\frac{1}{\mu_g}\right)^{-k-1}\left(\chi_{e_2}+\frac{\tilde{s}_{f_2}^{\alpha_g}}{\hat{\varrho}_g\mu_g}\right)^{\hat{k}}\Bigg)\Bigg(1-\sum_{k=0}^{K}\sum_{j=0}^{J}\sum_{t=0}^{m_d}\Lambda$$
$$\sqrt{(1-\phi_j^2)(1-\phi_k^2)}\left(\frac{s_j s_k}{\binom{m_d}{t}\mathcal{Y}^t\mathcal{X}^{m_d-t}}\right)\Bigg),$$

where, $\tilde{t}_{e\epsilon\{e_1,e_2\}}=\sqrt{t_e+(h_d-h_{\mathcal{B}})^2}$, $\tilde{s}_{f\epsilon\{f_1,f_2\}}=\sqrt{s_f+(h_g-h_{\mathcal{B}})^2}$, $\psi_f=\cos\left(\frac{2f-1}{2\mathcal{F}}\pi\right)$, $\psi_e=\cos\left(\frac{2e-1}{2\mathcal{E}}\pi\right)$, $\Lambda_*=\frac{\pi^2(\hat{\varrho}_g\chi_e)^k\sqrt{(1-\psi_e^2)(1-\psi_f^2)}}{\mathcal{R}_{\mathcal{D}}\mathcal{R}_{\mathcal{G}}k!\tilde{s}_f^{\alpha_g k}\mathcal{E}\mathcal{F}}$, $\chi_e=\frac{m_d\gamma_{\mathcal{T}}^{x_{ul}^{d}}\tilde{t}_e^{\alpha_d}}{\hat{\varrho}_d}$, $t_e=\frac{\mathcal{R}_{\mathcal{D}}(\psi_e+1)}{2}$, $s_f=\frac{\mathcal{R}_{\mathcal{G}}(\psi_f+1)}{2}$, $\mathcal{E}\epsilon\{\mathcal{E}_1,\mathcal{E}_2\}$, and $\mathcal{F}\epsilon\{\mathcal{F}_1,\mathcal{F}_2\}$ are Cheybshev approximation parameters.

Proof: See Appendix E.

Corollary 5: For the special case where SIC is ideal at $\mathcal{B}$, i.e., $\beta_{SIC}=0$, the outage probability of a user d in UL can be simplified as follows

$$P_{\mathcal{O}}^{x_{ul}^{d}} \approx \left(1-\sum_{e_1=0}^{\mathcal{E}_1}\sum_{k=0}^{m_d-1}\frac{\pi}{\mathcal{R}_{\mathcal{D}}\mathcal{E}_1}\left(\frac{m_d(2^{R_{\mathcal{T}}^{x_{dl}^{d}}}-1)}{\hat{\varrho}_d}\right)^{k}\sqrt{1-\psi_{e_1}^2}\,t_{e_1}^{(\alpha_d+1)}\right.$$
$$\left.e^{-\chi_d\tilde{t}_{e_1}^{\alpha_d}}\right)\times IDSP_g+\left(1-\sum_{k=0}^{m_d-1}\sum_{\hat{k}=0}^{k}\sum_{e_2=0}^{\mathcal{E}_2}\sum_{f_2=0}^{\mathcal{F}_2}\frac{\exp(-\chi_{e_2})\Lambda_*}{\hat{k}!}\right. \tag{4.25}$$
$$\left.\left(\frac{\hat{\varrho}_g\chi_{e_2}}{\tilde{s}_{f_2}^{\alpha_g}}+\frac{1}{\mu_g}\right)^{-k-1}\left(\chi_{e_2}+\frac{\tilde{s}_{f_2}^{\alpha_g}}{\hat{\varrho}_g\mu_g}\right)^{\hat{k}}\right)\times IDSP_d,$$

Proof: On substituting $\beta_{SIC}=0$ in (E.2), and after simplification, we obtain Corollary 5. This completes the proof.

System Throughput in Uplink Transmission

The uplink system throughput in the delay-sensitive transmission mode, based on the outage probabilities of aerial and ground users in NOMA pair [59] is given by

$$R_{UL} = (1 - P_{\mathcal{O}}^{x_{ul}^d}) R_{\mathcal{T}}^{x_{ul}^d} + (1 - P_{\mathcal{O}}^{x_{ul}^g}) R_{\mathcal{T}}^{x_{ul}^g}, \tag{4.26}$$

where, $P_{\mathcal{O}}^{x_{ul}^g}$ and $P_{\mathcal{O}}^{x_{ul}^d}$ are given in Theorem 3 and 4, respectively.

4.5 Numerical Studies

In this section, we investigate performance of the proposed NOMA transmissions and verify the accuracy of the derived outage expressions by comparing with Monte Carlo simulation runs. We assume normalised unit noise at all nodes, unless otherwise stated. We verify our results with numerical simulations as follows. We simulate in Matlab $\mathcal{N}_{\mathcal{G}}$ ground devices and a UAV on random locations in radius $\mathcal{R}_{\mathcal{G}}$ and $\mathcal{R}_{\mathcal{D}}$ respectively, based on the spatial model presented in Section 4.2 in MATLAB. In each simulation run, a ground user g is selected randomly and paired with user d to perform NOMA transmissions as explained in Section 4.3. The channel fading gain between ground devices and $\mathcal{B}$ is modelled by exponential random variable with mean μ_g (to model Rayleigh fading), while the channel fading gain between aerial user and $\mathcal{B}$ is modelled by a gamma random variable with shape and scale parameters of m_d and Ω_d respectively (to model Nakagami-m fading). For each realisation in downlink and uplink transmissions, if data rate at user node is less than threshold data rate, outage is declared. This is repeated for a number of realisations to evaluate outage probability of each user. These results are then compared with the outage probability results obtained from theorems 1 to 4 for verification of our analysis. The special cases are compared with corollaries presented in Section 4.4.

4.5.1 Instantaneous Distinct Signal Power Assumption

First, we study the assumption of this paper in which we stated that IDSP of ground user and aerial user needs to be evaluated before applying distinct power levels for DL NOMA transmissions and for applying SIC in UL transmissions. We study the impact of different system parameters on the assumption of $IDSP_g$ in the following.

Impact of Path Loss Exponent

As explained earlier, aerial and ground users have distinct channel conditions and may experience different path loss and have difference in spatial characteristics. Fig. 4.2 shows the impact of α_g on the probability of having IDSP of user g greater than user

Table 4.1: Simulation Parameters

Parameters	**Settings**
$p_{\mathcal{W}}$, $p_{\mathcal{S}}$	0.75, 0.25
P_d=P_g	20 dB
α_g	2 (free space), 3, 4, 5
α_d	1.992 , 2.05 [100]
Monte Carlo Runs	100,000
μ_g	≈ 1
Ω_d	1
$\mathcal{R}_{\mathcal{G}}$	50m, unless otherwise stated
$\mathcal{R}_{\mathcal{D}}$	50m, unless otherwise stated
h_d, h_g, $h_{\mathcal{B}}$	50-100m, 0m, 0m
m_d	2,3,4,5
Ω_d	1 [98]
Cheybshev Parameters (J, K, A, B, $\mathcal{E}_1, \mathcal{E}_2, \mathcal{F}_1, \mathcal{F}_2$)	500

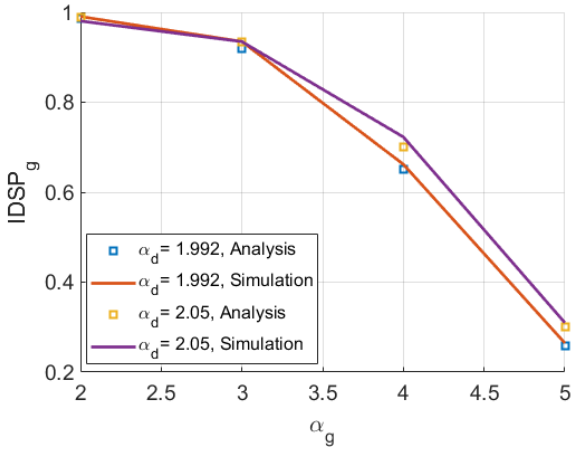

Figure 4.2: Impact of α_g on $IDSP_g$ with $m_d = 2$, $\mathcal{R}_{\mathcal{D}} = \mathcal{R}_{\mathcal{G}} = 50m, h_d = 50m$.

d. We have included the graph with different values of α_d as well. The solid lines show the results obtained from (15) which are well matched with Monte Carlo simulations represented by square boxes. When the value of α_g is small, for example, at $\alpha_g = 2$, the value of $IDSP_g$ is 0.9899 showing that it is reasonable to expect that a ground user will have better channel conditions than aerial user. However, when the path-loss exponent of ground user increases, for example, at α_g=5, $IDSP_g$ reduces significantly to 0.3219 reflecting that a ground user experience poor channel conditions than aerial user despite of its shorter distance to $\mathcal{B}$ than aerial user d. Hence in such conditions ranking aerial and ground users only on the basis of distance is not ideal and our model overcomes this shortcoming by including the assumption of $IDSP_d$ in outage analysis.

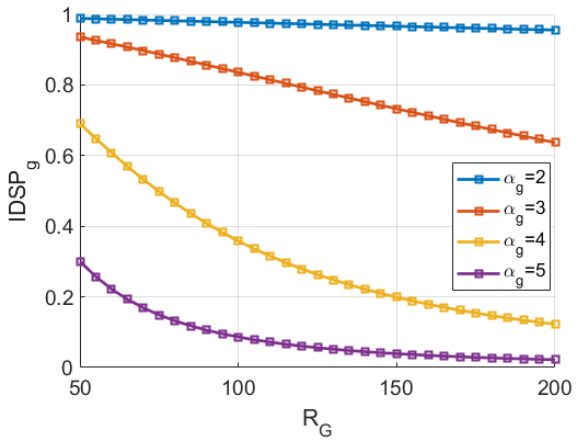

Figure 4.3: Impact of $\mathcal{R}_{\mathcal{G}}$ on $IDSP_g$ with $m_d = 2, \mathcal{R}_{\mathcal{D}} = 50m, \alpha_d = 2.05, h_d = 50m$.

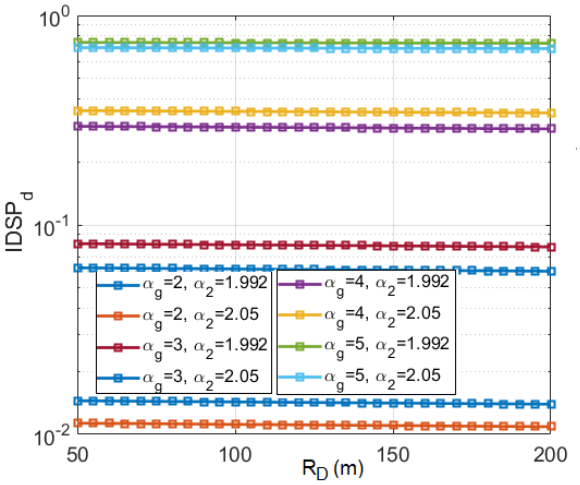

Figure 4.4: Impact of $\mathcal{R}_{\mathcal{D}}$ on $IDSP_d$ with $m_d = 2, \mathcal{R}_{\mathcal{G}} = 50m, \alpha_g = 2, h_d = 50m$.

Impact of Coverage Radius

In Fig. 4.3, we illustrate $IDSP_g$ as a function of $\mathcal{R}_{\mathcal{G}}$. $\mathcal{R}_{\mathcal{D}}$ is fixed at 50m. As is seen on Fig. 4.3, the probability of having instantaneous distinct signal power of ground user greater than aerial user decreases with an increase in the coverage radius of ground users. This can be understood as a user located farther away from the BS experiences higher large scale fading which in turn reduces the received IDSP of ground user and a decline in $IDSP_g$ occurs. It can also be noticed that when aerial and ground users are present within the same radius of, for example, 50m, the probability of having $IDSP_g$ greater than $IDSP_d$ is close to 1 for $\alpha_g = 2$ and it reduces substantially when the ground user experiences severe shadowing. To illustrate this observation further, we have plotted $IDSP_d$ versus $\mathcal{R}_{\mathcal{D}}$ in Fig. 4.4. We have taken $\alpha_d = 1.992$ and $\alpha_d = 2.05$ with ground radius fixed at $\mathcal{R}_{\mathcal{G}} = 50m$. We see that the larger radius of drone does

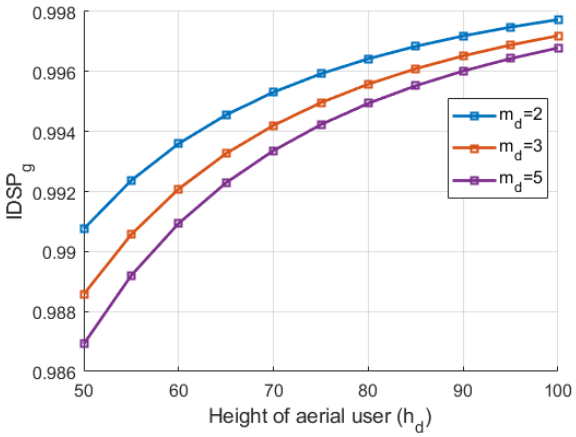

Figure 4.5: Impact of h_d on $IDSP_g$ with $\alpha_d = 2.05, \alpha_g = 2$.

not substantially affect the $IDSP_d$ as the total distance of drone from the source is measured in 3D coordinates by considering its altitude as well.

Impact of Fading and Height

In Fig. 4.5, $IDSP_g$ is plotted as a function of height of user d with multiple values of m_d. This finding coincides with the previous analysis of Fig. 4.3. Intuitively, as the height of aerial user increases it goes far away from $\mathcal{B}$ resulting in lower $IDSP_d$. We can see that with better fading conditions, the value of $IDSP_g$ is slightly less for the same height of user d the impact of BS-to-d channel fading is less significant. Intuitively, this looks reasonable as with improved fading conditions between B and user d, the impact of Nakagami-m fading channel power is less than that of distance-dependant path-loss.

4.5.2 Downlink Transmissions

After analysing the impact of different system parameters on the assumptions, we now explain the outage analysis of both users in DL transmission.

Impact of Transmit Power and Power Allocation

We study the impact of transmit power on the outage of user d and a typical user g in a NOMA pair with variable data rates in Fig. 4.6. The simulation parameters taken are $\alpha_d = 2.05$, $\alpha_g = 2$, $m_d = 2$, $h_d = 50m$, $\mathcal{R}_\mathcal{D} = \mathcal{R}_\mathcal{G} = 100m$, and $\beta_{SIC} = 0.1$. Fig. 4.6 shows that the outage probabilities of the aerial user and ground user decrease with increasing transmit SNR confirming that with a fixed power allocation, a ground-aerial user pair can be served with equal or unequal data rate requirements. The dashed lines in Fig. 4.6 represent $P_\mathcal{O}^{x^{dl}}$, that are the results obtained from (4.17), while solid straight lines represent $P_\mathcal{O}^{x^{dl}}$, depicting the results obtained from (4.19).

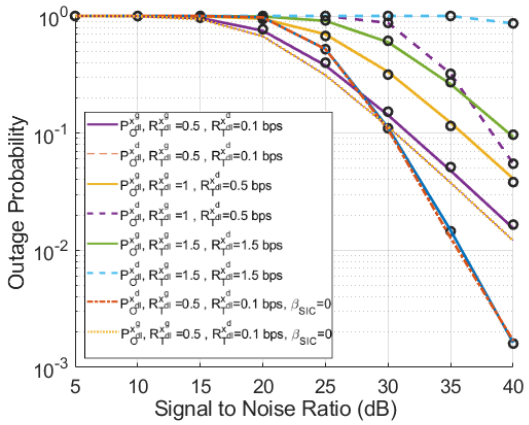

Figure 4.6: Outage of user d and user g in DL transmission, $\beta_{SIC} = 0.1$.

Monte Carlo simulations are represented with round markers which match closely with the theoretical results, verifying closed-form expressions obtained in Theorem 1 and Theorem 2 respectively. We plotted perfect SIC case for both users from (4.18) and (4.20) with dotted lines, as specified in the legend of Fig. 4.6. It is clear that with ideal SIC, the outage of users is improved. Furthermore, it can be observed that the data rates for both users need to be chosen carefully to achieve acceptable level of coverage. In Fig. 4.7, we illustrate the impact of power allocation coefficient on the outage probability of drone and aerial user. The associated parameters are chosen as $\alpha_d = 1.992$, $\alpha_g = 2$, $\mathcal{R}_{\mathcal{G}} = \mathcal{R}_{\mathcal{D}} = 50m$, $R_{\mathcal{T}}^{x_{dl}^d} = 0.1bps, R_{\mathcal{T}}^{x_{dl}^g} = 0.5bps$. From Fig. 4.7, on assigning more power, there is an apparent decrease in the downlink outage of strong user (ground user), which is evaluated on the basis of IDSP. An obvious increase in the outage of weak user is also observed here. While the data rate of the aerial user is less than that of the ground user, equal outage is observed at both users when approximately 35% of the power is dedicated for the ground user. The effect of increasing the value of m_d on $P_{\mathcal{O}}^{x_{dl}^g}$ and on $P_{\mathcal{O}}^{x_{dl}^d}$ is also visible in Fig. 4.7. Increasing m_d results in significant reduction in the outage of the aerial user due to reduced fading. It is demonstrated that in ground-aerial NOMA, with the static power allocation of aerial and ground user, existence of line of sight (increased value of m_d) in aerial user results in the variation of signal outage for both users. We also show the superiority of the proposed scheme against the baseline NOMA transmission in Fig. 4.8. The chosen parameters are $\alpha_d = 2.05$, $\alpha_g = 5$, $m_d = 5$, $R_{\mathcal{T}}^{x_{dl}^d} = 0.1bps, R_{\mathcal{T}}^{x_{dl}^g} = 0.5bps$, $\beta_{SIC} = 0.1$. By considering the environment and channel characteristics of the aerial and ground users individually, power allocation is done for both which results in reduced outage of the received signals. However, if these factors are not considered and power assignment is done conventionally, considering similar environmental conditions for the aerial and ground user, the outage appears to increase.

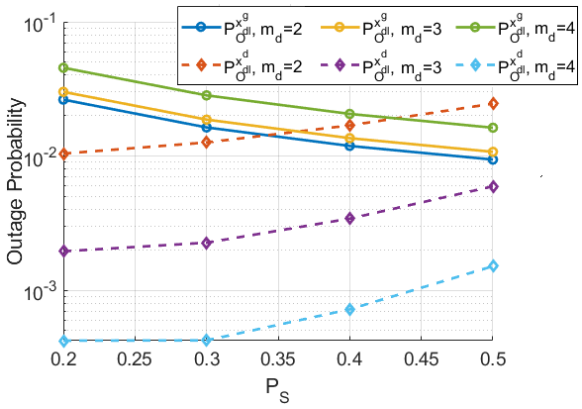

Figure 4.7: Outage of user d and user g in DL transmission vs. Power allocation, $\beta_{SIC} = 0.1$.

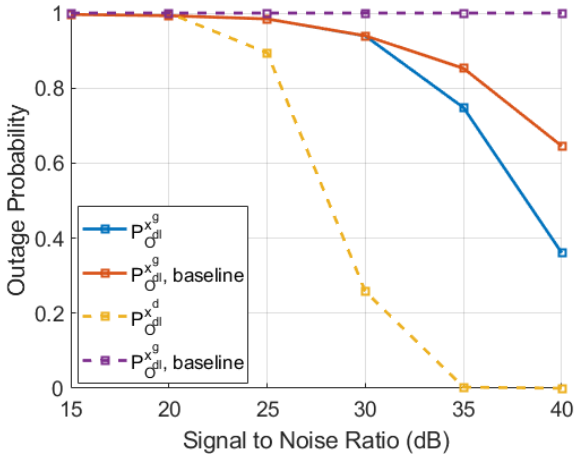

Figure 4.8: Comparison of Outage of user d and user g in DL transmission with baseline scheme.

Impact of Path Loss Exponent

Fig. 4.9 illustrates the impact of path loss exponent α_g on the outage of the ground user. To give a clear explanation, the outage of drone user is also plotted in the figure. It can be seen that with an increase in the value of α_g, the ground user experiences more outage and this is because of increased distance-dependant loss in ground user. Quite interestingly, the outage increases more dominantly when ground user experiences shadowed urban environment as compared to rural. This is because when aerial user has better channel conditions, the distance dependant path loss of aerial user is less than the ground user, in such cases the ground user acts as weak user and aerial user employs SIC which in return increases outage. This impact can be further explained with the plot of $P^{x^d_{dl}}_{\mathcal{O}}$ in Fig. 4.9 , where it can be noticed that outage of drone user also gets impacted with the increased value of α_g.

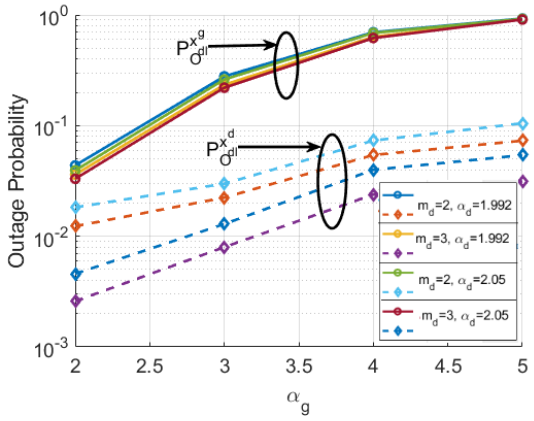

Figure 4.9: Outage Probability of the users vs. α_g, $p_{\mathcal{S}} = 30$dB, h_d= 50m, β_{SIC}= 0.1, $\mathcal{R}_{\mathcal{T}}^{x^d_{dl}} = 0.1$ bps, and $\mathcal{R}_{\mathcal{T}}^{x^g_{dl}} = 0.5$ bps.

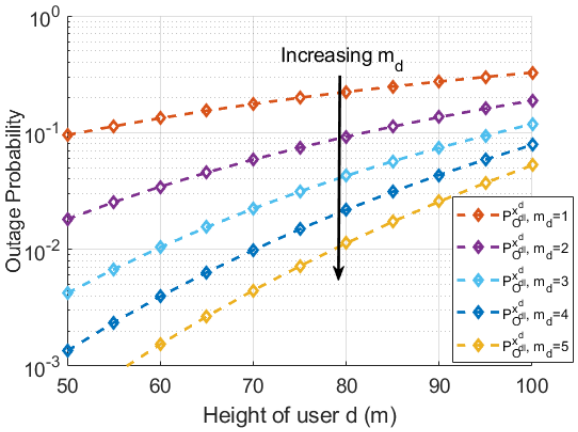

Figure 4.10: Outage Probability of user d vs. h_d, $\alpha_d = 2.05, \alpha_g = 1.992, \beta_{SIC} = 0.1$.

Impact of Fading and Height

We compute the outage probability of user d as a function of user d's height in Fig. 4.10. The other simulation parameters are $\alpha_d = 2.05$, $\alpha_g = 1.992$, $\mathcal{R}_{\mathcal{D}} = \mathcal{R}_{\mathcal{G}} = 100m$ and $\beta_{SIC} = 0.1$. As expected, when the height of user d is increased, the received SINR deteriorates leading to increased outage of user d. Note that when we simulate less-severe fading conditions for aerial user with increased value of m_d, the outage experienced is lesser due to decrease in variance of SINR. This is applicable to drone users since they are in the air and experience less fading than ground users deployed in densely-populated environment usually.

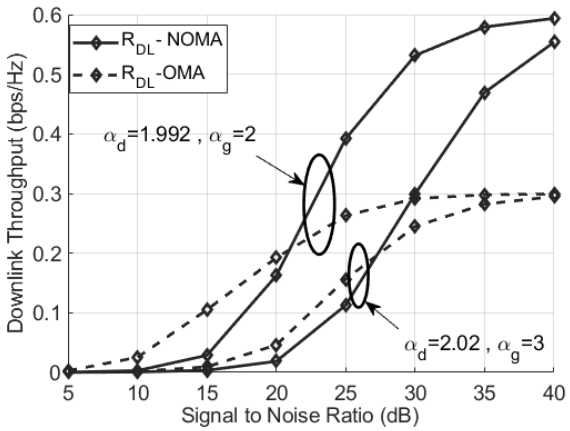

Figure 4.11: Downlink System Throughput (NOMA vs. OMA), $h_d = 50m$, $m_d = 2$, $\beta_{SIC} = 0.1$ $\mathcal{R}_{\mathcal{T}}^{x_{dl}^d} = 0.1$ bps, and $\mathcal{R}_{\mathcal{T}}^{x_{dl}^g} = 0.5$ bps.

Downlink Throughput

We obtain DL system throughput by (4.21) and plot in Fig. 4.11 with respect to transmit SNR. Fig. 4.11 illustrates that the proposed system achieves superior downlink throughput with improved spectral efficiency than OMA-based transmissions in high SNR region. Interestingly, even with different values of α_d and α_g, NOMA is superior in performance than OMA-based transmissions for serving a ground-aerial user pair in high SNR region.

4.5.3 Uplink Transmissions

In this section, we analyse the results obtained in UL transmissions on employing ground-aerial NOMA.

Impact of Data Rate

We illustrate the UL performance in Fig. 4.12, the outage in UL transmission for the aerial user d and ground user g is plotted vs. uplink SNR. Both users transmit with same power while the other simulation parameters are kept as $\beta_{SIC} = 0.1$, $m_d = 2$, $\alpha_d = 2.05$, $\alpha_g = 2$. It is evident from Fig. 4.12 that for multiple values of $R_{\mathcal{T}}^{x_{ul}^g}$ and $R_{\mathcal{T}}^{x_{ul}^d}$, the mathematical results in (4.22) and (4.24) match with simulations. The slight difference is because of the approximation scheme that we have used. First, we observe that there is poor reception for user d's message in UL even when $R_{\mathcal{T}}^{x_{ul}^g} > R_{\mathcal{T}}^{x_{ul}^d}$. This is because of the fact that user d is situated far at a certain height from $\mathcal{B}$ unlike user g and with the simulation settings, $IDSP_g > IDSP_d$ (see Fig. 4.2), which means that $\mathcal{B}$ decodes the x_{ul}^g first, subtracts it from received signal with 90% accuracy and then decodes x_{ul}^d. It is therefore important to maintain adequate threshold data rates to achieve desirable

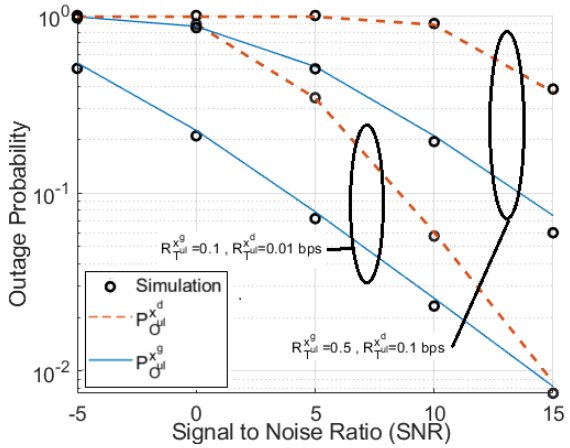

Figure 4.12: Outage of user d and user g in UL transmission, $\beta_{SIC} = 0.1$.

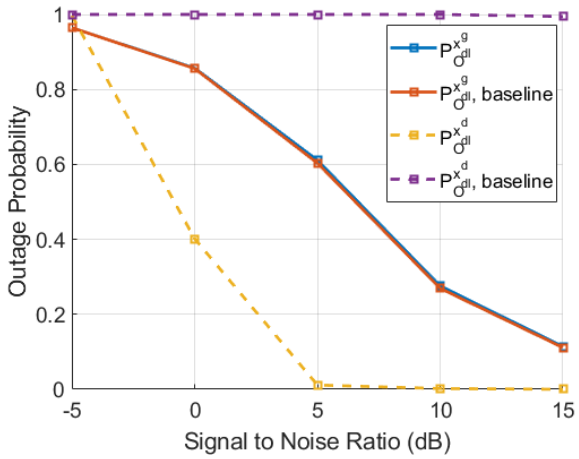

Figure 4.13: Comparison of Outage of user d and user g in UL transmission with baseline scheme.

performance. Similar to downlink transmission, we show the superiority of our scheme in uplink transmission in Fig. 4.13. As can be seen that, there is substantial decrease in the outage of aerial user with our proposed ranking method. This is because our scheme takes into account the individual characteristics of the environmental conditions of aerial users unlike baseline scheme.

Impact of Path Loss Exponent

Fig. 4.14 illustrates the impact of α_g on UL outage behaviour. We also plotted $P_{\mathcal{O}}^{x^d_{ul}}$ and $P_{\mathcal{O}}^{x^g_{ul}}$ for different values of m_d. First, it is to be noticed that $P_{\mathcal{O}}^{x^g_{ul}}$ gets affected significantly with an increased value of path-loss exponent in UL transmission. However, the impact on $P_{\mathcal{O}}^{x^d_{ul}}$ is almost negligible. Nonetheless, as m_d increases the outage performance of user d is reduced notably due to reduced fading effects.

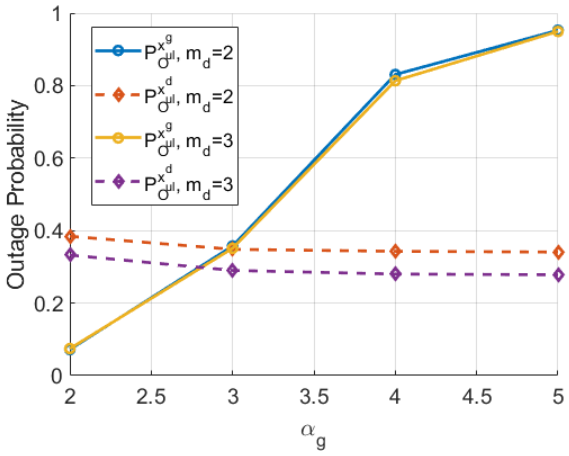

Figure 4.14: Outage of user d and user g vs. α_g, $\alpha_d = 2.05$, $\beta_{SIC} = 0.1$, $m_d = 2$, $h_d = 50m$, $\mathcal{R}_{\mathcal{T}}^{x^d_{ul}} = 0.01$ bps, and $\mathcal{R}_{\mathcal{T}}^{x^g_{ul}} = 0.1$ bps.

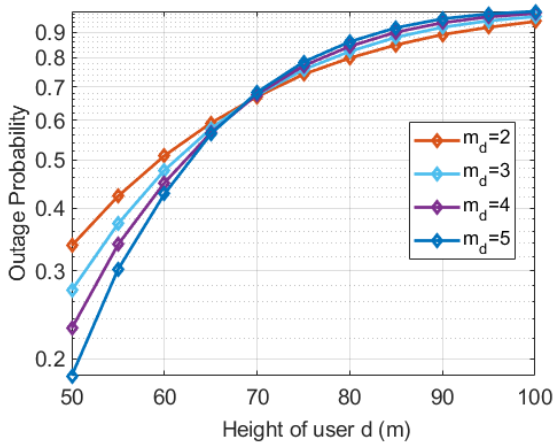

Figure 4.15: Outage of user d vs. h_d, $\beta_{SIC} = 0.1$, $\alpha_d = 2$, $\alpha_d = 1.992$, $\mathcal{R}_{\mathcal{T}}^{x^d_{ul}} = 0.01$ bps, and $\mathcal{R}_{\mathcal{T}}^{x^g_{ul}} = 0.1$ bps.

Impact of Fading and Height

Fig. 4.15 represents the outage performance of user d in UL transmission for increasing value of user d's height with multiple values of m_d. As can be seen in this figure, increasing the m_d has two effects on $P_{\mathcal{O}}^{x^d_{ul}}$: for lower heights of user d, decreasing channel variability ($m_d \uparrow$) improves outage probability, whereas for higher values of h_d, this trend is reversed. All curves intersect interestingly at one point, in this case at around 70m.

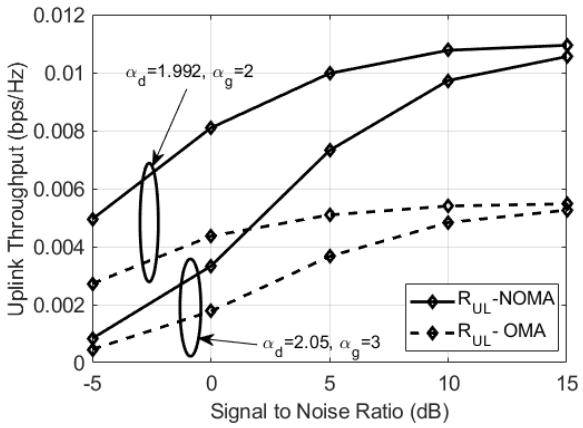

Figure 4.16: Uplink System Throughput (NOMA vs. OMA), $\beta_{SIC} = 0.1$, $\mathcal{R}_{\mathcal{T}}^{x_{ul}^{d}} = 0.01$ bps, and $\mathcal{R}_{\mathcal{T}}^{x_{ul}^{g}} = 0.1$ bps.

Uplink Throughput

The uplink system throughput is plotted against transmit SNR of users in Fig. 4.16 for NOMA-based and OMA-based transmissions. As can be seen that ground-aerial-NOMA-based transmission with IDSP ranking achieves higher throughput than OMA-based transmission. The results in conjunction with Fig. 4.11 affirms that ground-aerial NOMA brings superior throughput than conventional OMA.

4.6 Conclusion and Future Work

In this work, we investigated the outage performance of a ground-aerial user pair to transmit on DL and UL using NOMA. Unlike existing research works, we considered IDSP of the user pair before setting power levels in downlink transmissions. Similarly in decoding received signal in UL transmissions, IDSP is employed to determine the order of successive interference cancellation at BS. The work considered instantaneous-distinct-signal-power-based ranking of both users instead of distance-based ranking because of difference in path loss exponents and fading environments of ground users and the aerial user. We characterised the performance of our proposed model by evaluating outage behaviour at both user ends and system throughput in DL and UL transmissions. We presented simulation results to validate derived mathematical expressions of outage probabilities. We also studied the impact of path-loss exponent, spatial location and fading characteristics of aerial user on the assumption that instantaneous signal power of ground user is higher than that of aerial user. To provide more insights, we studied outage behaviour by varying data rates of the users, fading parameter, path loss exponents and height of aerial user. Subsequently, we showed that NOMA to ground

and aerial user is prevailing in performance than OMA. An interesting future extension of this work is to study the user-selection scheme of ground users and mobility effects of UAV on the transmission. This paper has investigated a single ground-aerial pair of users. Examining the performance with a larger number of users is also recognized as future work.

Appendices

A Proof of Corollary 1

Proof. With the details provided in Section 4.2, we can write $IDSP_g$ as

$$IDSP_g = \mathbb{E}_{u_g,r_d}\Bigg[\mathbb{E}_{|C_g|^2,|C_d|^2}\Bigg[\frac{|C_g|^2}{\left(\sqrt{u_g^2+(h_g-h_{\mathcal{B}})^2}\right)^{\alpha_g}} > \frac{|C_d|^2}{\left(\sqrt{r_d^2+(h_d-h_{\mathcal{B}})^2}\right)^{\alpha_d}}\Bigg]\Bigg], \tag{A.1}$$

As mentioned earlier $|C_g|$ experiences Rayleigh fading while $|C_d|$ exhibits Nakagami-m fading, based on the PDF of powers of channel gain $|C_d|^2$ and $|C_g|^2$ from (4.3) and (4.4) respectively, we express $IDSP_g$ as

$$IDSP_g \overset{(a)}{=} \mathbb{E}_{u_g,r_d}\Bigg[\frac{{m_d}^{m_d}}{{\Omega_d}^{m_d}}\left(\frac{{m_d}^{m_d}}{{\Omega_d}^{m_d}}+\frac{\mathcal{L}_d}{\mu_g\mathcal{L}_g}\right)^{-m_d}\Bigg], \tag{A.2}$$

where (a) is obtained by exponential and Gamma distribution characteristics of $|C_g|^2$ and $|C_d|^2$ respectively and by applying ([61], 3.384) after simplification, for $m_d > 0$. The expectation in (a) is further evaluated by using PDF of link distances of u_g and r_d from (4.1) and (4.2) respectively. Taking $\Delta = \frac{4{m_d}^{m_d}}{\mathcal{R}_{\mathcal{D}}^2\mathcal{R}_{\mathcal{G}}^2{\Omega_d}^{m_d}}$, we express $IDSP_g$ as

$$IDSP_g = \Delta\int_0^{\mathcal{R}_{\mathcal{D}}}\int_0^{\mathcal{R}_{\mathcal{G}}} xy\left(\frac{{m_d}^{m_d}}{{\Omega_d}^{m_d}}+\frac{\left(\sqrt{x^2+(h_g-h_{\mathcal{B}})^2}\right)^{\alpha_g}}{\mu_g\left(\sqrt{y^2+(h_d-h_{\mathcal{B}})^2}\right)^{\alpha_d}}\right)^{-m_d} dx\,dy, \tag{A.3}$$

For many communication scenarios with variable values of $m_d, \alpha_d, \alpha_g, h_g, h_d$, and $h_{\mathcal{B}}$, it is challenging to obtain closed-form expression for the above. In this case, we can use Gaussian Cheybshev Quadrature [81] to approximate double integral in (A.3) as

$$IDSP_g = \sum_{j=0}^{J}\sum_{k=0}^{K}\Lambda\sqrt{(1-\phi_j^2)(1-\phi_k^2)}\left[s_j s_k\left(\frac{{m_d}^{m_d}}{{\Omega_d}^{m_d}}+\frac{s_k'}{s_j'}\right)^{-m_d}\right], \tag{A.4}$$

On applying binomial expansion theorem $(x+y)^n = \sum_{k=0}^{n} {}^nC_k x^{n-k}y^k = \sum_{k=0}^{n} {}^nC_k x^k y^{n-k}$, we obtain Corollary 1 as expressed in (4.15). ■

B Proof of Theorem 1

Proof. We express outage of aerial user d as

$$P_{\mathcal{O}}^{x_{dl}^d} \approx \underbrace{\mathbb{P}\Big(\frac{P_{\mathcal{B}}\omega_d|C_d|^2\mathcal{L}_d}{P_{\mathcal{B}}\omega_g|C_d|^2\mathcal{L}_d+\sigma_d^2} < \gamma_{\mathcal{T}}^{x_{dl}^d}\Big)}_{\Psi_1} IDSP_g + \underbrace{\mathbb{P}\Big(\frac{P_{\mathcal{B}}\omega_d|C_d|^2\mathcal{L}_d}{P_{\mathcal{B}}\omega_g|C_d|^2\mathcal{L}_d\beta_{SIC}+\sigma_d^2} < \gamma_{\mathcal{T}}^{x_{dl}^d}\Big)}_{\Psi_2} IDSP_d, \tag{B.1}$$

where, $\gamma_{\mathcal{T}}^{x_{dl}^d} = 2^{\mathcal{R}_{\mathcal{T}}^{x_{dl}^d}} - 1$. First we apply some algebraic manipulations to obtain Ψ_1 as

$$\Psi_1 = \mathbb{E}_{r_d}\Big[\mathbb{E}_{|C_d|^2}\Big[|\mathcal{C}_d|^2 < \delta_d\Big(\sqrt{r_d^2+(h_d-h_{\mathcal{B}})^2}\Big)^{\alpha_d}|r_d\Big]\Big], \tag{B.2}$$

$$\Psi_1 \overset{(a)}{=} \mathbb{E}_{r_d}\Bigg[1 - \frac{\Gamma\Big(m_d, \frac{m_d}{\Omega_d}\delta_d\Big(\sqrt{r_d^2+(h_d-h_{\mathcal{B}})^2}\Big)^{\alpha_d}\Big)}{\Gamma(m_d)}\Bigg], \tag{B.3}$$

$$\Psi_1 \overset{(b)}{=} 1 - \sum_{s=0}^{m_d-1}\frac{2m_d^s\delta_d^s}{s!\Omega_d{}^s\mathcal{R}_{\mathcal{D}}^2}\int_0^{\mathcal{R}_{\mathcal{D}}} r_d\Big(\sqrt{r_d^2+(h_d-h_{\mathcal{B}})^2}\Big)^{s\alpha_d} \exp\Big(-\frac{m_d}{\Omega_d}\delta_d\Big(\sqrt{r_d^2+(h_d-h_{\mathcal{B}})^2}\Big)^{\alpha_d}\Big)dr_d, \tag{B.4}$$

where *(a)* follows from the cumulative density function (CDF) of gamma random variable $|\mathcal{C}_d|^2$, if $\frac{\omega_d}{\omega_g} > \gamma_T^{x_{dl}^d}$, else $\Psi_1 = 1$. *(b)* follows from the definition of incomplete gamma function for real values of m_d and expectation of r_d is based on its link distance with $\mathcal{B}$ in $\mathcal{R}_{\mathcal{D}}$ from (4.2). For multiple values of α_d and m_d, we approximate Ψ_1 using Gaussian Cheybshev Quadrature [81] as

$$\Psi_1 = \sum_{a=0}^{A}\sum_{s=0}^{m_d-1}\nabla_s\zeta_a\mathcal{J}_a^s\exp\big(-\delta_d m_d\mathcal{J}_a\big), \tag{B.5}$$

To obtain Ψ_2 in (B.1), we apply similar steps as of Ψ_1 and obtain

$$\Psi_2 = \sum_{b=0}^{B}\sum_{s'=0}^{m_d-1}\ddagger_{s'}\zeta_b\mathcal{J}_b^{s'}\exp\big(-\delta'_d m_d\mathcal{J}_b\big), \tag{B.6}$$

Substituting Ψ_1 and Ψ_2 in (B.1) and with the help of Corollary 1, we obtain Theorem 1 as given in (4.17). ■

C Proof of Theorem 2

Proof. The outage of a ground user selected randomly from a radius of $\mathcal{R}_{\mathcal{G}}$ is given as

$$P_{\mathcal{O}}^{x_{dl}^{g}} \approx \underbrace{\mathbb{P}\Big(\frac{P_{\mathcal{B}}\omega_g|C_g|^2\mathcal{L}_g}{P_{\mathcal{B}}\omega_d|C_g|^2\mathcal{L}_g+\sigma_g^2} < \gamma_{\mathcal{T}}^{x_{dl}^{g}}\Big)}_{\Xi_1} IDSP_d + \underbrace{\mathbb{P}\Big(\frac{P_{\mathcal{B}}\omega_g|C_g|^2\mathcal{L}_g}{P_{\mathcal{B}}\omega_d|C_g|^2\mathcal{L}_g\beta_{SIC}+\sigma_g^2} < \gamma_{\mathcal{T}}^{x_{dl}^{g}}\Big)}_{\Xi_2} IDSP_g \tag{C.1}$$

where $\gamma_{\mathcal{T}}^{x_{dl}^{g}} = 2^{\mathcal{R}_{\mathcal{T}}^{x_{dl}^{g}}} - 1$. First, after some algebraic adjustments, we obtain Ξ_1 as

$$\Xi_1 = \mathbb{E}_{u_g}\Big[\mathbb{E}_{|\mathcal{C}_g|^2}\Big[|\mathcal{C}_g|^2 < \tau\Big(\sqrt{u_g^2+(h_g-h_{\mathcal{B}})^2}\Big)^{\alpha_g}|u_g\Big]\Big], \tag{C.2}$$

if $\frac{\omega_g}{\omega_d} > \gamma_T^{x_{dl}^{g}}$, else $\Xi_1 = 1$.Based on PDF of $|\mathcal{C}_g|^2$ and u_g given in section II, we evaluate above expectations as

$$\Xi_1 = 1 - \frac{2}{\mathcal{R}_{\mathcal{G}}^2}\int_0^{\mathcal{R}_{\mathcal{G}}} \exp\Big(-\frac{\tau}{\mu_g}\Big(\sqrt{u_g^2+(h_g-h_{\mathcal{B}})^2}\Big)^{\alpha_g}\Big)u_g du_g, \tag{C.3}$$

$$\Xi_1 \overset{(a)}{=} 1 - \frac{2}{\mathcal{R}_{\mathcal{G}}^2}\int_{\sqrt{\tilde{h}_g}}^{\sqrt{\mathcal{R}_{\mathcal{G}}^2+\tilde{h}_g}} \exp\Big(-\frac{\tau}{\mu_g}x_1^{\alpha_g}\Big)x_1 dx_1, \tag{C.4}$$

$$\Xi_1 \overset{(b)}{=} 1 - \frac{2}{\mathcal{R}_{\mathcal{G}}^2}\int_{\tilde{h}_g^{\tilde{\alpha_g}}}^{(\mathcal{R}_{\mathcal{G}}^2+\tilde{h}_g)^{\tilde{\alpha_g}}} \exp\Big(-\frac{\tau}{\mu_g}x_2\Big)x_2^{\tilde{\alpha_g}-1} dx_2, \tag{C.5}$$

$$\Xi_1 \overset{(c)}{=} 1 - \frac{{\mu_g}^{\tilde{\alpha_g}^{-1}}}{\tilde{\alpha_g}\mathcal{R}_{\mathcal{G}}^2\tau^{\tilde{\alpha_g}^{-1}}}\Big[\Gamma\Big(\frac{1}{\tilde{\alpha_g}},\frac{\tau}{\mu_g}\tilde{h}_g^{\tilde{\alpha_g}}\Big) - \Gamma\Big(\frac{1}{\tilde{\alpha_g}},(\tilde{h}_g+\mathcal{R}_{\mathcal{G}}^2)^{\tilde{\alpha_g}}\frac{\tau}{\mu_g}\Big)\Big], \tag{C.6}$$

where (a) is obtained by change of variable and (b) follows with $x_2 \to x_1^{\alpha_g}$ and (c) on applying ([61], 3.351.1) $\int_0^u x^n e^{-\mu x}dx = \mu^{-(n+1)}(\Gamma(n+1)-\Gamma(n+1,\mu u))$ with some algebraic manipulations.

Following similar steps as Ξ_2, we obtain Ξ_2 as

$$\Xi_2 = 1 - \frac{1}{\tilde{\alpha_g}\mathcal{R}_{\mathcal{G}}^2\hat{\tau}^{\tilde{\alpha_g}^{-1}}}\Big[\Gamma\Big(\frac{1}{\tilde{\alpha_g}},\hat{\tau}\tilde{h}_g^{\tilde{\alpha_g}}\Big) - \Gamma\Big(\frac{1}{\tilde{\alpha_g}},(\tilde{h}_g+\mathcal{R}_{\mathcal{G}}^2)^{\tilde{\alpha_g}}\hat{\tau}\Big)\Big], \tag{C.7}$$

Substituting (C.6), (C.7), (15) and (16) in (C.1), we obtain Theorem 2 as given in (4.19). ∎

D Proof of Theorem 3

Proof. From details mentioned in Section 4.2, we can express $P_{\mathcal{O}}^{x_{ul}^g}$ as

$$P_{\mathcal{O}}^{x_{ul}^g} \approx \underbrace{\mathbb{P}\Big(\frac{P_g|C_g|^2\mathcal{L}_g}{P_d|C_d|^2\mathcal{L}_d+\sigma_{\mathcal{B}}^2} < \gamma_{\mathcal{T}}^{x_{ul}^g}\Big)}_{\Xi_1^*} IDSP_g + \underbrace{\mathbb{P}\Big(\frac{P_g|C_g|^2\mathcal{L}_g}{P_d|C_d|^2\mathcal{L}_d\beta_{SIC}+\sigma_{\mathcal{B}}^2} < \gamma_{\mathcal{T}}^{x_{ul}^g}\Big)}_{\Xi_2^*} IDSP_d \tag{D.1}$$

where, $\gamma_{\mathcal{T}}^{x_{ul}^g} = 2^{\mathcal{R}_{\mathcal{T}}^{x_{ul}^g}} - 1$. By considering, $\tilde{\kappa} = \dfrac{\gamma_{\mathcal{T}}^{x_{ul}^g}\sqrt{r_g^2+(h_g-h_{\mathcal{B}})^2}^{-\alpha_g}}{\hat{\varrho}_g}$, we simplify Ξ_1^* as follows

$$\Xi_1^* = \mathbb{P}\Big(|\mathcal{C}_g|^2 < \tilde{\kappa}\Big(\hat{\varrho}_d\Big(\sqrt{r_d^2+(h_d-h_{\mathcal{B}})^2}^{\alpha_d}\Big)|\mathcal{C}_d|^2+1\Big)\Big), \tag{D.2}$$

$$\Xi_1^* \overset{(a)}{=} 1 - \frac{1}{\Gamma(m_d)}\int_{\tilde{\kappa}}^{\infty}\Big(e^{-\frac{x}{\mu_g}}\gamma(m_d, m_d\wp)\Big), \tag{D.3}$$

where, $\wp = \dfrac{\sqrt{r_d^2+(h_d-h_{\mathcal{B}})^2}^{\alpha_d}(x-\tilde{\kappa})}{\tilde{\kappa}\hat{\varrho}_d}$. *(a)* is obtained using PDF of $|\mathcal{C}_d|^2$ and $|\mathcal{C}_g|^2$ defined in section II and after applying ([61], 3.381.1). For further simplification, we use $\gamma(n,x) = (n-1)![1-e^{-x}\sum_{k=0}^{n-1}x^k/k!]$ ([61], 8.352.6) and apply ([61], 3.382.2) on (D.3) and after taking $\breve{\Upsilon} \to \sqrt{r_d^2+(h_d-h_{\mathcal{B}})^2}^{\alpha_d}(\hat{\varrho}_d\tilde{\kappa})^{-1}$, we obtain

$$\Xi_1^* = 1 - \mathbb{E}_{r_d,u_g}\underbrace{\Big[e^{-\tilde{\kappa}\mu_g^{-1}}\Big(1-\sum_{n=0}^{m_d-1}\frac{m_d^n}{n!}(\breve{\Upsilon})^n(m_d\breve{\Upsilon}+\frac{1}{\mu_g})^{-n-1}\Gamma(n+1)\Big)\Big]}_{\tilde{\Delta}}, \tag{D.4}$$

To solve the expectation in (D.4), we apply PDF of u_g and r_d from (4.1) and (4.2) respectively to obtain Ξ_1^* as

$$\Xi_1^* = 1 - \frac{4}{\mathcal{R}_{\mathcal{G}}^2\mathcal{R}_{\mathcal{D}}^2}\int_0^{\mathcal{R}_{\mathcal{G}}}\int_0^{\mathcal{R}_{\mathcal{D}}}\tilde{\Delta}.u_g.r_d du_g dr_d, \tag{D.5}$$

As mentioned earlier, the communication scenarios are distinct with multiple values of α_d and α_g. Hence, conventional integration techniques may not be applicable on (D.5) for further simplification, so we apply Gaussian-Cheybshev Quadrature and obtain Ξ_1^* as

$$\Xi_1^* = 1 - \sum_{v=0}^{\mathcal{V}}\varkappa_v\sqrt{1-\mho_v^2}\sum_{w=0}^{\mathcal{W}}\varkappa_w\sqrt{1-\vartheta_w^2}\Big(e^{-\tilde{\kappa_v}} - \sum_{n=0}^{m_d-1}\frac{\aleph^n}{n!}\beth\Big), \tag{D.6}$$

Following the steps from (D.1) to (D.6), Ξ_2^* is obtained as

$$\Xi_2^* = 1 - \sum_{\tilde{v}=0}^{\tilde{\mathcal{V}}} \varkappa_{\tilde{v}} \sqrt{1-\mho_{\tilde{v}}^2} \sum_{\tilde{w}=0}^{\tilde{\mathcal{W}}} \varkappa_{\tilde{w}} \sqrt{1-\vartheta_{\tilde{w}}^2} \Big(e^{-\tilde{\kappa}_{\tilde{v}}} - \sum_{n=0}^{m_d-1} \frac{\digamma^n}{n!} \tilde{\beth} \Big), \tag{D.7}$$

Substituting (D.6), (4.15), (4.16) and (D.7) in (D.1), we get Theorem 3 as expressed in (4.22). ■

E Proof of Theorem 4

Proof. We express $P_{\mathcal{O}}^{x_{ul}^d}$ as

$$\begin{aligned} P_{\mathcal{O}}^{x_{ul}^d} \approx \underbrace{\mathbb{P}\Big(\frac{P_d |C_d|^2 \mathcal{L}_d}{P_g |C_g|^2 \mathcal{L}_g \beta_{SIC} + \sigma_{\mathcal{B}}^2} < \gamma_{\mathcal{T}}^{x_{ul}^d} \Big)}_{\Psi_1^*} IDSP_g + \\ \underbrace{\mathbb{P}\Big(\frac{P_d |C_d|^2 \mathcal{L}_d}{P_g |C_g|^2 \mathcal{L}_g + \sigma_{\mathcal{B}}^2} < \gamma_{\mathcal{T}}^{x_{ul}^d} \Big)}_{\Psi_2^*} IDSP_d \end{aligned} \tag{E.1}$$

where, $\gamma_{\mathcal{T}}^{x_{ul}^d} = 2^{\mathcal{R}_{\mathcal{T}}^{x_{ul}^d}} - 1$.

We now compute Ψ_1^*, after some simplification, Ψ_1^* is expressed as

$$\Psi_1^* = \mathbb{P}\Bigg(|C_d|^2 < \frac{\gamma_{\mathcal{T}}^{x_{ul}^d} \beta_{SIC} \hat{\varrho}_g \mathcal{L}_g}{\mathcal{L}_d} |C_g|^2 + \frac{\gamma_{\mathcal{T}}^{x_{ul}^d}}{\hat{\varrho}_d \mathcal{L}_d} \Bigg) \tag{E.2}$$

After some algebraic manipulation, and taking $\wp \to \frac{\gamma_{\mathcal{T}}^{x_{ul}^d} \beta_{SIC} \hat{\varrho}_g \mathcal{L}_g}{\mathcal{L}_d}, \varsigma \to \frac{\gamma_{\mathcal{T}}^{x_{ul}^d}}{\hat{\varrho}_d \mathcal{L}_d}, \mathcal{U} \to \frac{1}{\hat{\varrho}_g \beta_{SIC} \mathcal{L}_g}$, where (a) is obtained on applying PDF of gamma random variable $|C_d|^2$ and PDF of exponential random variable $|C_g|^2$ and on substituting $\Gamma(n,x) = (n-1)![e^{-x}\sum_{k=0}^{n-1} x^k/k!]$ ([61], 8.354.4). (b) is computed using ([61], 3.382.4) with some algebraic simplification, while (c) is obtained by applying series representation of gamma variable mentioned earlier. On applying the PDF of r_d and u_g, we obtain (d). Since double integral in (E.6) is difficult to solve with conventional integration techniques for multiple values of m_d, so we apply Gaussian Cheybshev Quadrature technique on (d) to obtain (e) as in (E.7) where, using similar steps from (E.2) to (E.7), Ψ_2^* is given as in (E.9). Substituting (E.8), (E.9), (4.12) and (4.13) in (E.1), we obtain Theorem 4. This completes the proof. ■

F DRC 16 Form

$$\Psi_1^* \overset{(a)}{=} 1 - \sum_{k=0}^{m_d-1} \frac{(m_d \wp)^k}{\mu_g k!} \int_{z=0}^{\infty} \exp\big(- (m_d(\varsigma + \wp y) + \mu_g^{-1} y)\big)(y+\mathcal{U})^k dy, \tag{E.3}$$

$$\Psi_1^* \overset{(b)}{=} 1 - \sum_{k=0}^{m_d-1} \frac{(m_d \wp)^k}{k!} e^{\mathcal{U}\mu_g^{-1}} \Big(m_d \wp + \frac{1}{\mu_g}\Big)^{-k-1} \Gamma\Big(k+1, (m\varsigma + \mathcal{U}\mu_g^{-1})\Big), \tag{E.4}$$

$$\Psi_1^* \overset{(c)}{=} 1 - \mathbb{E}_{r_d,u_g}\Big[\sum_{k=0}^{m_d-1} \sum_{\hat{k}=0}^{k} \frac{(m_d \wp)^k}{\hat{k}! \mu_g} \Big(m_d \wp + \frac{1}{\mu_g}\Big)^{-k-1} e^{-m_d \varsigma} \Big(m_d \varsigma + \mathcal{U}\mu_g^{-1}\Big)^{\hat{k}}\Big], \tag{E.5}$$

$$\begin{aligned}\Psi_1^* \overset{(d)}{=} 1 - \sum_{k=0}^{m_d-1} \sum_{\hat{k}=0}^{k} \int_0^{\mathcal{R}_\mathcal{D}} \int_0^{\mathcal{R}_\mathcal{G}} & \frac{4 r_d u_g (m_d \gamma_\mathcal{T}^{x_{ul}^d} \beta_{SIC} \hat{\varrho}_g)^k}{\mathcal{R}_\mathcal{D}^2 \mathcal{R}_\mathcal{G}^2 \hat{k}! \mu_g \hat{\varrho}_d} \left(\frac{\sqrt{r_d^2 + (h_d - h_\mathcal{B})^2}^{\alpha_d}}{\sqrt{u_g^2 + (h_g - h_\mathcal{B})^2}^{\alpha_g}} \right)^k \\ & \left(\frac{m_d \gamma_\mathcal{T}^{x_{ul}^d} \beta_{SIC} \hat{\varrho}_g \sqrt{r_d^2 + (h_d - h_\mathcal{B})^2}^{\alpha_d}}{\hat{\varrho}_d \sqrt{u_g^2 + (h_g - h_\mathcal{B})^2}^{\alpha_g}} + \frac{1}{\mu_g} \right)^{-k-1} \exp\left(- \frac{m_d \gamma_\mathcal{T}^{x_{ul}^d} \sqrt{r_d^2 + (h_d - h_\mathcal{B})^2}^{\alpha_d}}{\hat{\varrho}_d} \right) \\ & \left(\frac{m_d \gamma_\mathcal{T}^{x_{ul}^d} \sqrt{r_d^2 + (h_d - h_\mathcal{B})^2}^{\alpha_d}}{\hat{\varrho}_d} + \frac{\sqrt{u_g^2 + (h_g - h_\mathcal{B})^2}^{\alpha_g}}{\hat{\varrho}_g \beta_{SIC} \mu_g} \right)^{\hat{k}} dr_d du_g,\end{aligned} \tag{E.6}$$

$$\begin{aligned}\Psi_1^* \overset{(e)}{=} 1 - \sum_{k=0}^{m_d-1} \sum_{\hat{k}=0}^{k} \sum_{e=0}^{\mathcal{E}} \sum_{f=0}^{\mathcal{F}} & \frac{\pi^2 (m_d \gamma_\mathcal{T}^{x_{ul}^d} \beta_{SIC} \hat{\varrho}_g)^k \sqrt{(1-\Phi_e^2)(1-\Phi_f^2)}}{\mathcal{R}_\mathcal{D} \mathcal{R}_\mathcal{G} \hat{k}! \hat{\varrho}_d \mathcal{E} \mathcal{F}} \left(\frac{\tilde{t}_e^{\alpha_d}}{\tilde{s}_f^{\alpha_g}} \right)^k \\ & \left(\frac{m_d \gamma_\mathcal{T}^{x_{ul}^d} \beta_{SIC} \hat{\varrho}_g \tilde{t}_e^{\alpha_d}}{\hat{\varrho}_d \tilde{s}_f^{\alpha_g}} + \frac{1}{\mu_g} \right)^{-k-1} \exp\left(- \frac{m_d \gamma_\mathcal{T}^{x_{ul}^d} \tilde{t}_e^{\alpha_d}}{\hat{\varrho}_d} \right) \\ & \left(\frac{m_d \gamma_\mathcal{T}^{x_{ul}^d} \tilde{t}_e^{\alpha_d}}{\hat{\varrho}_d} + \frac{\tilde{s}_f^{\alpha_g}}{\hat{\varrho}_g \beta_{SIC} \mu_g} \right)^{\hat{k}},\end{aligned} \tag{E.7}$$

$$\Psi_1^* = 1 - \sum_{k=0}^{m_d-1} \sum_{\hat{k}=0}^{k} \sum_{e_1=0}^{\mathcal{E}_1} \sum_{f_1=0}^{\mathcal{F}_1} \frac{\exp(-\chi_{e_1}) \Lambda_*}{\hat{k}!} \left(\frac{\beta_{SIC} \hat{\varrho}_g \chi_{e_1}}{\tilde{s}_{f_1}^{\alpha_g}} + \frac{1}{\mu_g} \right)^{-k-1} \left(\chi_{e_1} + \frac{\tilde{s}_{f_1}^{\alpha_g}}{\hat{\varrho}_g \beta_{SIC} \mu_g} \right)^{\hat{k}}, \tag{E.8}$$

$$\Psi_2^* = 1 - \sum_{k=0}^{m_d-1} \sum_{\hat{k}=0}^{k} \sum_{e_2=0}^{\mathcal{E}_2} \sum_{f_2=0}^{\mathcal{F}_2} \frac{\exp(-\chi_{e_2}) \Lambda_*}{\hat{k}!} \left(\frac{\hat{\varrho}_g \chi_{e_2}}{\tilde{s}_{f_2}^{\alpha_g}} + \frac{1}{\mu_g} \right)^{-k-1} \left(\chi_{e_2} + \frac{\tilde{s}_{f_2}^{\alpha_g}}{\hat{\varrho}_g \mu_g} \right)^{\hat{k}}, \tag{E.9}$$

DRC 16

MASSEY UNIVERSITY
GRADUATE RESEARCH SCHOOL

STATEMENT OF CONTRIBUTION
DOCTORATE WITH PUBLICATIONS/MANUSCRIPTS

We, the candidate and the candidate's Primary Supervisor, certify that all co-authors have consented to their work being included in the thesis and they have accepted the candidate's contribution as indicated below in the *Statement of Originality*.

Name of candidate:	Syeda Kanwal Zaidi
Name/title of Primary Supervisor:	Syed Faraz Hasan
Name of Research Output and full reference:	
S. K. Zaidi, S. F. Hasan, and X. Gui, "Outage Analysis of Ground-Aerial NOMA with Distinct Instantaneous Channel Gain Ranking",IEEE Transactions on Vehicular Technology, doi: 10.1109/TVT.2019.2938516, September 2019.	
In which Chapter is the Manuscript /Published work:	Chapter 4
Please indicate:	
• The percentage of the manuscript/Published Work that was contributed by the candidate:	90%
and	
• Describe the contribution that the candidate has made to the Manuscript/Published Work:	
The candidate has proposed the system model, conducted model simulations and mathematical analysis. Illustration and interpretation of the results has also been done by the candidate. Related manuscript has been written by the candidate majorly. The supervisors were throughout involved in the review of the work.	
For manuscripts intended for publication please indicate target journal:	
Candidate's Signature:	Syeda Kanwal Zaidi Digitally signed by Syeda Kanwal Zaidi Date: 2020.01.06 08:53:08 +13'00'
Date:	06/Jan/2020
Primary Supervisor's Signature:	Faraz Hasan Digitally signed by Faraz Hasan Date: 2020.01.06 10:46:57 +13'00'
Date:	6 Jan 2020

(This form should appear at the end of each thesis chapter/section/appendix submitted as a manuscript/ publication or collected as an appendix at the end of the thesis)

GRS Version 4– January 2019

Figure F.1: DRC 16 -Chapter 4.

Chapter 5

Conclusion and Future Directions

5.1 Conclusion

This thesis has studied the communication scenarios with emerging non-orthogonal multiple access mechanism for effective relaying in future wireless networks. The use of radio frequency based energy harvesting in uplink and downlink communication has also been explored. We had provided baseline scheme to establish uplink communication with base station by harvesting energy from downlink radio signals. Extending this concept further, we had investigated the relaying techniques to extend the coverage of a base station to cell-edge users. Foreseeing the variety of cellular connected devices in future wireless networks, the access mechanism for ground and aerial devices has also been studied as a part of this research. We had shown that the potential of non-orthogonal multiple access to connect ground and aerial devices in a cellular network is still largely unexplored. Consequently, for a pair of an aerial and a ground device, we proposed a novel idea of ground-aerial NOMA where devices are ranked on the basis of instantaneous distinct signal power. The key contributions of this thesis are as follows.

Our study had revealed that maintaining distinct power levels between the received signals at the source in uplink communication with non-orthogonal multiple access is still a research issue. Processing overhead to provide distinguished power levels is still present in existing uplink schemes. We had proposed a scheme to harvest energy utilising power-splitting SWIPT protocol while receiving downlink signals. The uplink communication with information source is then established with the power obtained from radio frequency energy harvesting. We had derived ergodic rates in downlink and uplink communication for the participating users to evaluate the performance of our proposed model. The results illustrate that this scheme successfully provided distinction in the received uplink signals at the source and the users communicated solely on the basis of harvested energy. Furthermore, the portion of the downlink power used

in harvesting energy impacts the data rate achieved in UL communication. Power-splitting parameter shows positive correlation on the uplink rate performance whereas the choice of time-splitting parameter either improves uplink data rate or downlink data rate. This system is applicable in future low data rate applications, where users will be able to transmit high priority UL messages to the source at the cost of compromised DL data rate.

Proceeding from the first scheme, a model of intermediate wireless powered NOMA relays (WPNR) had been established to provide connectivity to cell-edge users by harvesting energy from the radio frequencies. These WPNRs aid data ferrying in uplink and downlink transmission. Unlike existing research works, where cooperative communication with NOMA provides coverage to single users only, this model had provided coverage extension for multiple users. Along with the coverage extension, these relays also eliminate doubly-near far problem in a wireless network. Our study had also emphasised that the geographical location of WPNRs and an appropriate choice of uplink and downlink data rate of users also require careful consideration for adequate and satisfactory network performance. This scheme is highly useful in time-critical scenarios for example, if an emergency signal needs to be transmitted to remote devices and a single relay is unable to communicate to both of them, then the use of a WPNR pair can serve the purpose effectively

For providing connectivity for a multitude of devices in future networks, we had further investigated the case of providing coverage to a ground and an aerial user. Unlike the existing NOMA schemes, where only ground users are considered for cellular connectivity, this scheme allows the multiple access of ground users and aerial users together. So far recent literature focused on the communication scenario of ground users only which share similar channel and environmental conditions. Notwithstanding, this novel scheme gives attention to the large and small scale fading, and geographical location of the devices to evaluate instantaneous distinct signal power (IDSP) first. Based on the IDSP, the power allocation factors are considered for the devices. Contrary to the existing schemes, our approach derives outage probability for ground and aerial users both in uplink and downlink transmission. Our results illustrate that an increase in large scale fading of ground users yield positive impact on the probability of instantaneous channel gain of the aerial user being greater than that of ground users. We argue that evaluating IDSP of the users is an important metric before providing access to two different kinds of users non-orthogonally. The results also unveil that path-loss exponent of ground users affects the outage probability of aerial users, while the outage of ground user is less influenced with the changes in the path-loss exponent of aerial users. Furthermore, the altitude of aerial user impacts the signal reception in downlink and uplink significantly. In the end, we had also compared the system throughput of

ground-aerial NOMA with OMA based transmission and illustrate that the proposed scheme provides superior throughput than conventional OMA based transmission.

5.2 Future Research Directions

This research opens up several directions for future work. We summarise a few of them below.

5.2.1 Extension of WPNRs on a large scale network

Although we had provided a baseline concept of utilising both of the users in a NOMA pair for relaying data to cell-edge users, the scalability of current scheme is still needs to be explored for a large scale network. We have assumed static location of the nodes and the cell edge users. A future extension is to analyse the concept on a larger scale for example, by considering WPNRs in a homogeneous poisson based network where the nodes are evenly distributed. Considering the distance distribution of WPNRs and the cell edge users, selection of efficient WPNRs in terms of data rate is an interesting direction. For such scenario, our proposed model can be utilised in finding key performance indicators such as outage probability and ergodic rate for a general cell-edge user. We have not investigated the amount of power harvested from radio frequency signals experimentally and have considered the energy efficiency factor stated in the recent literature studies. Another research domain is to employ full duplex relays to reduce the overhead of additional time slots of this scheme. A compelling research area is to explore incentive mechanisms for theses relays other than providing energy for data transfer.

5.2.2 Ground Aerial NOMA Aided Relays

The extensive use of aerial devices, such as UAVs motivated us to explore the opportunity to provide cellular connectivity to aerial devices along with ground devices with the proposal of ground-aerial NOMA. An interesting future direction to aid relaying in future wireless networks is use of aerial nodes as relays in a wireless network. We had proposed an initial idea towards this direction in [85]. We studied a network where we consider a ground users closer to the source and an aerial user farther from the source. Based on their different locations, we access ground user and aerial UAV non-orthogonally. In this work we used the UAV as decode-and-forward relay to extend the coverage of source to a farther located user. Working towards this direction, we further extended this work by applying ground-aerial NOMA. Instead of assuming UAV as a fixed relay, we proposed to select the relay node dynamically. More specifically, a device which establishes strong communication link with transmit source is selected as a relay.

The relay communication is further fuelled by harvesting energy from the radio signals of transmit source using power-splitting energy harvesting protocol. We argue that the channel fading characteristics and path-loss environment of a ground and an aerial user are different in nature, contributing towards the relay selection. This dynamic relaying scheme which is an extension of our contributed work [106], achieves improved signal reception at the end user. A substantial future work is to analyse the proposed model mathematically and compare the performance with our numerically proposed model. It is required to evaluate the analytical expressions for the outage probabilities and ergodic rates of cell edge user which is served with dynamically selected aerial or ground relay.

With advancements in drone technology, considering the impact of mobility of aerial user on the performance of ground-aerial NOMA needs to be explored. In a large scale network, the selection of a mobile aerial user to pair with a static ground user is a novel research direction which has not been rigorously investigated.

Bibliography

[1] CommScope, "Cellular wireless 1G, 2G, 3G, 4G, 5G – watch the evolution." [Online]. Available: https://blog.commscopetraining.com/cellular-wireless-watch-the-evolution/

[2] J. Deng, A. A. Dowhuszko, R. Freij, and O. Tirkkonen, "Relay selection and resource allocation for D2D-relaying under uplink cellular power control," in *IEEE Globecom Workshops (GC Wkshps)*, 2015, pp. 1–6.

[3] B. Badic, C. Drewes, I. Karls, and M. Mueck, *Rolling Out 5G: Use Cases, Applications, and Technology Solutions*. Apress, 2016. [Online]. Available: https://www.amazon.com/Rolling-Out-Applications-Technology-Solutions-ebook/dp/B01HUOWMKY?SubscriptionId=AKIAIOBINVZYXZQZ2U3A&tag=chimbori05-20&linkCode=xm2&camp=2025&creative=165953&creativeASIN=B01HUOWMKY

[4] J. McCann, "5G in the UK: everything you need to know," https://www.techradar.com/au/news/5g-uk, accessed 2019-10-16.

[5] Vodafone, "Life to the power of 5G," https://www.vodafone.co.nz/5g/, accessed 2019-10-16.

[6] M. N. Tehrani, M. Uysal, and H. Yanikomeroglu, "Device-to-device communication in 5G cellular networks: challenges, solutions, and future directions," *IEEE Communications Magazine*, vol. 52, no. 5, pp. 86–92, 2014.

[7] N. Instruments, "Applications of Device-to-Device Communication in 5G Networks," http://https://spectrum.ieee.org/computing/networks/applications-of-devicetodevice-communication-in-5g-networks, accessed 2019-09-24.

[8] M. Gharbieh, A. Bader, H. ElSawy, M. Alouini, and A. Adinoyi, "The advents of device-to-device relaying for massively loaded 5G networks," in *IEEE Global Communications Conference*, Dec 2017, pp. 1–7.

[9] A. Li, Y. Lan, X. Chen, and H. Jiang, "Non-orthogonal multiple access (NOMA) for future downlink radio access of 5G," *China Communications*, vol. 12, no. Supplement, pp. 28–37, December 2015.

[10] A. Benjebbour, Y. Saito, Y. Kishiyama, A. Li, A. Harada, and T. Nakamura, "Concept and practical considerations of non-orthogonal multiple access (NOMA) for future radio access," in *IEEE International Symposium on Intelligent Signal Processing and Communication Systems*, 2013, pp. 770–774.

[11] J. B. Kim and I. H. Lee, "Capacity analysis of cooperative relaying systems using NOMA," *IEEE Comm. Letters*, vol. 19, no. 11, pp. 1949–1952, Nov 2015.

[12] L. Dai, B. Wang, Y. Yuan, S. Han, I. Chih-Lin, and Z. Wang, "Non-orthogonal multiple access for 5G: solutions, challenges, opportunities, and future research trends," *IEEE Comm. Magazine*, vol. 53, no. 9, pp. 74–81, 2015.

[13] Z. Ding, M. Peng, and H. V. Poor, "Cooperative non-orthogonal multiple access in 5G systems," *IEEE Communications Letters*, vol. 19, no. 8, pp. 1462–1465, 2015.

[14] J. Men, J. Ge, and C. Zhang, "Performance analysis of nonorthogonal multiple access for relaying networks over nakagami-m fading channels," *IEEE Trans. on Vehicular Technology*, vol. 66, no. 2, pp. 1200–1208, Feb 2017.

[15] T. Nadkar, V. Thumar, G. Shenoy, U. B. Desai, and S. Merchant, "Cognitive relaying with time incentive: protocol design for multiple primary users," in *IEEE 22nd International Symposium on Personal, Indoor and Mobile Radio Communications*, 2011, pp. 577–582.

[16] G. Zhang, K. Yang, Q. Hu, P. Liu, and E. Ding, "Bargaining game theoretic framework for stimulating cooperation in wireless cooperative multicast networks," *IEEE Communications letters*, vol. 16, no. 2, pp. 208–211, 2011.

[17] S. Sudevalayam and P. Kulkarni, "Energy harvesting sensor nodes: Survey and implications," *IEEE Communications Surveys Tutorials*, vol. 13, no. 3, pp. 443–461, Third 2011.

[18] X. Zhou, R. Zhang, and C. K. Ho, "Wireless information and power transfer: Architecture design and rate-energy tradeoff," *IEEE Transactions on Communications*, vol. 61, no. 11, pp. 4754–4767, November 2013.

[19] A. A. Nasir, X. Zhou, S. Durrani, and R. A. Kennedy, "Relaying protocols for wireless energy harvesting and information processing," *IEEE Transactions on Wireless Communications*, vol. 12, no. 7, pp. 3622–3636, 2013.

[20] B. Medepally and N. B. Mehta, "Voluntary energy harvesting relays and selection in cooperative wireless networks," *IEEE Transactions on Wireless Communications*, vol. 9, no. 11, pp. 3543–3553, 2010.

[21] P. T. Venkata, S. A. U. Nambi, R. V. Prasad, and I. Niemegeers, "Bond graph modeling for energy-harvesting wireless sensor networks," *Computer*, vol. 45, no. 9, pp. 31–38, 2012.

[22] CBInsights, "38 ways drones will impact society: From fighting war to forecasting weather, UAVs change everything," https://www.cbinsights.com/research/drone-impact-society-uav/, accessed 2019-11-12.

[23] M. M. Azari, F. Rosas, and S. Pollin, "Cellular connectivity for uavs: Network modeling, performance analysis, and design guidelines," *IEEE Transactions on Wireless Communications*, vol. 18, no. 7, pp. 3366–3381, July 2019.

[24] L. Gupta, R. Jain, and G. Vaszkun, "Survey of important issues in uav communication networks," *IEEE Communications Surveys & Tutorials*, vol. 18, no. 2, pp. 1123–1152, 2015.

[25] H. Nishiyama, M. Ito, and N. Kato, "Relay-by-smartphone: realizing multihop device-to-device communications," *IEEE Communications Magazine*, vol. 52, no. 4, pp. 56–65, April 2014.

[26] J. Liu, N. Kato, J. Ma, and N. Kadowaki, "Device-to-device communication in LTE-advanced networks: A survey," *IEEE Communications Surveys & Tutorials*, vol. 17, no. 4, pp. 1923–1940, 2014.

[27] D. Tsolkas, E. Liotou, N. Passas, and L. Merakos, "LTE-A access, core, and protocol architecture for D2D communication," in *Smart Device to Smart Device Communication*. Springer, 2014, pp. 23–40.

[28] Z. Li, M. Moisio, M. A. Uusitalo, P. Lunden, C. Wijting, F. S. Moya, A. Yaver, and V. Venkatasubramanian, "Overview on initial metis D2D concept," in *1st IEEE International Conference on 5G for Ubiquitous Connectivity*, 2014, pp. 203–208.

[29] P. Popovski, G. Mange, A. Roos, T. Rosowski, G. Zimmermann, J. Söder *et al.*, "Deliverable d6. 3 intermediate system evaluation results," *ICT-317669-METIS/D6. 3*, 2014.

[30] G. Liu, F. R. Yu, H. Ji, V. C. M. Leung, and X. Li, "In-band full-duplex relaying: A survey, research issues and challenges," *IEEE Communications Surveys Tutorials*, vol. 17, no. 2, pp. 500–524, Secondquarter 2015.

[31] Z. Wu, K. Lu, C. Jiang, and X. Shao, "Comprehensive study and comparison on 5G noma schemes," *IEEE Access*, vol. 6, pp. 18 511–18 519, 2018.

[32] Z. Ding, X. Lei, G. K. Karagiannidis, R. Schober, J. Yuan, and V. K. Bhargava, "A survey on non-orthogonal multiple access for 5G networks: Research challenges and future trends," *IEEE Journal on Selected Areas in Communications*, vol. 35, no. 10, pp. 2181–2195, Oct 2017.

[33] U. Uyoata and M. Dlodlo, "Incentive/reward based relay selection for device to device communication," in *IEEE AFRICON*, Sep. 2017, pp. 256–261.

[34] N. Mastronarde, V. Patel, and L. Liu, "Device-to-device relay assisted cellular networks with token-based incentives," in *IEEE International Conference on Communication Workshop (ICCW)*, June 2015, pp. 698–704.

[35] N. Zhao, Y. Liang, and Y. Pei, "Dynamic contract incentive mechanism for cooperative wireless networks," *IEEE Transactions on Vehicular Technology*, vol. 67, no. 11, pp. 10 970–10 982, Nov 2018.

[36] Y. Zhai, X. Bai, and Q. Liu, "Incentive mechanisms in mobile delay tolerant network," in *7th IEEE International Conference on Electronics Information and Emergency Communication (ICEIEC)*, July 2017, pp. 184–188.

[37] A. Ali, H. Mehdi, Z. Hussain *et al.*, "Analysis of SWIPT based relaying network," in *IEEE International Conference on Information Science and Communication Technology (ICISCT)*, 2019, pp. 1–6.

[38] A. Rajaram, R. Khan, S. Tharranetharan, D. N. K. Jayakody, R. Dinis, and S. Panic, "Novel swipt schemes for 5G wireless networks," *Sensors*, vol. 19, no. 5, p. 1169, 2019.

[39] M. A. Hossain, R. M. Noor, K.-L. A. Yau, I. Ahmedy, and S. S. Anjum, "A survey on simultaneous wireless information and power transfer with cooperative relay and future challenges," *IEEE Access*, vol. 7, pp. 19 166–19 198, 2019.

[40] M. Ju and H.-C. Yang, "Optimum swipt relaying in bidirectional non-regenerative relay networks," *IET Communications*, vol. 13, no. 6, pp. 679–686, 2019.

[41] Y. Liu, Y. Ye, H. Ding, J. Shen, and H. Yang, "Performance analysis in df based cooperative swipt networks with direct link," *arXiv preprint arXiv:1902.10403*, 2019.

[42] B. Su, Q. Ni, W. Yu, and H. Pervaiz, "Outage constrained robust beamforming design for SWIPT-enabled cooperative NOMA system," in *IEEE International Conference on Communications (ICC)*, 2019, pp. 1–6.

[43] Y. Liu, H. Ding, J. Shen, R. Xiao, and H. Yang, "Outage performance analysis for swipt-based cooperative non-orthogonal multiple access systems," *IEEE Communications Letters*, vol. 23, no. 9, pp. 1501–1505, 2019.

[44] M. Vaezi, G. Amarasuriya, Y. Liu, A. Arafa, F. Fang, and Z. Ding, "Interplay between NOMA and other emerging technologies: A survey," *arXiv preprint arXiv:1903.10489*, 2019.

[45] K. S. Ali, M. Haenggi, H. ElSawy, A. Chaaban, and M.-S. Alouini, "Downlink non-orthogonal multiple access (NOMA) in poisson networks," *arXiv preprint arXiv:1803.07866*, 2018.

[46] J.-B. Kim and I.-H. Lee, "Non-orthogonal multiple access in coordinated direct and relay transmission," *IEEE Communications Letters*, vol. 19, no. 11, pp. 2037–2040, 2015.

[47] Y. Zeng, J. Lyu, and R. Zhang, "Cellular-connected UAV: Potential, challenges, and promising technologies," *IEEE Wireless Communications*, vol. 26, no. 1, pp. 120–127, 2019.

[48] Y. Chen, W. Feng, and G. Zheng, "Optimum placement of UAV as relays," *IEEE Communications Letters*, vol. 22, no. 2, pp. 248–251, 2018.

[49] F. Ono, H. Ochiai, and R. Miura, "A wireless relay network based on unmanned aircraft system with rate optimization," *IEEE Transactions on Wireless Communications*, vol. 15, no. 11, pp. 7699–7708, Nov 2016.

[50] S. Timotheou and I. Krikidis, "Fairness for non-orthogonal multiple access in 5G systems," *IEEE Signal Processing Letters*, vol. 22, no. 10, pp. 1647–1651, 2015.

[51] Y. Liu, Z. Qin, Y. Cai, Y. Gao, G. Y. Li, and A. Nallanathan, "UAV communications based on non-orthogonal multiple access," *arXiv preprint arXiv:1809.05767*, 2018.

[52] P. K. Sharma and D. I. Kim, "UAV-enabled downlink wireless system with non-orthogonal multiple access," in *IEEE Globecom Workshops (GC Wkshps)*. IEEE, 2017, pp. 1–6.

[53] M. S. Ali, H. Tabassum, and E. Hossain, "Dynamic user clustering and power allocation for uplink and downlink non-orthogonal multiple access (NOMA) systems," *IEEE Access*, vol. 4, pp. 6325–6343, 2016.

[54] N. Zhang, J. Wang, G. Kang, and Y. Liu, "Uplink nonorthogonal multiple access in 5G systems," *IEEE Communications Letters*, vol. 20, no. 3, pp. 458–461, 2016.

[55] Z. Zhang and R. Q. Hu, "Uplink non-orthogonal multiple access with fractional power control," in *IEEE Wireless Comm. and Networking Conference (WCNC)*, 2017, pp. 1–6.

[56] P. D. Diamantoulakis, K. N. Pappi, Z. Ding, and G. K. Karagiannidis, "Wireless-powered communications with non-orthogonal multiple access," *IEEE Trans. on Wireless Communications*, vol. 15, no. 12, pp. 8422–8436, 2016.

[57] H. Chingoska, Z. Hadzi-Velkov, I. Nikoloska, and N. Zlatanov, "Resource allocation in wireless powered communication networks with NOMA," *IEEE Wireless Comm. Letters*, vol. 5, no. 6, pp. 684–687, 2016.

[58] K. Zaidi, S. Hasan, and X. Gui, "SWIPT-aided uplink in hybrid non-orthogonal multiple access," in *IEEE Wireless Comm. and Networking Conference (WCNC)*, 2018, p. (in press).

[59] Y. Liu, Z. Ding, M. Elkashlan, and H. V. Poor, "Cooperative non-orthogonal multiple access with simultaneous wireless information and power transfer," *IEEE Journal on Selected Areas in Communications*, vol. 34, no. 4, pp. 938–953, 2016.

[60] J. Cui, Z. Ding, and P. Fan, "Power minimization strategies in downlink MIMO-NOMA systems," in *IEEE International Conference on Communications (ICC)*, May 2017, pp. 1–6.

[61] I. S. Gradshteyn and I. M. Ryzhik, *Table of integrals, series, and products.* Academic press, 2014.

[62] S. Peng, A. Liu, L. Song, I. Memon, and H. Wang, "Spectral efficiency maximization for deliberate clipping-based multicarrier faster-than-nyquist signaling," *IEEE Access*, vol. 6, pp. 13 617–13 623, 2018.

[63] X. Zhao, A. M. A. Abdo, C. Xu, S. Geng, J. Zhang, and I. Memon, "Dimension reduction of channel correlation matrix using cur-decomposition technique for 3-D massive antenna system," *IEEE Access*, vol. 6, pp. 3031–3039, 2018.

[64] Y. Zhao, Y. Li, D. Wu, and N. Ge, "Overlapping coalition formation game for resource allocation in network coding aided D2D communications," *IEEE Trans. on Mobile Computing*, vol. 16, no. 12, pp. 3459–3472, 2017.

[65] D. Wu, D. I. Arkhipov, T. Przepiorka, Y. Li, B. Guo, and Q. Liu, "From intermittent to ubiquitous: Enhancing mobile access to online social networks with opportunistic optimization," *Proceedings of the ACM on Interactive, Mobile, Wearable and Ubiquitous Technologies*, vol. 1, no. 3, p. 114, 2017.

[66] A. M. A. Abdo, X. Zhao, R. Zhang, Z. Zhou, J. Zhang, Y. Zhang, and I. Memon, "MU-MIMO downlink capacity analysis and optimum code weight vector design for 5G big data massive antenna mm-wave comm." *Wireless Comm. and Mobile Computing*, vol. 2018, 2018.

[67] G. Chen, P. Xiao, J. R. Kelly, B. Li, and R. Tafazolli, "Full-duplex wireless-powered relay in two way cooperative networks," *IEEE Access*, vol. 5, pp. 1548–1558, 2017.

[68] "Proposed solutions for new radio access," METIS, Deliverable D2.4, Tech. Rep. ICT-317669, Feb 2015.

[69] Y. Liu, Z. Qin, M. Elkashlan, Z. Ding, A. Nallanathan, and L. Hanzo, "Non-orthogonal multiple access for 5G and beyond," *arXiv preprint arXiv:1808.00277*, 2018.

[70] J. Choi, "Non-orthogonal multiple access in downlink coordinated two-point systems," *IEEE Comm. Letters*, vol. 18, no. 2, pp. 313–316, February 2014.

[71] X. Y. et. al., "Exploiting full/half-duplex user relaying in NOMA systems," *IEEE Trans. on Comm.*, vol. 66, no. 2, pp. 560–575, Feb 2018.

[72] X. Lu, P. Wang, D. Niyato, D. I. Kim, and Z. Han, "Wireless networks with RF energy harvesting: A contemporary survey," *IEEE Comm. Surveys & Tutorials*, vol. 17, no. 2, pp. 757–789, 2015.

[73] S. K. Zaidi, S. F. Hasan, and X. Gui, "Time switching based relaying for coordinated transmission using NOMA," in *IEEE Eleventh International Conference on Mobile Computing and Ubiquitous Network (ICMU)*, 2018, pp. 1–5.

[74] Z. Wei, X. Zhu, S. Sun, Y. Jiang, A. Al-Tahmeesschi, and M. Yue, "Research issues, challenges, and opportunities of wireless power transfer-aided full-duplex relay systems," *IEEE Access*, vol. 6, pp. 8870–8881, 2018.

[75] Z. Wei, X. Zhu, S. Sun, J. Wang, and L. Hanzo, "Energy-efficient full-duplex cooperative nonorthogonal multiple access," *IEEE Trans. on Vehicular Technology*, vol. 67, no. 10, pp. 10 123–10 128, Oct 2018.

[76] N. T. Do, D. B. Da Costa, T. Q. Duong, and B. An, "A BNBF user selection scheme for NOMA-based cooperative relaying systems with swipt," *IEEE Comm. Letters*, vol. 21, no. 3, pp. 664–667, 2017.

[77] S. K. Zaidi, S. F. Hasan, and X. Gui, "Wireless-powered NOMA relays for out-of-coverage devices," in *IEEE 28th Annual International Symposium on Personal, Indoor, and Mobile Radio Communications (PIMRC)*, Oct 2017, pp. 1–5.

[78] K. Huang and V. K. N. Lau, "Enabling wireless power transfer in cellular networks: Architecture, modeling and deployment," *IEEE Trans. on Wireless Comm.*, vol. 13, no. 2, pp. 902–912, February 2014.

[79] S. K. Zaidi, S. F. Hasan, and X. Gui, "Evaluating the ergodic rate in SWIPT-aided hybrid NOMA," *IEEE Comm. Letters*, vol. 22, no. 9, pp. 1870–1873, 2018.

[80] J. Men, J. Ge, and C. Zhang, "Performance analysis for downlink relaying aided non-orthogonal multiple access networks with imperfect CSI over nakagami- m fading," *IEEE Access*, vol. 5, pp. 998–1004, 2017.

[81] J. Stoer and R. Bulirsch, *Introduction to numerical analysis*. Springer Science & Business Media, 2013, vol. 12.

[82] M. M. Molu, P. Xiao, M. Khalily, L. Zhang, and R. Tafazolli, "A novel equivalent definition of modified bessel functions for performance analysis of multi-hop wireless communication systems," *IEEE Access*, vol. 5, pp. 7594–7605, 2017.

[83] L. Comtet, *Advanced Combinatorics: The art of finite and infinite expansions*. Springer Science & Business Media, 2012.

[84] R. S. Sinha, Y. Wei, and S.-H. Hwang, "A survey on LPWA technology: LoRa and NB-IoT," *Ict Express*, vol. 3, no. 1, pp. 14–21, 2017.

[85] S. K. Zaidi, S. F. Hasan, X. Gui, N. Siddique, and S. Ahmad, "Exploiting UAV as NOMA based relay for coverage extension," in *2nd International Conference on Computer Applications Information Security (ICCAIS)*, May 2019, pp. 1–5.

[86] M. F. Sohail, C. Y. Leow, and S. Won, "Non-orthogonal multiple access for unmanned aerial vehicle assisted communication," *IEEE Access*, vol. 6, pp. 22 716–22 727, 2018.

[87] Z. Ding, Z. Yang, P. Fan, and H. V. Poor, "On the performance of non-orthogonal multiple access in 5g systems with randomly deployed users," *IEEE Signal Processing Letters*, vol. 21, no. 12, pp. 1501–1505, 2014.

[88] M. T. Le, G. C. Ferrante, G. Caso, L. DeNardis, and M.-G. Di Benedetto, "On information-theoretic limits of code-domain NOMA for 5G," *IET Communications*, vol. 12, no. 15, pp. 1864–1871, 2018.

[89] A. Benjebbour, K. Saito, A. Li, Y. Kishiyama, and T. Nakamura, "Non-orthogonal multiple access (NOMA): Concept, performance evaluation and experimental trials," in *IEEE International Conference on Wireless Networks and Mobile Communications (WINCOM)*, 2015, pp. 1–6.

[90] M. Zeng, A. Yadav, O. A. Dobre, G. I. Tsiropoulos, and H. V. Poor, "Capacity comparison between MIMO-NOMA and MIMO-OMA with multiple users in a cluster," *IEEE Journal on Selected Areas in Communications*, vol. 35, no. 10, pp. 2413–2424, 2017.

[91] M. Zeng, A. Yadav, O. A. Dobre, G. I. Tsiropoulos, and H. V. Poor, "On the sum rate of MIMO-NOMA and MIMO-OMA systems," *IEEE Wireless Communications Letters*, vol. 6, no. 4, pp. 534–537, 2017.

[92] L. Dai, B. Wang, Z. Ding, Z. Wang, S. Chen, and L. Hanzo, "A survey of non-orthogonal multiple access for 5G," *IEEE Communications Surveys & Tutorials*, 2018.

[93] A. A. Nasir, H. D. Tuan, T. Q. Duong, and H. V. Poor, "UAV-enabled communication using NOMA," *arXiv preprint arXiv:1806.03604*, 2018.

[94] T. Hou, Y. Liu, Z. Song, X. Sun, and Y. Chen, "Multiple antenna aided NOMA in UAV networks: A stochastic geometry approach," *arXiv preprint arXiv:1805.04985*, 2018.

[95] M. M. Selim, M. Rihan, Y. Yang, L. Huang, Z. Quan, and J. Ma, "On the outage probability and power control of D2D underlaying NOMA UAV-assisted networks," *IEEE Access*, vol. 7, pp. 16 525–16 536, 2019.

[96] N. Rupasinghe, Y. Yapıcı, I. Güvenç, and Y. Kakishima, "Non-orthogonal multiple access for mmWave drone networks with limited feedback," *IEEE Transactions on Communications*, vol. 67, no. 1, pp. 762–777, 2019.

[97] T. Qi, W. Feng, and Y. Wang, "Outage performance of non-orthogonal multiple access based unmanned aerial vehicles satellite networks," *China Communications*, vol. 15, no. 5, pp. 1–8, 2018.

[98] T. Hou, X. Sun, and Z. Song, "Outage performance for non-orthogonal multiple access with fixed power allocation over nakagami-$m$fading channels," *IEEE Communications Letters*, vol. 22, no. 4, pp. 744–747, April 2018.

[99] P. D. Diamantoulakis, K. N. Pappi, G. K. Karagiannidis, H. Xing, and A. Nallanathan, "Joint downlink/uplink design for wireless powered networks with interference," *IEEE Access*, vol. 5, pp. 1534–1547, 2017.

[100] A. A. Khuwaja, Y. Chen, N. Zhao, M. Alouini, and P. Dobbins, "A survey of channel modeling for UAV communications," *IEEE Communications Surveys Tutorials*, pp. 1–1, 2018.

[101] W. Khawaja, I. Guvenc, D. W. Matolak, U. Fiebig, and N. Schneckenburger, "A survey of air-to-ground propagation channel modeling for unmanned aerial vehicles," *IEEE Communications Surveys Tutorials*, vol. 21, no. 3, pp. 2361–2391, 2019.

[102] M. Salehi, H. Tabassum, and E. Hossain, "Accuracy of distance-based ranking of users in the analysis of noma systems," *IEEE Transactions on Communications*, vol. 67, no. 7, pp. 5069–5083, 2019.

[103] M. Mozaffari, W. Saad, M. Bennis, and M. Debbah, "Unmanned aerial vehicle with underlaid device-to-device communications: Performance and tradeoffs," *IEEE Transactions on Wireless Communications*, vol. 15, no. 6, pp. 3949–3963, 2016.

[104] ——, "Unmanned aerial vehicle with underlaid device-to-device communications: Performance and tradeoffs," *IEEE Trans. on Wireless Comm.*, vol. 15, no. 6, pp. 3949–3963, 2016.

[105] H. Sun, B. Xie, R. Q. Hu, and G. Wu, "Non-orthogonal multiple access with SIC error propagation in downlink wireless MIMO networks," in *IEEE 84th Vehicular Technology Conference (VTC-Fall)*. IEEE, 2016, pp. 1–5.

[106] S. K. Zaidi, S. F. Hasan, and X. Gui, "Outage analysis of ground-aerial noma with distinct instantaneous channel gain ranking," *IEEE Transactions on Vehicular Technology*, vol. 68, no. 11, pp. 10 775–10 790, Nov 2019.